BEHAVIOR OF HIGH-STRENGTH CONCRETE PLATES UNDER IMPACT LOADING

SURYAWAN MURTIADI

INFORMATION TO USERS

This manuscript has been reproduced from the microfilm master. UMI films the text directly from the original or copy submitted. Thus, some thesis and dissertation copies are in typewriter face, while others may be from any type of computer printer.

The quality of this reproduction is dependent upon the quality of the copy submitted. Broken or indistinct print, colored or poor quality illustrations and photographs, print bleedthrough, substandard margins, and improper alignment can adversely affect reproduction.

In the unlikely event that the author did not send UMI a complete manuscript and there are missing pages, these will be noted. Also, if unauthorized copyright material had to be removed, a note will indicate the deletion.

Oversize materials (e.g., maps, drawings, charts) are reproduced by sectioning the original, beginning at the upper left-hand corner and continuing from left to right in equal sections with small overlaps.

Photographs included in the original manuscript have been reproduced xerographically in this copy. Higher quality 6" x 9" black and white photographic prints are available for any photographs or illustrations appearing in this copy for an additional charge. Contact UMI directly to order.

Bell & Howell Information and Learning
300 North Zeeb Road, Ann Arbor, MI 48106-1346 USA

UMI®
800-521-0600

BEHAVIOR OF HIGH-STRENGTH CONCRETE PLATES UNDER IMPACT LOADING

by

© Suryawan Murtiadi

A thesis submitted to the School of Graduate

Studies in partial fulfillment of the

requirements for the degree of

Master of Engineering

Faculty of Engineering and Applied Science

Memorial University of Newfoundland

March 1999

St. John's Newfoundland Canada

ABSTRACT

High-strength concrete plates are frequently used in various structural engineering systems and varieties of civil engineering applications. A research program was carried out at Memorial University of Newfoundland to investigate the behavior of high-strength concrete two-way plates subjected to impact loading. The research program included both experimental investigation and numerical investigation.

The current research includes an experimental investigation on sixteen concrete plates with dimension of 950x950 mm and 100-mm thickness. The plates were supported by a special frame designed for this investigation. The support frame is made from concrete and steel with free opening of 700x700 mm. Normal-strength and high-strength concrete plates were tested under two end conditions, i.e. fixed and simply supported. All of the specimens were two-way reinforced plates with reinforcement ratio that varied from 1%-2.5% in tension face and 0.7%-0.8% in compression face. A rigid projectile was used to apply the impact load to the tested reinforced concrete specimens. The rigid projectile was a solid steel cylinder with 220-kg mass and 304.5 mm diameter contact area. The projectile was dropped from a variable height of up to 4 m. An accelerometer with $\pm$200-g capacity was attached to the cylinder steel to record the actual test acceleration. A data acquisition system based on a personal computer acquired the data at a sampling rate of 1000 Hz. The structural behavior with respect to displacement, concrete and steel strains, failure mode, and energy absorption were examined. The effect of dynamic loading, concrete strength, reinforcement ratio, and support patterns were the test parameters.

A numerical investigation was conducted to evaluate the test results with respect to the North American code and some European design codes. A linear elastic fracture mechanics impact load expression was used to evaluate the effect of rate of loading on the dynamic behavior of high-strength concrete plates. Based on the experimental test results it has been found that the punching failures of the impact loading were about twice the static punching shear capacity. The critical velocities of perforation can be estimated accurately for all high-strength concrete specimens according to CEB dynamic code expression. The ratio of impact versus static fracture energy for high-strength concrete plate was found to be much higher than that for normal-strength concrete. Therefore, high-strength concrete plates are considered to be more efficient than normal-strength concrete plates under impact loading.

ACKNOWLEDGEMENTS

This thesis was completed at Memorial University of Newfoundland as part of Master of Engineering degree program. The experimental work has been carried out at the concrete and structure laboratory of Memorial University of Newfoundland, Canada. Funding in the form of graduate fellowship from the Government of Republic Indonesia and research supplement from Memorial University are gratefully acknowledged.

Grateful acknowledgement is also due to Dr. H. Marzouk, Professor of Civil Engineering, under whose guidance and supervision the thesis was carried out. Acknowledgement is also addressed to Dr. M.R. Haddara, Associate Dean of Engineering Graduate Studies and Research, for his encouragement and the facilities provided.

Acknowledgements are also made to the Technical Staff for their assistance in the experimental program, especially Mr. C. Ward, Mr. A. Bursey, and Mr. R. O'Driscoll for their preparation of the test specimens and test equipment. Special thanks to Dr. A. Hussein and Dr. M.A. Fard for their support and discussion during experimental work.

Last, but not least, the author takes this chance to express his profound gratitude to all his family members, especially his parents for their prayer and blessing, also his wife and son for their patience, continuing encouragement, and affection.

Table of Contents

Chapter 3

EXPERIMENTAL INVESTIGATION

Chapter 4

TEST RESULTS AND DISCUSSION

List of Figures

List of Tables

List of Symbols

A_s	area of steel reinforcement
a	crack length
a_f	final crack on fracture
a_i	initial crack before testing
a_p	acceleration of projectile
a_t	total acceleration
b	side dimension of square loaded area
b_o	perimeter of critical section for shear in plates
c	periphery around the column excluding openings
d	effective depth of the slab
$\frac{da}{dt}$	rate of crack extension
$\frac{d\sigma}{dt}$	stress rate or variation of stress with time
E	modulus of elasticity
E_c	modulus of elasticity of concrete
E_s	modulus elasticity of steel
E_{imp}	dynamic (impact) modulus of elasticity
E_{stat}	static modulus of elasticity
$F(t)$	impact loading
f_{cm}	mean concrete strength

f_{cu} cube strength of concrete

f_{cy} cylinder compressive strength

f_t tensile strength

f_{td} design tensile strength of concrete

f_y yield strength of flexural steel reinforcement

f_{imp} impact strength

f_{stat} static strength

f_c' concrete compressive strength

G_c critical strain energy release rate

G_f fracture energy required to form an unit area of crack surface

$G_f(t)$ impact energy received by the specimen

h concrete slab thickness

K intrinsic material property called fracture toughness

K_a = 0.13 for normal concrete 0.105 for lightweight concrete

K_c critical stress intensity factor

K_I stress intensity factor

K_{sc} = $1.15\,[4\,\pi\,(\text{column area}) / (\text{column perimeter})^2\,]^{1/2}$

M missile mass

m mass of cylindrical dropped object

m_p mass of projectile

m_s mass of specimen

$P(t)$ impact test load

p missile perimeter

u perimeter of the governing section at a distance 1.0 d from the loaded area

$u(t)$ deflection at the load point

$\ddot{u}(t)$ acceleration at the load point

$\dot{V}$ velocity of crack extension

V_u ultimate shear force

V_{flex} ultimate load for flexural failure

v_c nominal shear stress

v_u ultimate shear stress

W concrete density

w crack width

w_c width of the fracture process zone

w_o crack width when f_t reaches zero

$\dot{w}$ crack opening velocity

α dynamic material property

α_s factor which adjusts v_c for support dimensions

β_c ratio of long side to short side of the concentrated load

γ fracture surface energy

γ_c material coefficient for reinforced

ε_t tensile strain

ε_y yield strain of steel reinforcement

ε_{max} maximum tensile strain

$\varepsilon_{u,imp}$ impact ultimate strain

$\varepsilon_{u,stat}$ static ultimate strain

$\dot{\varepsilon}$ strain rate

$\dot{\varepsilon}_o$ strain rate at quasi static condition

ρ tensile reinforcement ratio

ρ' compressive reinforcement ratio

$\sum C$ perimeter of the column

σ_c fracture strength of concrete

σ_f final stress of a specimen measured in a fracture test

σ_i initial stress of a specimen

$\dot{\sigma}$ stress rate or variation of stress with time

$\dot{\sigma}_o$ stress rate at quasi static condition.

Chapter 1

INTRODUCTION

1.1. General

It is appropriate to discuss and clarify a number of fundamental points in the subject or dealing with specific design arrangement. There are three points that should be clarified before examining the behavior of concrete plates under impact loading. Firstly, the high-strength concrete plate should be defined. Secondly, the definition of impact loading should be outlined. Finally, the objectives of the research should be described clearly.

High-strength concrete is defined as any concrete with compressive-strength over 41 MPa. High-strength is realized through the use of silica fume as a partial replacement for cement to produce extremely strong, highly abrasion resistant, impermeable, very durable concrete against freeze-thaw damage and salt water attack. This material has already been successfully used for offshore platforms, marine structures, tall buildings, and long span bridges.

Impact loading is a result of a collision between two bodies that occur in a very small interval of time, one with a high initial speed striking another at a stationary

position by generating large forces. The struck object, in civil engineering, is usually a structural element that has to be designed to resist impact loading. This loading is mostly extreme loading with infrequent probability of existence during the lifetime of the structure. However, failure due to impact loading often results in a serious structural damage. Material properties like high-energy absorption have to be taken into consideration in the design of safe concrete structure.

Many structures experience impact loading. Some of the structures that must have the possibility of impact loading considered in their design are offshore facilities, piles, defense shelters, and structures in seismic areas. The impact loading can be ignored in the design process when the loading intensity has small fluctuations. However, when the magnitude of the fluctuating component of loading is large, the impact loading can be very significant. Engineers should be able to decide whether the impact loading must be accounted for in design or neglect it. The responsibility of the design engineer is to solve problems in a safe, efficient, and economic manner. Therefore, the design engineer should consider how the overall structure behaves under impact loading.

The use of high-strength concrete is increasing faster than the development of appropriate design code recommendation. In spite of the wide use of high-strength concrete, little research has been conducted on the structural behavior of high-strength concrete beams, slabs and columns under dynamic loading. The structural behavior of concrete plates, especially under impact loading, needs further investigation. The concrete plate is a simple, economical, and popular structural system. Therefore, high-strength concrete flat plate was chosen in this research, since it has several civil engineering applications.

1.2. Research Scope

The scope of this study is to investigate the dynamic behavior of two-way reinforced concrete plates under impact loading. The investigation includes an experimental investigation and a numerical evaluation. The two phases of the investigations are described as follows:

The experimental testing program will be conducted on several specimens subjected to impact loading. The impact load speed target range between 4 to 9 m/s as acceleration is range between 70 to 120 g. The specimens will be tested under fixed and simply supported end-conditions. The behavior of high-strength concrete plates will be evaluated with respect to deflection, concrete and steel strains, energy absorption capacity, and fracture energy.

The numerical evaluation will be carried out to verify the validity of the current code predictions. The impact load capacities will be compared with static capacities of the codes. A fracture mechanics impact load analysis based on linear elastics fracture mechanics (LEFM) will be conducted. The purpose of the numerical evaluation is to provide a more detail analysis on the effect of the rate of loading on the dynamic behavior of high-strength concrete plates. The dynamic fracture energies of the tested plates will be compared to static fracture energies calculated from previous investigators. The study will provide a design guide for engineers on the effect of rate of loading on the behavior of high-strength concrete plate.

1.3. Research Objectives

This research will investigate the test results of 16 different specimens. Based on the experimental investigation a better understanding of the behavior of high-strength reinforced concrete plates under impact loading will be realized. The major objectives are not limited to but will contain the following objectives:

(1) Investigate the structural behavior of high-strength concrete plate under dynamic impact loading.

(2) Study the effect of the end conditions on the structural behavior of high-strength concrete plate under impact loading.

(3) Examine the effect of reinforcement ratio on the behavior of high-strength concrete plates.

(4) Record actual concrete strains, steel strains, and deflection of high-strength concrete plates under impact loading.

(5) Investigate the influence of the rate of loading on the impact behavior of specimens using fracture mechanics equations and test results.

(6) Provide new information on the force-displacement relationships of high-strength concrete plates.

(7) Compare the result of the investigation with theoretical expressions and code equations.

(8) Evaluate the fracture energy of the concrete plate under impact loading.

1.4. Format

This thesis can be divided into three parts. Part I appears under Chapters 1 and 2. Chapter 1 covers the introduction and the objectives of this investigation. Chapter 2 presents the literature review of previous investigations.

Part II appears under Chapter 3 that cover all the experimental investigation carried out to study the effect of concrete strength and reinforcement ratio on the behavior of reinforced concrete plates subjected to impact loading. This chapter covers the set-up of laboratory and experimental program.

Part III appears under Chapters 4 and 5, cover the entire research findings, test results and analytical investigation including evaluation of several models to predict the shear-strength of high-strength concrete plate. This chapter also presents a numerical evaluation based on a fracture mechanics analysis to evaluate the effect of rate of loading on the behavior of concrete plates. Finally, a conclusion summarizes the experimental and analytical investigations are given in Chapter 6.

Chapter 2

REVIEW OF LITERATURE

2.1. High-Strength Concrete

2.1.1. General

Quality of concrete is generally described by its compressive strength. According to the American Concrete Institute, ACI 363 (1992), ordinary structural concrete has been used with a compressive strength in the range of 20 to 40 MPa. While, high-strength concrete is defined as any concrete with over 41 MPa compressive strength. But, in the last two decades, concrete with higher compressive strength has been used in the construction of high-rise buildings, long-span bridges, and offshore structures. The new high-strength concrete has a compressive strength of 70 MPa and 100 MPa.

The use of high-strength concrete is spreading rapidly all over the world and increasing faster than the development of appropriate design code recommendations. Several recent investigations have been conducted on high-strength concrete behavior to find the characteristic behavior of high-strength concrete and to upgrade the current

design recommendations so that the potential of high-strength concrete can be fully exposed.

Recent investigations on high-strength concrete can be classified into three main categories, i.e. behavior of material properties, behavior of structural members, and development of testing equipment. These three main categories can be described briefly in the following:

(1) With attention to the material properties, several studies have been carried out to investigate the behavior of high-strength concrete subjected to different stress conditions.

(2) With respect to the behavior of structural members, several studies have been conducted to investigate the behavior of structural elements constructed with high-strength concrete.

(3) Finally, with consideration to the development of testing equipment, several researches have been given to improve the testing equipment in order to investigate accurately the behavior of high-strength concrete.

During the past decade, several concrete material and structural investigations were conducted at Memorial University of Newfoundland. Marzouk and Hussein (1990) conducted the development of high-strength mix design from local materials. It has been concluded that local materials can be used with silica fume and fly ash to provide strength of 70 MPa at 28 days. Marzouk and Chen (1995) recommended a constitutive relationship for the behavior of high-strength concrete under uniaxial tension load including the post-peak softening response and fracture energy.

Marzouk and Hussein (1991) reported that the use of the cubic root of the compressive strength to predict the punching shear resistance of high-strength concrete slabs is much better expression compared to the square root expression used in all North American codes. Marzouk and Jiang (1994) investigated six different methods to enhancement of the punching shear capacity. The structural behavior of high-strength concrete plates was evaluated in terms of overall load-deflection response, ultimate loading capacity, ductility and energy absorption. Failure patterns and strain distribution were also discussed.

2.1.2. Mix Design of High-Strength Concrete

High-strength concrete is made with the same basic ingredients as normal-strength concrete. Farny and Panarese (1993) reported that the production of high-strength concrete is achieved by optimization of the following factors:

(1) characteristics of the cementing medium,

(2) characteristics of the aggregates,

(3) proportions of the paste,

(4) paste-aggregates interaction,

(5) mixing, consolidating, and curing, and

(6) testing procedures.

Some selection of materials and mixing methods are being explored through research. However, attention to the above six basic areas is of extreme importance whether using existing or new materials and techniques. In the United States and Canada, the ACI

Committee 363 (1992) report is used as a guide for the design and construction of high-strength concrete structures.

2.1.2.1. Cement

Cement paste is an important factor in making high-strength concrete. Selection of a portland cement for high-strength concrete should be based on comparative strength tests of cement at 28 and 90 days. A cement that yields the highest compressive strength at the later age, 90 days, is obviously preferable.

Zia et al. (1993) described that the choice of appropriate cementitious materials was governed by considerations of:

(1) cost,

(2) availability,

(3) evidence of satisfactory performance,

(4) the engineer's confidence in specifying the material, and

(5) the contractor's ability to produce, handle, and place concrete containing the product.

In the United States and Canada, ACI-363 (1992) recommendations require a minimum cement content of 360 kg/m^3. In order to make high-strength concrete; the mixture should have a cementitious materials content of between 360 to 600 kg/m^3. However, the use of high cement content in massive structures frequently leads to thermal cracking. Thermal cracking increases the permeability and reduces the durability. Therefore, developing high-strength cement with moderate heat of hydration is recommended in order to avoid this problem. In the United States ASTM type I cement

and in Canada CSA type 10 cement are the most used type of cements to produce high-strength concrete.

Water-cement ratio is typically expressed as the total weight of water to the total weight of cement. In addition, water-cementitious material ratio is expressed as the total weight of water to the total combined weight of all cementitious materials. In both cases, the total weight of water excludes that absorbed by the aggregates, but includes any water introduced into the mixture as part of an admixture. Some of the more finely ground portland cements such as ASTM type III (high-early-strength) will have higher mixing water requirement for equal workability, particularly at low water-cement ratios, and may promote rapid stiffening in hot weather. Unfortunately, this type of cement is not recommended for high-strength concrete.

2.1.2.2. Aggregates

Aggregates are those parts of the concrete that constitute the bulk of the finished product. Aggregates constitute the major part of the mix and comprise 60% to 80% of the volume of the concrete. They have to be so graded that the whole mass of concrete acts as a relatively solid, homogeneous, dense combination, with the smaller sizes acting as an filler of the voids.

Usually, the main components of aggregates can be divided into two types: (1) coarse aggregate: gravel, crushed stone, or blast furnace slag; and (2) fine aggregate: natural or manufactured sand. The coarse and fine aggregates are described briefly in the following discussion.

2.1.2.2.1. Coarse Aggregates

The characteristics of the aggregate significantly influence the properties of concrete, including strength. The strength of aggregates is always greater than the strength of cement paste. However, for high-strength concrete production, the strength of the cement paste is high enough to rival the strength and other vital properties of the aggregate. The strength of the aggregate, the bond or adhesion between cement paste and aggregate, and the absorption characteristic of the aggregate all become more important for high-strength concrete than for normal-strength concrete. For this reason, any one of these properties could be a limit factor for ultimate strength.

There is a practical value in determining the optimum size of coarse aggregate for different concrete strength levels. The optimum size depends on the following factors:

(1) relative strength of the cement paste,

(2) cement-aggregate bond, and

(3) strength of the aggregate particles.

The chemical content of the aggregates, that is the mineral present, does lend some insight into predicting the interaction between cement paste and aggregate particles. Still, trial batches provide the most practical information for choosing the best aggregate for a concrete mixture.

For normal-strength concrete, Walker and Bloem (1960) explained that mixing water requirement is reduced as coarse aggregate size is increased. The net effect is a lower water-cement ratio and higher strength. Water requirement is a function of the overall fineness of the solid ingredients.

For high-strength mixtures, the use of small aggregates with maximum nominal size of 19.0, 12.5, and 9.5 mm, usually is sufficient to offset the effect of the higher mixing water demand. Carrasquillo (1985) reported that the use of crushed aggregates is recommended for the production of high-strength concrete, rather than round aggregates. This was attributed to the reduced aggregate-mortar interface bond strength of natural gravel aggregates.

However, the role of aggregates in high-strength concrete is minor compared with the role of cementitious materials. Marzouk, Osman, and Helmy (1998) reported that it has been produced a high-strength lightweight concrete up to 80 MPa at the concrete laboratory of Memorial University.

2.1.2.2.2. Fine Aggregates

Saucier, Smith, and Tynes (1964) indicated that fine aggregates contain a much higher surface area than coarse aggregates for a given weight. Because it has a much larger surface area, the fine aggregate (sand) can influence the amount of mixing water required and affect the properties of fresh and hardened paste more than the coarse aggregate. In sands of the same grading, 1% increase in fine aggregate voids may induce a 5 l/m^3 increase in water demand to maintain an equal slump.

Since all aggregate in concrete must be coated with paste, the shape and grading of fine aggregate as well as its proportion to coarse aggregate will have a direct impact on paste requirement. More cement paste is required when more fine aggregate is used. The less sand used, however, the harsher mixture and workability maybe seriously impaired. A balance must be struck in proportioning high-strength mixtures. In general, using at

least sand consistent with necessary workability has given the best strength for a given paste.

The bond of paste to fine aggregate is less significant than bond to coarse aggregate because of the large surface area available in the fine aggregate for bonding. Maximizing the coarse to fine aggregate ratio (CA/FA) can result in the most efficient, and therefore economical, use of cementitious materials. The optimum ratio of CA/FA will probably be apparent from trial batches based on workability of the mixture.

Rounded and smooth fine aggregate particles (natural sand) are better from the viewpoint of workability than sharp and rough particles (manufactured sand). Concrete mixtures of the same slump and cement factor containing natural sand produce higher strengths than concrete containing manufactured sand as reported by Farny and Panarese (1994). The particle shape and grading of these materials are probably responsible for the strength differences.

Washing the sand may be necessary. When natural sands containing large quantities of mica, clay, and other deleterious materials. These harmful materials should be avoided as they may increase water demand and affect hydration and bond of cement paste to aggregate. Uniformity of grading from batch to batch is also important for both the fine and coarse aggregates because of its effect on workability.

2.1.2.3. Admixtures

Admixtures are materials other than water, aggregates, and cement that are used as ingredients of concrete. ACI Committee 212 (1983) reported that the function of admixtures is to modify the properties of concrete to improve workability, or for

economy, or for other purposes such as improving concrete strength. These materials are added to the batch immediately before or during the mixing. These properties help the concrete to achieve high strength and water reduction without loss of workability.

Trial mixtures should be made with the admixture and job materials at the same temperatures and humidity anticipated on the job. This permits an evaluation of the compatibility of an admixture with other admixtures and concrete materials. It also serves an evaluation of the admixture effects on the properties of fresh and hardened concrete. A recommendation by the manufacturer or the optimum amount determined by laboratory trial batches should be used. The major type of admixtures can be summarized as mineral admixtures and chemical admixtures, which will be described briefly in the following discussion.

2.1.2.3.1. Mineral Admixtures

The most important mineral admixtures to the production of high-strength concrete are pozzolans. The two pozzolans most commonly used in high-strength concrete are fly ash and silica fume. However, especially in Canada, ground granulated blast-furnace slag has been used more recently instead of silica fume. Ground slag for use in concrete should conform to section C989 of the ASTM (1997), specification for ground granulated blast-furnace slag for use in concrete and mortar.

Fly ash is produced as a by-product of the combustion of pulverized coal in electric power generating plant. This material is used to amend insufficiencies in a concrete mix by providing missing fines from the fine aggregate. Using fly ash type F to the mix can improve qualities of concrete such as reducing permeability, expansion, and

the cost of concrete-making materials. Unfortunately, the properties of fly ash can vary greatly because of the wide range of composition of coals. Considering the acceptance and uniformity, tests should made according to section C618 of the ASTM (1997), specification for fly ash and raw or calsined natural pozzolan for use as a mineral admixture in portland cement concrete.

Silica fume is a new pozzolanic material that has received considerable attention in both research and application. This material is a by-product resulting from high-purity quartz with coal in the electric arc furnace in the production of silicon and ferrosilicon alloys. Unlike fly ash, silica fume is extremely fine. Most of particles are less than 1μm, and the average particle diameter is about 0.1 μm with surface area of about 20,000 m^2/kg. For comparison, fly ash surface area typically ranges from 300 to 500 m^2/kg, ground slag from about 400 to 600 m^2/kg, and type I cement from 300 to 400 m^2/kg.

Aitcin and Neville (1993) reported that the addition of silica fume to the mix increases the cohesiveness, viscosity, and water demand of fresh concrete. In hardened concrete, the addition of silica fume can produce significant increase in strength, modulus of elasticity, and flexural strength. The use of silica fume should conform to section C1240 of the ASTM (1997), specification for silica fume for use in hydraulic-cement concrete and mortar.

2.1.2.3.2. Chemical Admixtures

The benefits to be realized from use of admixtures in high-strength concrete have practically mandated their use. These admixtures increase the workability and enable reducing the cement content in proportion to the reduction in water content. A common

practice is to use a water-reducing admixture (superplasticizer) in combination with a water-reducing retarder.

The type of sulphonated naphthalene formaldehyde superplasticizer normally used reduces the amount of water required by 15-40%. However, using this superplasticizer often results in high rate of slump loss, making it difficult to place the concrete properly. The high rate of slump loss will be overcome by the addition of the water-reducing retarder which extends the time of set and permits the placement of a very low water-cement ratio concrete.

The compatibility of the admixtures with the choice of cement is a very important consideration. In order to reduce any undesirable effects in concrete, all chemical admixtures should meet the requirements of section C494 of the ASTM (1997), specifications for chemical admixtures for concrete. The use of retarder should be conformed to section C494 type B and D of the ASTM (1997), while the use of superplasticizer should be conformed to section C494 type F of the ASTM (1997).

2.1.3. Batching and Mixing Sequences

The incorporation of silica fume and high-range water reducers makes it possible to attain high-strength concrete at early ages. The following batching and mixing procedure has been developed by earlier researchers in the concrete laboratory of the Memorial University of Newfoundland for the production of workable high-strength mix.

(1) Charge 100% of coarse aggregates,

(2) Batch 100% of cement,

(3) Batch 100% of fly ash,

(4) Batch 100% of sand,

(5) Mix for 3-5 minutes after adding 50% the estimated water with water reducing agent,

(6) Prepare a slurry of silica fume, together with 25% of gross superplasticizer dose and 20% of water,

(7) Mix for 5 minutes,

(8) Add 30% of mixing water together with air entraining admixtures,

(9) Retemper with the rest of superplasticizer dose to target slump.

Flowing concrete was generally achieved using those mixtures including superplasticizer and retarder. The air content in the majority of the mixtures lies within 3% to 5%. Slump values were loosely at the 100-mm target, while an average value of the unit weight of fresh concrete was 2400 kg/m^3.

2.2. Punching Shear Strength

Respective suggested approaches can be represented as either the result of an empirical study or a rational study to establish a relationship between the load and stress at failure of concrete plates. The empirical study used a statistical analysis of the available test results, while the rational study described and idealized mathematically the mechanism of failure.

In the case of empirical studies, Forsell and Holemberg (1946) described that the critical section located at a distance $h/2$ from the loaded area. It has also been reported that the shear stress distribution over the slab thickness is assumed parabolic,

$$v = \frac{V}{4(c + \frac{h}{2})h} \tag{2.1}$$

where v is the ultimate shear stress, V is the ultimate shear force, c is the side dimension of a square column, and h is the effective depth of the slab.

Moe (1961) conducted an experimental investigation to analysis of shear strength where shear and flexure were considered as a combined loading problem. Moe stated that the critical section of a slab subjected to a concentrated load was located at the column perimeter and that the shear strength is to some extent dependent upon the flexural strength. Based on the experimental program, a semi-empirical type of equation was developed to calculate the ultimate shear strength,

$$v_u = \frac{V_u}{cd} = \frac{15\left(1 - \frac{0.075}{d}\right)\sqrt{f_c'}}{1 + \frac{5.25bd\sqrt{f_c'}}{V_{flex}}} \qquad (2.2)$$

where, v_u = ultimate shear stress

V_u = ultimate shear force

V_{flex} = ultimate load for flexural failure

b = side dimension of square loaded area

c = periphery around the column excluding openings

d = effective depth of the slab

f_c' = compressive strength of concrete

It was suggested that Equation (2.2) was the best equation to date for prediction of the failure load in the report of ACI-ASCE committee 316 (1962). The Committee recommended that the following design equation for calculating ultimate shear load,

$$V = vbd \qquad (2.3)$$

where b take as the perimeter at a distance of $d/2$ from the periphery of loaded area, and $v \leq 4.0\sqrt{f_c'}$, f_c' is the concrete compressive strength, and d is the effective depth of the slab.

The shear design methods of ACI-318 Building Code (1995) and CSA A23.3-94 (1994) are based on the developed in the most part on the work Moe (1961). The ratio of the ultimate shearing capacity of the slab to the ultimate flexural capacity of the slab is defined as $\Phi_o = \frac{V_u}{V_{flex}}$, the following empirical expression was developed from Equation (2.2) for the prediction of the ultimate shear stress:

$$v_u = \left(15\left(1 - 0.075\,\frac{b}{d}\right) - 5.25\Phi_o\right)\sqrt{f_c'} \qquad (2.4)$$

The development of design approaches of the British Codes, BS 8110 (1985), and is based primarily on the work of Regan (1981). An equation was developed to calculate punching shear capacity as:

$$V_u = K_a\,K_{sc}\sqrt[3]{\frac{100\,A_s}{bd}\,f_{cu}}\,(2.69\,d)\left(\sum C + 7.85\,d\right) \qquad (2.5)$$

where, V_u = ultimate shear force

K_a = 0.13 for normal concrete and 0.105 for lightweight concrete

K_{sc} = 1.15 [4 π (column area) / (column perimeter)^2]$^{1/2}$

$\frac{100\,A_s}{b\,d}$ = steel ratio

f_{cu} = cube strength of concrete

d = effective depth of the slab

$\sum C$ = perimeter of the column

The shear perimeter for a rectangle column is located at distance 1.25 d out from the column, for a circular column is located 1.25 d out from the column.

Marzouk and Hussein (1991) investigated the structural behavior of normal-strength and high-strength concrete slabs with respect to punching resistance. The result showed that high-strength concrete exhibits a more brittle failure than normal-strength concrete. The researchers have also indicated that the Moe's Equation (2.4) cannot be recommended to predict the punching shear capacity of high-strength concrete slabs. The punching resistance is proportional to the cubic root of concrete compressive strength. Therefore, the assumption of the British codes is better than the use of square root of the concrete strength as given in the present North American codes such as ACI-318 (1995) and CSA A23.3-94 (1994).

Gardner and Shao (1996) confirmed the use of cubic root of compressive strength using their experimental results regarding the punching shear of a two-way flat reinforced concrete slab. An empirical method using a shear perimeter around the loaded area was presented. The empirical recommended equation was expressed as follows:

$$v_u = \frac{V_u}{u\,d} < v_c = 0.79\left[1 + \left(\frac{200}{d}\right)^{0.5} (\rho f_y)^{1/3} (f_{cm})^{1/3} \left(\frac{d}{u}\right)^{0.5}\right] \qquad (2.6)$$

where, v_u = ultimate shear stress

v_c = nominal shear stress

V_u = ultimate shear force

u = perimeter of loaded area

d = effective depth of the slab

ρ = flexural steel reinforcement ratio, calculated over width $c + 6d$

f_y = yield strength of flexural steel

f_{cm} = mean concrete strength

2.3. Impact Performance of Concrete Plates

2.3.1. Overview of Material Modeling

CEB (1988) report No. 187, recommended that generally the mechanical behavior of the concrete material is described by a stress-strain relationship:

$$\sigma = f(\varepsilon) \tag{2.7}$$

taking strain rate into account leads to:

$$\sigma = f(\varepsilon, \dot{\varepsilon}) \tag{2.8}$$

where the strain rate is defined as:

$$\dot{\varepsilon} = \frac{d\varepsilon}{dt} \tag{2.9}$$

and it expresses the variation of strain with time.

More recently, several investigations have revealed that also the loading history should be taken into account:

$$\sigma = f(\varepsilon, \dot{\varepsilon}, \textit{load history}) \tag{2.10}$$

It is obvious that material models covering the relation in Equation (2.10) are much more complicated than those for Equation (2.7). In this sense, a broad varieties of different material models exist which may be grouped into the main categories of elasticity theory, plasticity, viscoplasticity, etc.

The different theories applicable to the modeling of concrete and steel reinforcement will be discussed briefly according to CEB (1988) report No. 187 as follows:

(1) Linear and non-linear elastic models

Linear elastic models are best known due to their simplicity, but as impact loading in general cause non-linear deformation it is not suited for any application in this field. The same may be stated for non-linear elastic models.

(2) Viscoelastic models

Models based on viscoelasticity have been used for the description of creep and relaxation phenomena. A few authors have used this theory with the idea that similarity between creep and strain-rate-effects should exist.

(3) Viscoplastic models

Models based on the theory of viscoplasticity have been used for many years also for the description of impact problem. The theory of viscoplasticity is very convenient especially for the modeling of the reinforcing steel, and may be simplified to a vast extent at least for the one-dimensional case.

(4) Models based on plasticity

Models based on the theory of plasticity can be arranged into two categories such as:

(a) Elastic-perfectly plastic material behavior

The material shows elastic behavior up to a certain level, for example compressive strength where strain is increased at constant stress. The influence of stress rate can be taken into account by increasing the yield level according to this stress rate.

(b) Elastic plastic behavior with hardening

Instead of undergoing unlimited deformation at a constant stress level, the stresses increase with increasing strain. Rate effects upon the yield surface are introduced, for example in the form of rate hardening parameters.

(5) Endochronic models

Models based on endochronic theory have been developed for concrete and reinforcing steel. Originally the endochronic theory was based on the viscoplastic theory, supplemented by a new internal variable, the intrinsic time. Although the endochronic theory was the subject of controversial discussions, it seems that some phenomena, like the influence of the loading history upon the stress-strain relationship and the strain-rate dependancy, are very well represented. For reinforcing steel this model is adequate, but for concrete, the problem of dilatancy at high strain is not solved yet.

(6) Fracture mechanics models

Fracture mechanics has to be subdivided into a linear and a non-linear theory. The linear theory provides a good basis to predict unstable or catastrophic propagation. Relations exist between fracturing stress, crack length, and strain rate. Linear fracture mechanics does not take any plastic deformation or micro-cracking in the region of the crack tip into account. However, as concrete and ductile steel are concerned, this must be included because of the fact that the energy consumed in the plastic or micro-cracked process zone is more relevant than the elastic part.

(7) Damage mechanics models

Models based on damage theory are relatively recent, especially on concrete. The method is based on the idea that damage occurs as an irreversible degradation of the material under deformation. A damage parameter is introduced as a scalar or vectorial function of this degradation process. The degradation process is a continuous and global process and does not consider only degradation within a default like the fracture mechanics concept.

(8) Stochastic models

The fracture process within the matrix of concrete is formulated using stochastic formulation. Concrete is modelled as a group of coupled elements with two or three different phases. A logarithmic relation between the resistance of concrete and stress or strain rate can be formulated.

2.3.2. Strain Rate for Various Types of Loading

In recent years, respectable attention has been given to the influence of strain rate or stress rate on the mechanical properties of concrete, reinforcing steel, and pre-stressing steel. Steel and concrete will be treated in two subsequent sections. The presentation of the data will be such that a design engineer can use such parameters in simple hand calculations and in a limited manner also in advanced computer codes. The properties will be given in graphs and or in functional form with respect to strain or stress rate.

Table 2.1 gives some global estimates of strain rates which occur during various types of loading. As reported in CEB (1988) report No. 187, these values are not expert estimates and have to be determined more exactly for specific structures and loading

configurations. On the other hand, it will be shown that most relations between strength and strain rate, or ultimate strain and strain rate, are linear-logarithmic or double logarithmic which means that exact accuracy is not necessary. With regard to the second remark, there is no mechanical property which decreases its value at higher strain rates.

Table 2.1. Typical strain rates for various types of loading

Type of Loading	Strain Rate (s^{-1})
Traffic	10^{-6} - 10^{-4}
Gas explosions	5.10^{-5} - 5.10^{-4}
Earthquake	5.10^{-3} - 5.10^{-1}
Pile driving	10^{-2} - 10^{0}
Air plane impact	5.10^{-2} - 2.10^{0}
Hard impact	10^{0} - 5.10^{1}
Hypervelocity impact	10^{2} - 10^{6}

2.3.3. Properties of Concrete under Dynamic Loading

A proceeding of the international symposium released in Germany, BAM (1982), reported that the most of the dynamic loading research were confined to plain concrete with normal-weight natural aggregates. The mechanical properties which were investigated include the compressive and tensile strength, ultimate strain at compressive and tensile strength, Young's modulus, biaxial strength, and fracture energy at tensile

loading. Some of these properties are well established as a function of stress or strain rate, defined as stress or strain increase in time, others are much less investigated.

Unfortunately, not all of research papers on this subject contain the information required to relate high stress rate tests to standard static test. This information is very important to give enough details in order to judge the validity of the results and the range of application. However, an attempt was made to examine the reported result to derive more relations.

Since most investigations at high strain rates were intended to determine the strength of material, data on ultimate strain are rather limited. Furthermore, data are sometimes not complete in the sense that static references are not given. That makes comparison dependent on assumptions that are based on general knowledge. Although these relations, for strain, are weaker than the strength relations they may still be useful.

2.3.3.1. Compressive Strength

A bulletin synthesis report on concrete structure under impact and impulsive loading was published by Comite Euro-International du Beton, CEB (1988), stated that the static testing rate was taken as $\dot{\sigma}_o$ = 1 MPa/s. Stress rate is converted into strain rate by assuming elastic material behavior with a modulus of elasticity of E_c = 33000 MPa. The strength relationship started at unity for static testing and reached a value of about 2 for low grade concrete, and about 1.4 for high grade concrete, when loaded more rapidly at a rate of $\dot{\sigma}_o = 10^6$ MPa/s. Beyond this stress rates the increase higher reaching values of four and greater. It should be noted, however, that this steep increase has been determined theoretically and that experimental evidence is only attainable for natural

rocks. Malvern, et al. (1985) reported that recent experimental results for concrete have not fully confirmed this prediction.

Ammann and Nussbaumer (1995) described that the compressive strength of concrete can be written in terms of strain rate as:

$$\frac{f_{imp}}{f_{stat}} = \left(\frac{\dot{\varepsilon}}{\dot{\varepsilon}_o}\right)^{1.026\alpha} \quad with\ \alpha = \frac{1}{5 + 0.75 f_c'} \quad for\ \dot{\varepsilon} \leq 30\ s^{-1} \tag{2.11}$$

where, $\dot{\varepsilon}$ = strain rate

$\dot{\varepsilon}_o$ = strain rate at quasi static condition

f_c' = static cube strength of concrete

This relationship reveals that the influence of loading rate decreases as the grade of concrete increases. If the influence of the loading rate on the modulus were not considered, the power of the equation above would be 1.0 α where α is the dynamic material property as defined in Equation (2.11).

2.3.3.2. Modulus of Elasticity

The modulus of elasticity (Young's modulus) of the concrete in compression increases with stress and strain rate. The relation between static and dynamic (impact) modulus of elasticity is given by Ammann and Nussbaumer (1995) in the following equation:

$$\frac{E_{imp}}{E_{stat}} = \left(\frac{\dot{\sigma}}{\dot{\sigma}_o}\right)^{0.025} \quad \text{with} \quad \dot{\sigma}_o = 1\ \text{MPa/s} \tag{2.12}$$

or

$$\frac{E_{imp}}{E_{stat}} = \left(\frac{\dot{\varepsilon}}{\dot{\varepsilon}_o}\right)^{0.025} \quad with\ \dot{\varepsilon}_o = 30.10^{-6}\ s^{-1} \tag{2.13}$$

where, $\dot{\sigma}$ = stress rate or variation of stress with time, or

$$\dot{\sigma} = \frac{d\sigma}{dt}$$

$\dot{\sigma}_o$ = stress rate at quasi static condition.

$\dot{\varepsilon}$ = strain rate

$\dot{\varepsilon}_o$ = strain rate at quasi static condition

2.3.3.3. Ultimate Strain

The ultimate strain in compression is the strain that occurs at maximum stress. The ultimate strain as a function of strain rate given by Ammann and Nussbaumer (1995) is:

$$\frac{\varepsilon_{u,\,imp}}{\varepsilon_{u,\,stat}} = \left(\frac{\dot{\sigma}}{\dot{\sigma}_o}\right)^{0.020} \quad with\ \dot{\sigma}_o = 1\ \text{MPa/s} \tag{2.14}$$

and

$$\frac{\varepsilon_{u,imp}}{\varepsilon_{u,stat}} = \left(\frac{\dot{\varepsilon}}{\dot{\varepsilon}_o}\right)^{0.020} \quad with\ \dot{\varepsilon}_o = 30.10^{-6}\ s^{-1} \tag{2.15}$$

2.3.3.4. Compressive Fracture Energy

The fracture energy is usually defined as the area under the complete stress-strain curve multiplied by the appropriate volume element. Whereas numerous results were available for static loading, there was no complete stress-strain curve available for high strain rates of compression loading. However, from the occurrence of higher strength and ultimate strain together with evidence of enhanced cracking, it may be concluded that the fracture energy increases with increasing stress rate and strain rate.

2.3.3.5. Tensile Loading

Ammann and Nussbaumer (1995) have also described the properties of concrete under tensile loading. In contrast to compressive failure, tensile failure is always a discrete phenomenon. Usually one crack occurs which divides a specimen into two parts. These two parts would unload as the crack width increases. Energy consumption occurs in the cracking zone. The relationships between a mechanical property and the stress or strain rate are similar to those obtained. The formulation is also similar to compressive strength except for the value of the coefficient.

Taking account again of the influence of strain rate on modulus of elasticity, a relation can be defined between strain rate and tensile strength in the following.

$$\frac{f_{imp}}{f_{stat}} = \left(\frac{\dot{\varepsilon}}{\dot{\varepsilon}_o}\right)^{1.016\delta} \quad with\ \delta = \frac{1}{10 + 0.5 f_c^{\cdot}} \quad for\ \dot{\varepsilon} \le 30\ s^{-1} \tag{2.16}$$

where $f_c^{\cdot}$ is static cube strength of concrete.

Tensile strength is more sensitive to strain or stress rate if the concrete has a low grade and is more sensitive to strain rate than compressive strength. Usually compressive strength is the reference value for the concrete grade and is therefore known. The tensile strength can be estimated from:

$$f_t = 0.20(f_c^{\cdot})^{2/3} \text{ MPa} \tag{2.17}$$

These values of concrete strength have also been recommended by CEB-FIP (1990).

2.3.3.6. Tension Modulus of Elasticity

The influence of stress rate on modulus of elasticity for tension is smaller than for compression. The formulation presented by Ammann and Nussbaumer (1995) such as:

$$\frac{E_{imp}}{E_{stat}} = \left(\frac{\dot{\sigma}}{\dot{\sigma}_o}\right)^{0.016} \quad with\ \dot{\sigma}_o = 0.1\ \text{MPa/s} \tag{2.18}$$

or

$$\frac{E_{imp}}{E_{stat}} = \left(\frac{\dot{\varepsilon}}{\dot{\varepsilon}_o}\right)^{0.016} \quad with\ \dot{\varepsilon}_o = 3.10^{-6}\ s^{-1} \tag{2.19}$$

are valid for all stress and strain rates, and all concrete grade.

The definition of strain in a tensile experiment only makes sense up to the moment where a discrete crack starts to open, i.e., until the maximum stress is reached. Beyond this point, the cracks open and the remaining undamaged part of the concrete unloads. Ultimate strain is just the strain at maximum stress. Few experiments are available which allow one to establish a relation between strain and the stress or strain rate. This relation is also given by Ammann and Nussbaumer (1995) such as:

$$\frac{\varepsilon_{u,\,imp}}{\varepsilon_{u,\,stat}} = \left(\frac{\dot{\sigma}}{\dot{\sigma}_o}\right)^{0.020} \quad with\ \dot{\sigma}_o = 0.1\ \text{MPa/s} \tag{2.20}$$

and

$$\frac{\varepsilon_{u,imp}}{\varepsilon_{u,stat}} = \left(\frac{\dot{\varepsilon}}{\dot{\varepsilon}_o}\right)^{0.020} \quad with\ \dot{\varepsilon}_o = 3.10^{-6}\ s^{-1} \tag{2.21}$$

These relationships are valid for all stress rates, strain rates, and concrete grade.

2.3.3.7. Tensile Fracture Energy

The fracture energy is defined as area under the stress-crack opening curve multiplied by the cross-sectional area of the specimen. The post-cracked behavior was treated with a brittle fracture concept proposed by Hillerborg (1985). The value can be calculated from

integrating the complete tensile stress-crack opening displacement or crack width such as follow:

$$G_f = \int_0^{w_o} f_t \, dw \tag{2.22}$$

where, G_f = fracture energy required to form an unit area of crack surface

f_t = tensile stress, as a function of w

w = crack width

w_o = crack width when f_t reaches zero.

More common in the description of engineering material, the expression for G_f can be arranged and expressed as a function of a stress-strain law. Thus, W_f is defined as the fracture energy density, or work per unit volume, dissipated by cracking, can be expressed as:

$$W_f = \frac{G_f}{w_c} = \int_0^{\varepsilon_{max}} f_t \, d\varepsilon_t \tag{2.23}$$

where, f_t = tensile stress expressed in terms of tensile strain

w_c = width of the fracture process zone

ε_t = tensile strain

ε_{max} = maximum tensile strain when f_t reaches zero at the end of the tension softening branch.

As reported by Marzouk and Chen (1995), the fracture energy of high-strength concrete is about five times the area under ascending portion of its complete stress-strain curve. Fracture energy is estimated about ten times the area under ascending portion of its complete stress-strain curve for normal-strength concrete as reported by Massicotte, Elwi,

and MacGregor (1990). This indicates that the high-strength concrete is more brittle in tension than normal-strength concrete.

CEB (1988) stated that the relation between fracture energy under static and dynamic (impact) loading is expressed by the following equation:

$$\frac{G_{tot,imp}}{G_{tot,stat}} = \left(\frac{\dot{w}}{\dot{w}_o} \right)^{0.045} \tag{2.24}$$

where, $\dot{w}$ = the crack opening velocity

$\dot{w}_o = 10^{-3}\ mm/s$.

2.3.4. Impact Resistance of Reinforced High Strength Concrete Slabs

2.3.4.1. Design Practice

In order to evaluate the damage due to impact caused by missile, fragments or dropped objects on reinforced concrete plates, different models are used in the design practice. These different models can be represented in the following:

(a) Determination of impact loads based on energy principles and penetration estimates. The impact loads are then to be compared with the punching shear capacity and the flexure capacity according to the yield line theory.

(b) CEB (1988) stated the determination of impact velocity to avoid scabbing based on empirical scabbing limits

(c) CEB (1988) has also represented the calculation of the critical impact velocity concerning perforation. This calculation is based on empirical data. The real impact velocity has to be compared with the critical velocity.

Jensen, Hoiseth, and Hansen (1993) concluded that the essential element in the first method is the ductility and the punching shear capacity of high-strength concrete under impact and impulsive loading. The validity of the two other methods are limited to certain missile velocities and concrete types, therefore the methods have to be verified. An experimental investigation on the capacity of reinforced high-strength concrete slabs under impact loading is recommended. The results may provide verification of analytical methods as well as design recommendations.

Banthia, Mindess, and Trottier (1996) conducted an experimental impact resistance of steel fiber reinforced concrete using a simple instrument impact machine designed to test concrete in uniaxial tension. It has been reported that fiber reinforcement is sensitive material to stress rate and is effective in improving fracture energy absorption under impact. While, Banthia, Yan, and Sakai (1998) studied the impact resistance of concrete plates reinforced with a fiber reinforced plastic grid. The plates reinforced with fiber reinforced plastic were found to fail in a brittle manner and absorb only a third of the energy absorbed by those reinforced with a traditional steel grid. It has also been reported that the most improvements in the impact performance occur with the use of fiber reinforced concrete. Improvements occur in both the ultimate load carrying capacity and the energy absorption capability.

Barr et al. (1982) studied the applicability of replica scaling to the dynamic behavior of reinforced concrete slabs impacted by rigid missiles. Experimental results were presented for models with relative linear scales of 1, 0.37, and 0.12. It has been found that the rear faces of all 3 scales of target showed very similar damage and cracking. A slight tendency of more rear face damage and more concrete stripping

occurred in the bigger target case than in the smaller targets. The general shapes of perforation craters were also similar on all 3 sizes of target. It has been concluded that the use of scale models, over the size range tested, to provide data on the perforation performance of reinforced concrete are justified.

2.3.4.2. European Design Codes for Punching Shear Capacity and Critical Perforation Velocity

The static punching shear capacity as specified in the Norwegian Code is expressed as follows:

$$V_{cd} = 0.33\left(f_{td} + \frac{k_A \rho}{\gamma_c} \right) u\, d\, k_v \leq 0.66\, f_{td}\, u\, d\, k_v \qquad (2.25)$$

where, f_{td} = design tensile strength of concrete

γ_c = material coefficient for reinforced

k_A = 100 N/mm^2

$1.0 < k_v\,(= 1.5d/d_1) < 1.4$, d_1 = 1.0 m

d = mean slab depth in the two reinforcement directions

u = length of perimeter of the governing section at a distance 1.0 d from the loaded area

ρ = geometrical mean of the orthogonal tension reinforcement ratio.

The upper value of the design punching shear capacity is limited by compressive failure. However, this limitation is not relevant in the case discussed here.

The critical velocity of perforation for the dynamic loading of a two-way plate as recommended by Committee Euro-International du Beton, CEB (1988) will be examined.

The critical velocity of perforation can be expressed as:

$$v_c = 1.3\, W^{1/6}\, f_{cy}^{1/2} \left(\frac{p h^2}{\pi M} \right)^{2/3} (\rho + 0.3)^{1/2} \qquad (2.26)$$

where, W = concrete density

f_{cy} = cylinder compressive strength

p = missile perimeter

h = concrete slab thickness

M = missile mass

ρ = reinforcement quantity.

Barr, et al. (1982) indicated that the crack pattern in the concrete target, as well as the transient displacement measurements, indicates that bending and shear failure mechanism were involved in concrete behavior. The researchers provided further justification for the suggestion that Equation (2.26) should be modified. An alternate bending reinforcement quantity dependent was included in the following:

$$v_c = 1.3\, W^{1/6}\, f_{cy}^{1/2} \left(\frac{d h^2}{m} \right)^{2/3} \rho^{0.27} \qquad (2.27)$$

where d is diameter of dropped object, h is concrete slab thickness, and m is mass of cylindrical dropped object.

Chapter 3

EXPERIMENTAL INVESTIGATION

3.1. Introduction

As a result of several advances in the manufacturing of chemical additives and material selection, it has been possible to produce high-strength concrete of 80 MPa and higher. The main objective of this experimental work, as discussed in the previous chapter, is to investigate the structural behavior of high-strength concrete two-way plates subjected to impact loading.

The experimental program consisted of testing and evaluation of the structural performance of sixteen plates. The details of test specimens and laboratory setup arrangements are described in the following section. The experimental test results will be compared with North American codes, ACI-318 (1995) and CSA-A23.3 (1994), Norwegian Standard NS-3473 (1992), British Code BS-8110 (1985), and European code CEB-FIP (1990) for predicting the shear strength. The experimental test results are presented in the following chapters.

3.2. Materials

3.2.1. Concrete

Ordinary Portland cement type 10, produced in Newfoundland, quartzite sandstone, and a crushed granite of 19 mm maximum nominal size were used for all test specimens. In order to produce high-strength concrete with low water cementitious ratio (w/c) of about 0.27, the following materials were added:

(1) Silica fume in a powder form in the ratio 8% of cement weight,

(2) Class F lignan fly ash from Nova Scotia in the ratio 12% of cement weight,

(3) Superplasticizer of sulfonated naphthaline formaldehyde base (Eucon 37),

(4) Retarder of polyhydroxycarboxylic base (TCDA type DX) supplied by Euclid Admixture Canada Inc.

The recommendation of the earlier investigation by Marzouk and Hussein (1990) was used for the mix proportion of selected materials. The mix proportions for 1 m^3 are given in Table 3.1 for normal-strength concrete and Table 3.2 for high-strength concrete. The mix was designed for a compressive-strength targets of 35 MPa for normal-strength and 80 MPa for high-strength concrete.

Table 3.1. Mix proportion for 1 m^3 of normal-strength concrete

Ingredients	Unit
Portland Cement	350 kg
Coarse Aggregates (granite 19-mm)	1160 kg
Fine Aggregates (graded sand)	690 kg
Water	175 liter

Table 3.2. Mix proportion for 1 m^3 of high-strength concrete

Ingredients	Unit
Portland Cement	400 kg
Silica Fume	40 kg
Fly Ash	60 kg
Coarse Aggregates (granite 19-mm)	1160 kg
Fine Aggregates (graded sand)	690 kg
Water	135 liter
W/cementitious materials ratio	0.27
Superplasticizer	7000 ml
Retarder	600 ml

3.2.2. Reinforcement

Grade 400 steel reinforcing with deformed rebars were used conforming to CSA standards. The steel reinforcements were obtained from one supplier. Two typical No. 10 M and No. 15 M bars were used as specimen reinforcement. The diameters of No. 10 M and No. 15 M bars are 11.3 mm and 16.0 mm, respectively, as detailed by the Canadian code. A 300 kips (1335 kN) Tinus Oslen hydraulic testing machine was used to test the tensile strength of the two samples of the reinforcing rebars. While, electrical strain gages were applied to determine the strain of the reinforcing rebars and LPDTs (Linear Potential Differential Transducers) were utilized to measure the specimen deformation up to the failure. The properties of the steel reinforcements are summarized in Table 3.3.

Table 3.3. Properties of steel reinforcement

Bar number	Diameter (mm)	Area (mm^2)	Yield strain ε_y	Mean yield stress f_y (MPa)	Mean ultimate stress (MPa)	Modulus Elasticity E_s (GPa)
No.10 M	11.3	100	0.00235	450	660	191
No.15 M	16.0	200	0.00225	435	670	193

3.3. Test Specimens

This study has been conducted on over 16 specimens. Two specimens were used at the beginning as a reference to establish the testing procedure, to check the instrumentation accuracy, to set the rate of loading and the rate of scanning data. The dimension for all test specimens were 950 mm square and 100 mm thick and several variables were considered in the investigation. The variables included the effect of concrete strength, support pattern, and reinforcement ratio. Details of the individual specimens and its variables are given in Table 3.4.

As given in the table, each specimen is identified in column two by three letters and one numeral. The first and second letters indicate the strength of concrete: HS indicates high-strength and NS indicates normal-strength. The third letter indicates the type of support pattern, where F indicates fixed and S indicates simply supported. The last numeral indicates the variable of the tension reinforcement ratio, where number 1 indicates reinforcement ratio of about 1%, 2 indicates 1.5%, 3 indicates 2% and 4 indicates 2.5%. A typical size of the tested specimen is given in Figure 3.1, and Figure 3.2 presents a typical reinforcements pattern on tension and compression faces.

Table 3.4. Details of test specimens

Series No:	Notation	Support Condition	fc' (MPa)	Reinforcement ρ (%)	Reinforcement ρ' (%)	Projectile's Velocities (m/s)
1	HSS1	Simply supported	81.7	1.0	0.68	7.00
2	HSS2	Simply supported	81.7	1.5	0.68	7.67
3	HSS3	Simply supported	81.7	2.0	0.74	8.29
4	HSS4	Simply supported	81.7	2.5	0.82	8.86
5	HSF1	Fixed	79.1	1.0	0.68	7.00
6	HSF2	Fixed	79.1	1.5	0.68	7.67
7	HSF3	Fixed	79.1	2.0	0.74	8.29
8	HSF4	Fixed	79.1	2.5	0.82	8.86
9	NSS1	Simply supported	33.1	1.0	0.68	5.42
10	NSS2	Simply supported	33.1	1.5	0.68	6.26
11	NSS3	Simply supported	33.1	2.0	0.74	7.00
12	NSS4	Simply supported	33.1	2.5	0.82	7.67
13	NSF1	Fixed	36.6	1.0	0.68	4.43
14	NSF2	Fixed	36.6	1.5	0.68	4.95
15	NSF3	Fixed	36.6	2.0	0.74	5.42
16	NSF4	Fixed	36.6	2.5	0.82	5.86

3.4. Fabrication of Specimens

3.4.1. Formwork

The formwork for the test specimens was fabricated in the concrete laboratory. The formwork consisted of four 960 x 960 mm decks made with 20 mm thickness plywood

with 100 mm height. The bottom of the form was made of steel plates. The form was constructed such that it can be disassembled and re-used. Before each casting, all of the steel plates and plywood surface were cleaned and coated with light mould oil. During casting, great care was also given to ensure that the four specimens provided were uniform.

3.4.2. Steel Reinforcement

The tension steel reinforcement at bottom face and the compression steel reinforcement at top face were arranged based on the design spacing. The tension steel reinforcement were supported on the compression steel reinforcement by 10-mm diameter spacers. The spacers also provided the concrete clear cover. The spacers were welded to the steel reinforcement at selected location to eliminate the effect of welding. The reinforcement cage was placed in the form, both the tension and compression steel reinforcement were tied together with steel wires. As shown in Figure 3.3, the steel reinforcement were placed in the form before casting

3.4.3. Mixing, Casting, and Curing

The capacity of concrete mixer was 0.1 m^3. The quantity was required to cast one specimen using one batch. Before concrete was placed, the formwork and the reinforcing rebars were thoroughly cleaned.

Figure 3.4 shows the pouring of fresh concrete from the batch to the formwork. Each concrete batch was poured into the formwork and then was vibrated using an electrical rod vibrator. The vibrator was applied to the whole plate to consolidate the

concrete and to ensure its consistency. When a full compaction was attained, the surface of the specimen was then leveled and finished with wooden and steel trowel. Four hours after casting, the surface of the specimens were cured under polyethylene sheets in the forms. This curing continued for a week by pouring water to its surface every 24 hours. The formwork for the specimen was stripped at an average age of one week after casting.

In order to determine the compressive strength f_c' of the specimens, three 150x300 mm concrete cylinders were taken from each batch according to the procedure of section C192 of the ASTM (1997). The test cylinders were subjected to the same curing conditions as the test specimens. The compressive strengths for the test cylinders were carried out of the 28 days of casting. A soil test 2670 kN machine was used to determine the concrete compressive strength. Figure 3.5. shows a specimen during compressive strength test.

3.5. Test Set-up

The specimens were simply-supported along the edge on a reinforced concrete frame with a free opening of 650x650-mm. In order to simulate a fixed-support, four steel plates were bolted to fix the upper face of the specimens. A special testing frame was designed including four concrete beams for supporting the specimen and steel beams to fix the edge of specimen as detailed in Figures 3.6 and 3.7. Figure 3.8 shows a specimen under fixed support.

The special testing frame was placed on a 2000x2000x200 mm concrete base. The concrete base was made in order to protect the basement laboratory floor. Figures 3.9 and

3.10 show the details of steel reinforcement of concrete base in bottom face and top face, respectively.

In order to ensure that the projectile strikes the specimen exactly at center and keep it in that place after hitting the specimens, a hollow steel cylinder was used to guide the flying projectile. The hollow steel cylinder was 6 mm thickness steel with 50 mm diameter and 1000 mm height. The steel cylinder was welded to the supported steel as part of the testing frame to provide a clear distance from the specimen surface. A photograph of the special test frame and the guide steel cylinder is shown in Figure 3.11.

3.6. Instrumentation System

3.6.1. Testing Load

Impact tests on the specimens were carried out after a minimum of 28 days from casting. The impact load was applied vertically to the test specimens using a drop rigid projectile. A solid steel cylinder was used as a projectile. The cylinder has a 220-kg mass and 304.5 mm diameter flat contact area, which can be dropped from variable heights of up to 4 m. The photographs in Figures 3.12 and 3.13 show the rigid projectile to be ready to be dropped for fixed and simply supported specimen, respectively. While, Figure 3.14 shows the rigid projectile was moving to hit against the tested specimen.

The stationary specimen is suddenly subjected to very high acceleration in the direction of the projectile when the rigid projectile dropping at a high speed strikes the specimen. An accelerometer was attached to the projectile. The accelerometer can read up to ± 200 g, where g is Earth's gravitational acceleration. Before each test, the accelerometer was calibrated. The calibration chart for the accelerometer was supplied by

the manufacturer. This accelerometer recorded the vertical acceleration of the projectile together with the plate. The impact velocity was then calculated.

3.6.2. Deflections

Deflection of the test specimen was measured during experimental by an external LPDT gage. Deflection was recorded at the center of the plate. The master panel recorded the deflection data, and the electrical strain gages reading were stored at the data acquisition system.

The voltage readings were converted to deflections using the LPDT calibration factor. The analog electrical signals came from the instruments were converted through the data acquisition board to digital signals and recorded in a digital computer files at sampling rate of 1000 Hz as well. The LPDT at the center of the tested specimen was placed in its position before securing the specimen in position as shown in Figure 3.15.

3.6.3. Strains

3.6.3.1. Steel Strains

In order to obtain the strain distribution at the cracking process zone, four electrical resistance steel strain gages with gage length of 10 mm were attached at different locations. The electrical resistance strain gages had a resistance of $120 \pm 0.3\%$ ohms and a gage factor of $2.04 \pm 0.5\%$ was used for calibration.

For protection against any possible water damage during concrete casting, the steel strain gages were coated with a protective sealant and then covered with a shrink

tube waxed at both ends. A typical locations of the steel strain gages on tension and compression faces are shown in Figure 3.16.

3.6.3.2. Concrete Strains

The concrete strains were measured on the compression face of the concrete plates by means of special concrete strain gages with gage length of 50 mm. The strain gages were glued using epoxy to the compression plate surface after it was ground and cleaned. The electrical concrete strain gages had a resistance of $120 \pm 0.3\%$ ohms and a gage factor of $2.04 \pm 0.5\%$.

The steel strain gages and concrete strain gages output together with accelerometer and deformation data were continuously scanned and recorded into data acquisition system. Figure 3.17 shows the location of measured concrete strain gages of compression face only.

3.7. Test Procedure

As mentioned before, the tests were carried out under a drop rigid projectile. The rigid projectile was a solid steel cylinder with 220-kg mass and 304.5 mm diameter flat contact area. The cylinder was dropped from variable heights up to 4 m. During impact testing, an accelerometer (± 200 g) was attached to the steel cylinder. The impact velocities were calculated while accelerometer recorded the vertical accelerations of the plate specimens.

Deflection at the center of specimen was measured with LPDT gage. As mentioned in the previous section, steel strain gages were used to record strains at four locations for each specimen, three gages on tension face and one gage on compression

face. Concrete strain was recorded on the compression surface only. Before conducting the test, the concrete specimen and the equipment were carefully inspected. Careful attention had also been given to the scrutiny of gages, wires and data acquisition system during testing.

A data acquisition system based on a personal computer at a sampling rate of 1000 Hz was used in this experiment. Labtech Notebook software was used for data acquisition and process control software was utilized. The data acquisition system has a build-time that enables to configure the set-up, and a run-time that controls the data acquisition and other function. This data acquisition system can be used to continuously monitor and record all types of process variables including voltage, strains, displacement, and accelerations at the scanning time of 1 micro-second.

There are two basic types of process control, open loop and closed loop. In an open loop controlling process, as used in this research, analog output blocks transmit waveforms to the control hardware during run-time operation. In closed loop control, the controlled system sends response data through the interface device to the run-time. The data output function uses this information to convert raw data from an interface device into appropriate scientific or engineering unit such as strain, displacement and acceleration. The data acquisition system used in this study is shown in Figure 3.18 and instrumentation block-diagram is given in Figure 3.18.

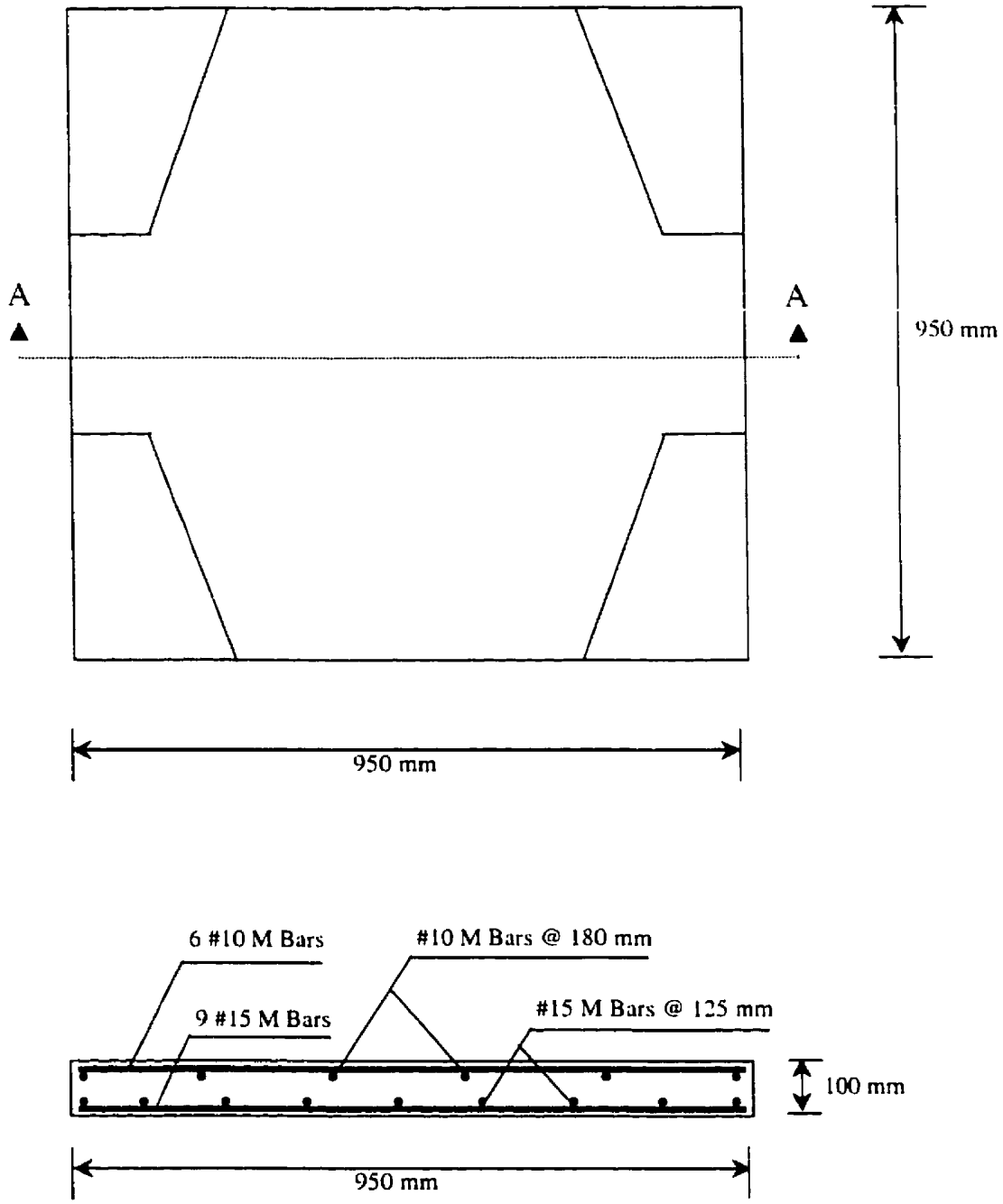

Figure 3.1. Cross section A-A of a typical specimen under fixed-support

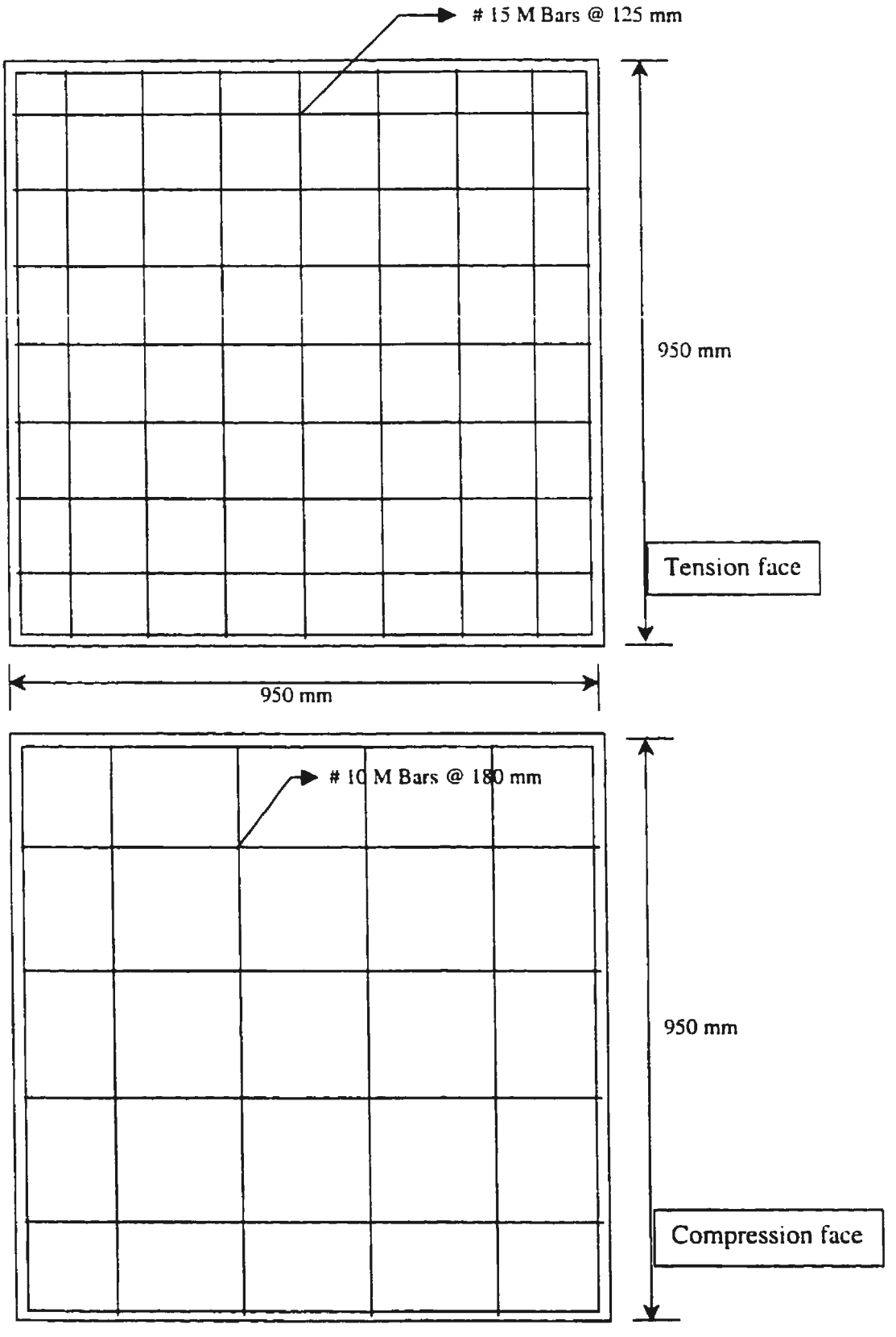

Figure 3.2. Typical steel reinforcement of a test specimen

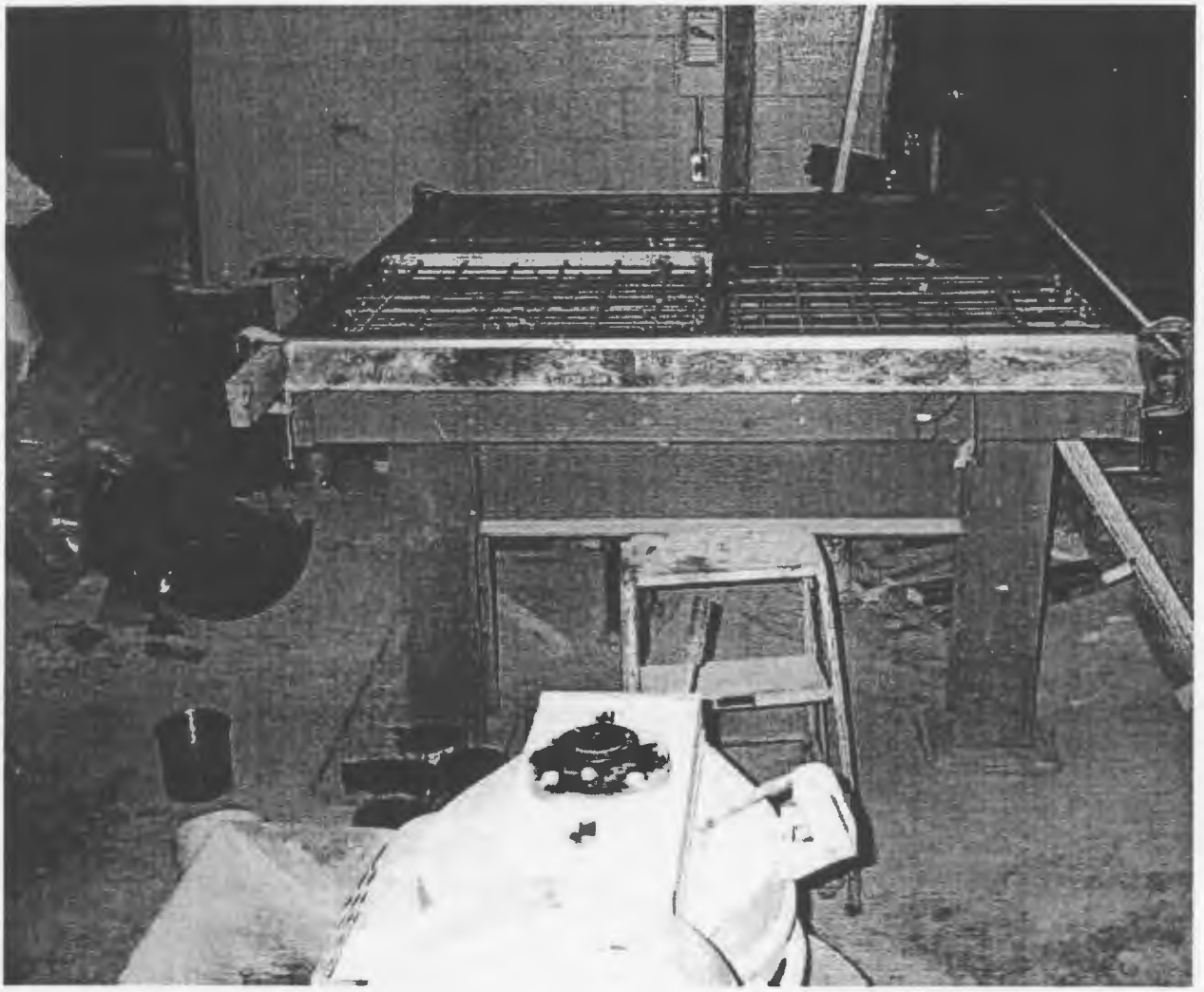

Figure 3.3. Arrangement of steel reinforcement rebars in the formwork before casting

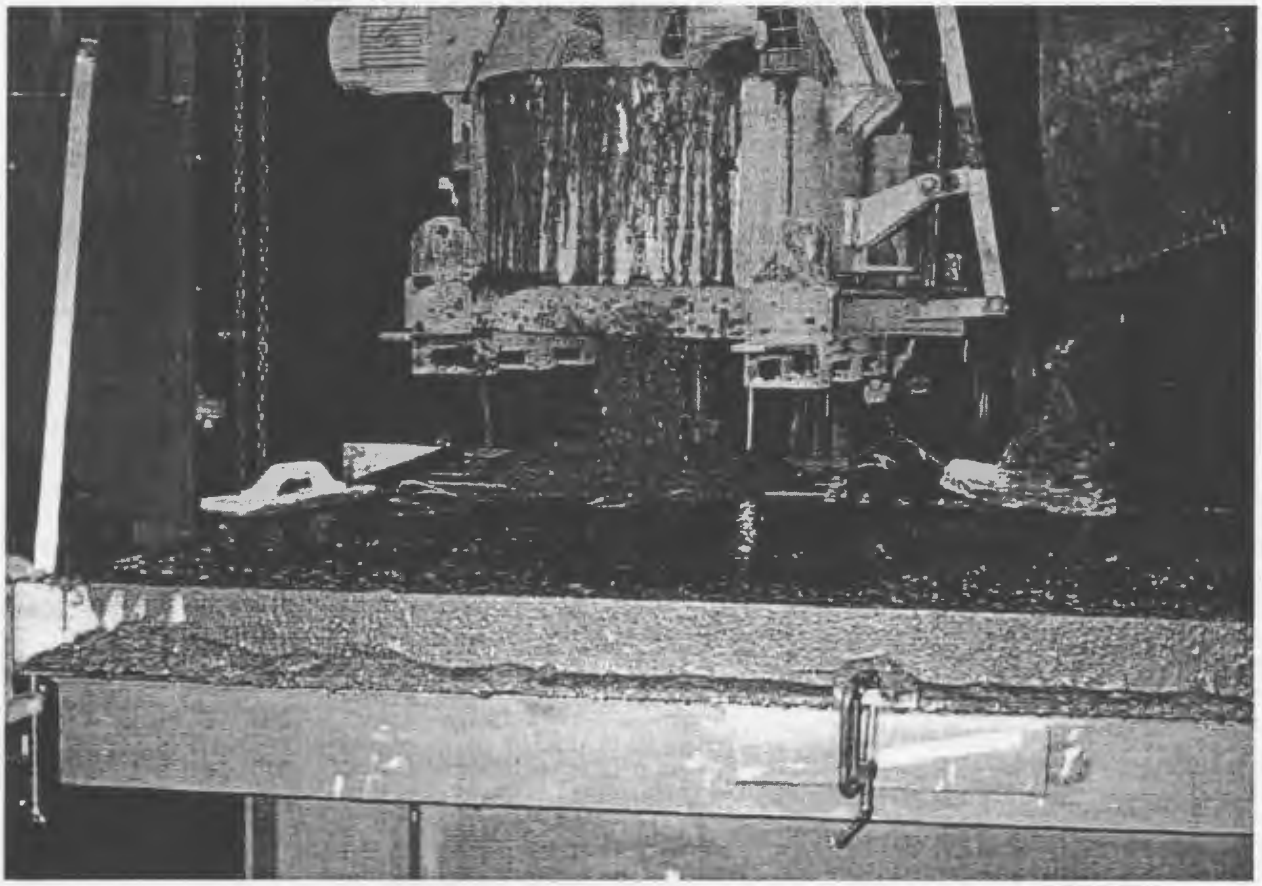

Figure 3.4. Casting of fresh concrete from the mixer to the formwork

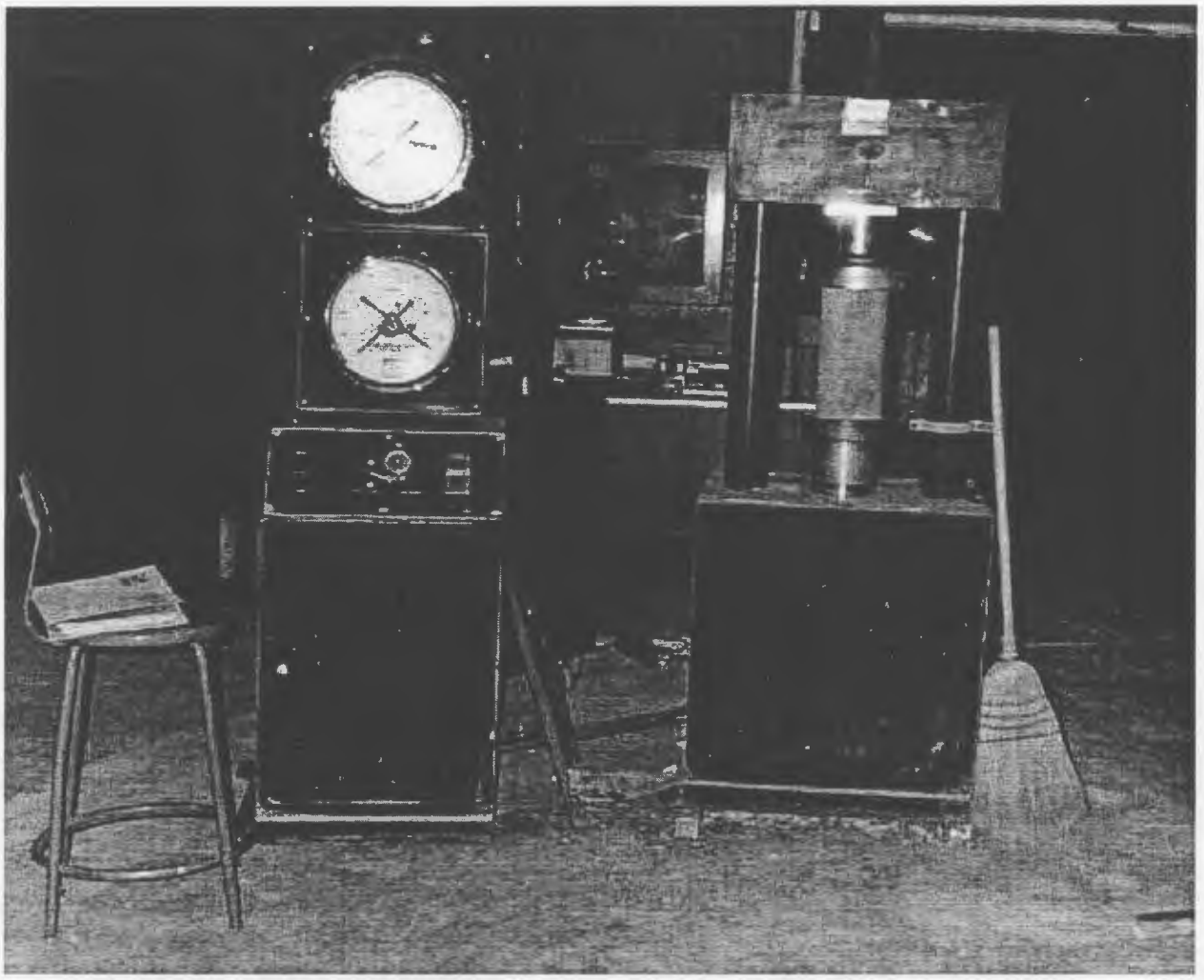

Figure 3.5. Compressive strength test of a concrete cylinder

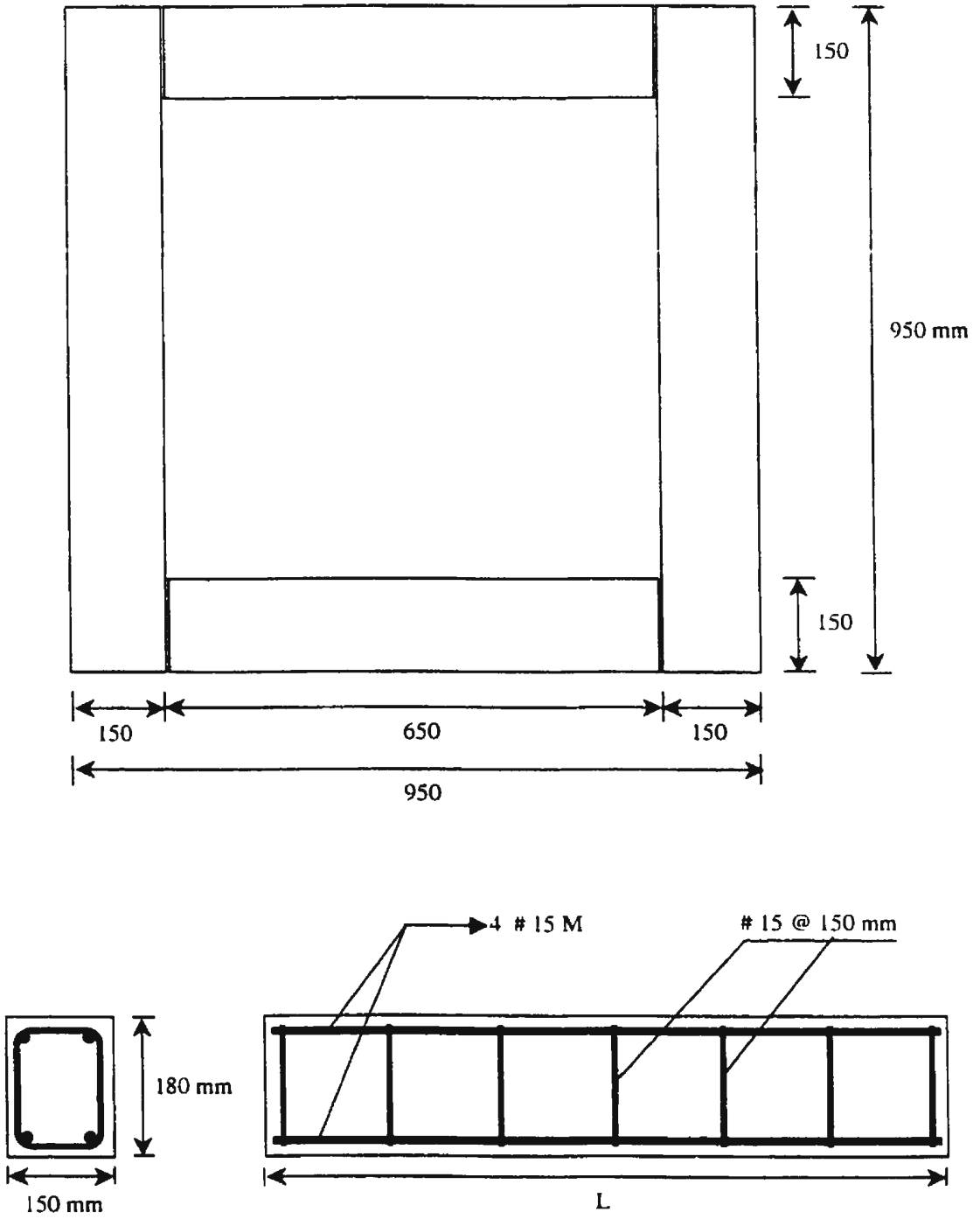

Note: - L has two values: 650 mm and 950 mm

Figure 3.6. Concrete beams of the test frame

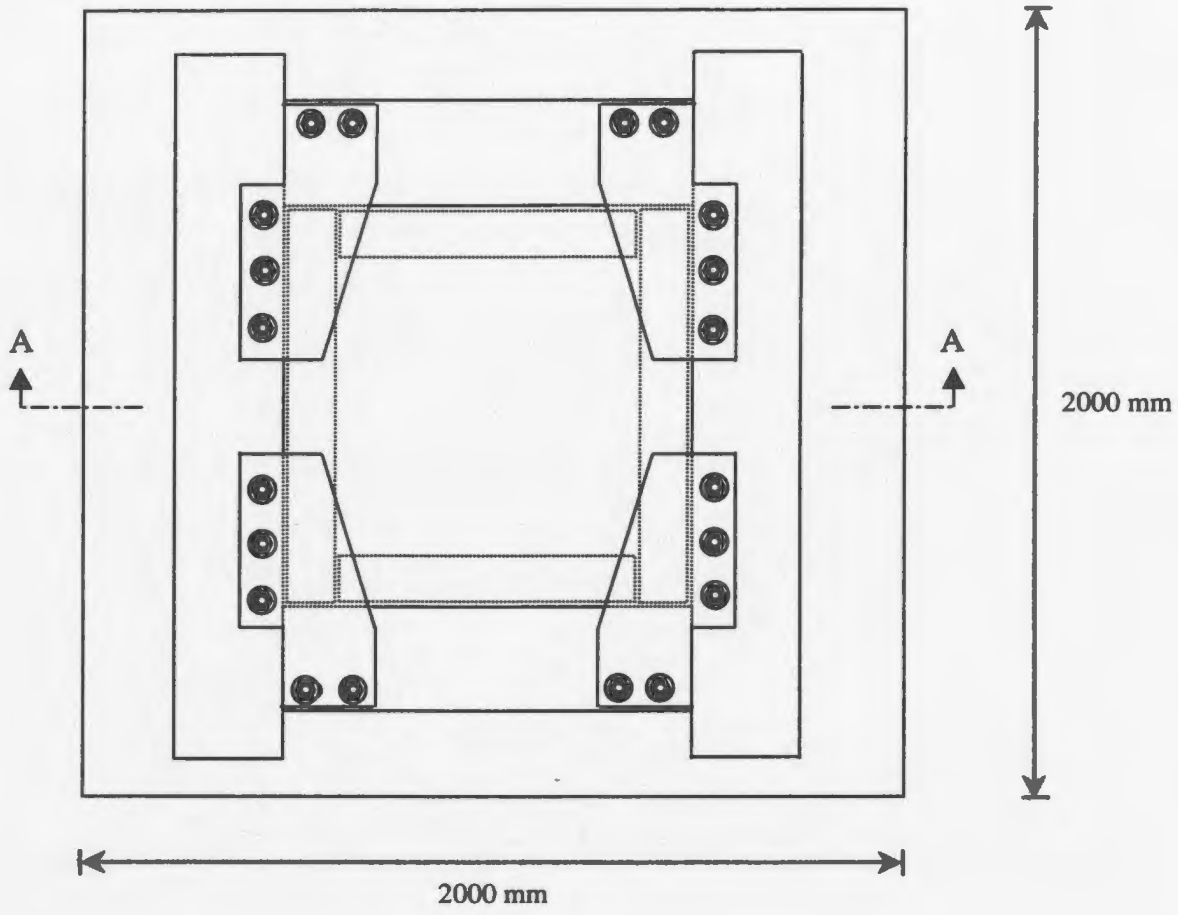

Section A – A :

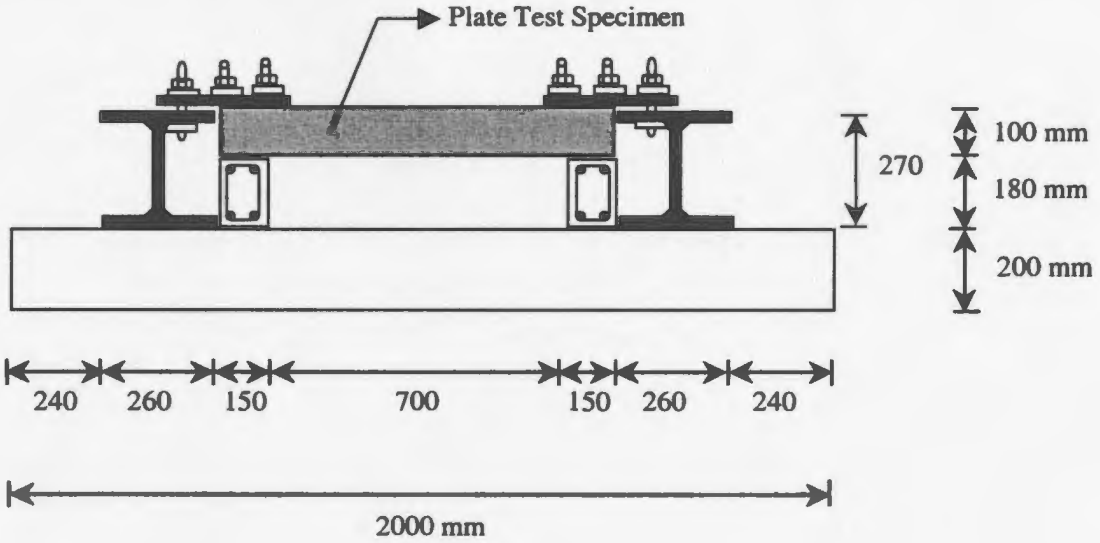

Figure 3.7. Concrete and steel beams for fixed-support

Figure 3.8. Specimen under fixed support

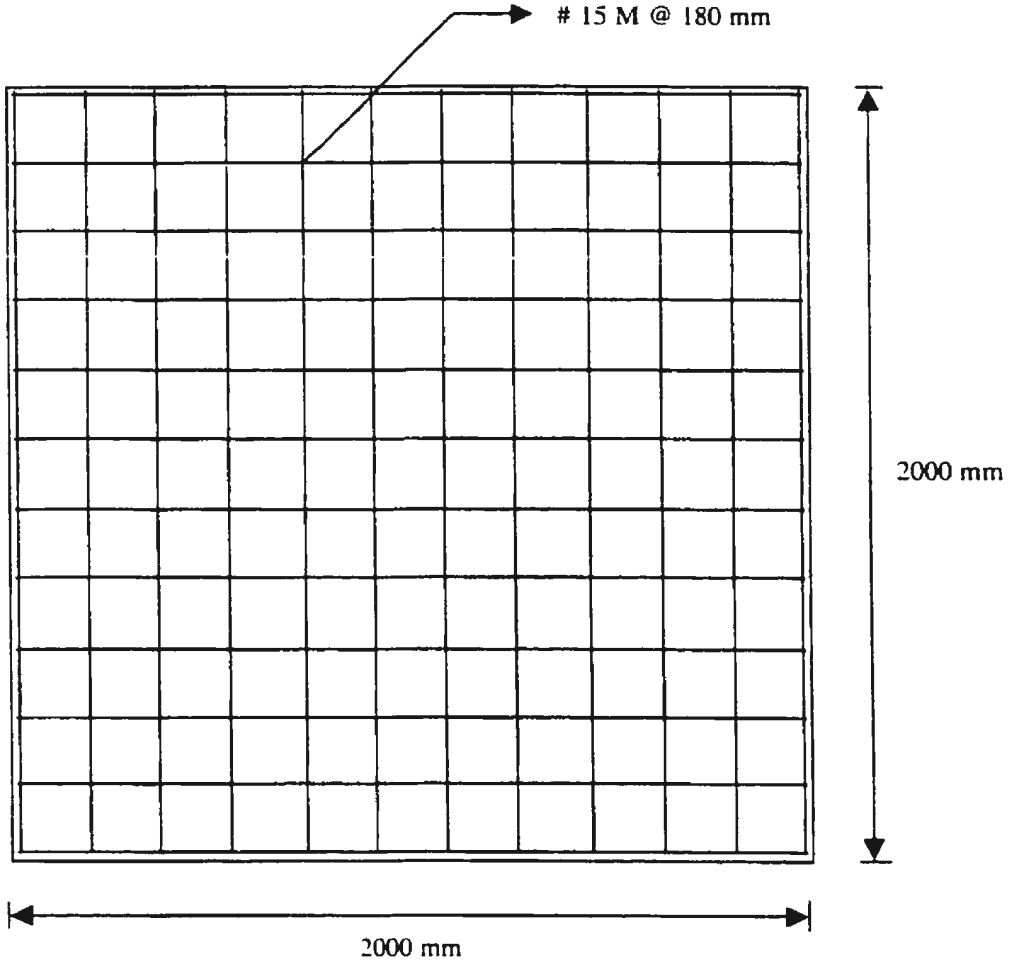

Figure 3.9. Bottom reinforcement of the concrete base of the testing frame

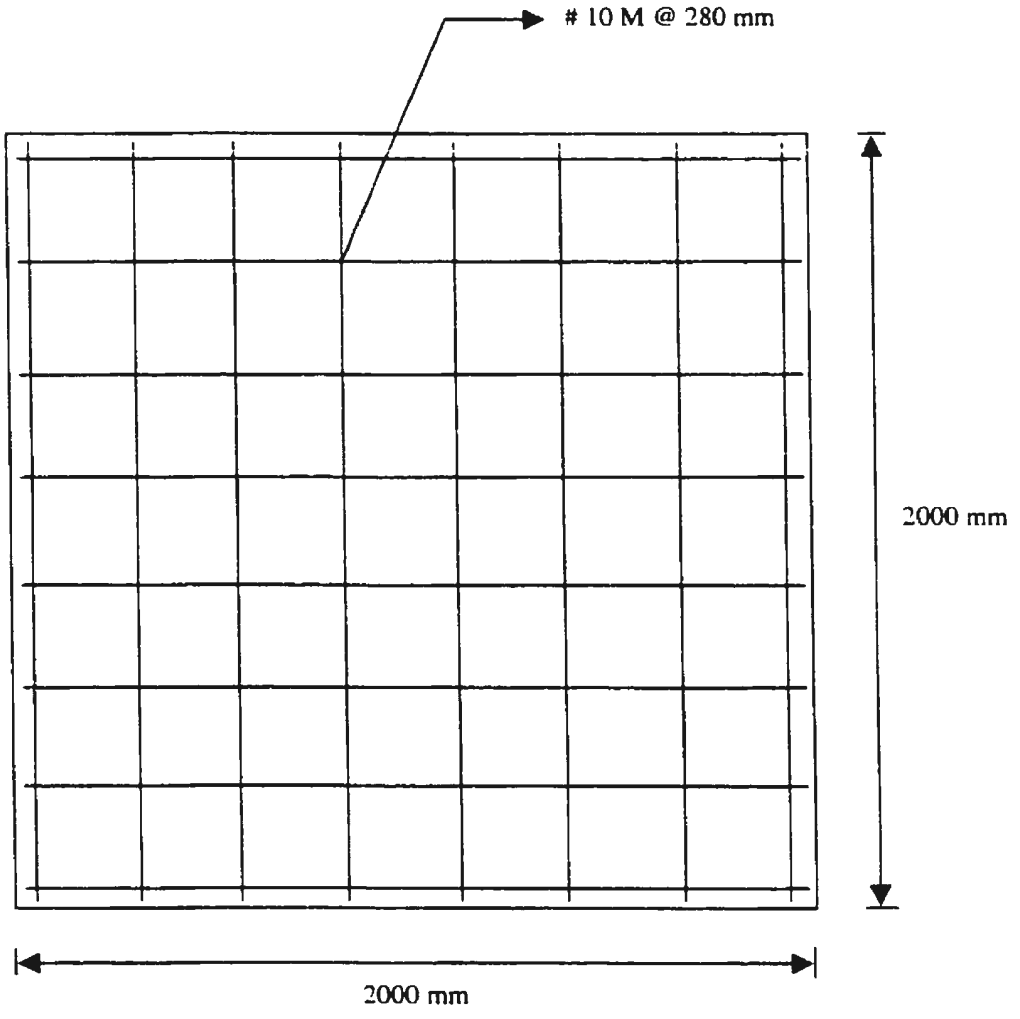

Figure 3.10. Top reinforcement of the concrete base of the testing frame

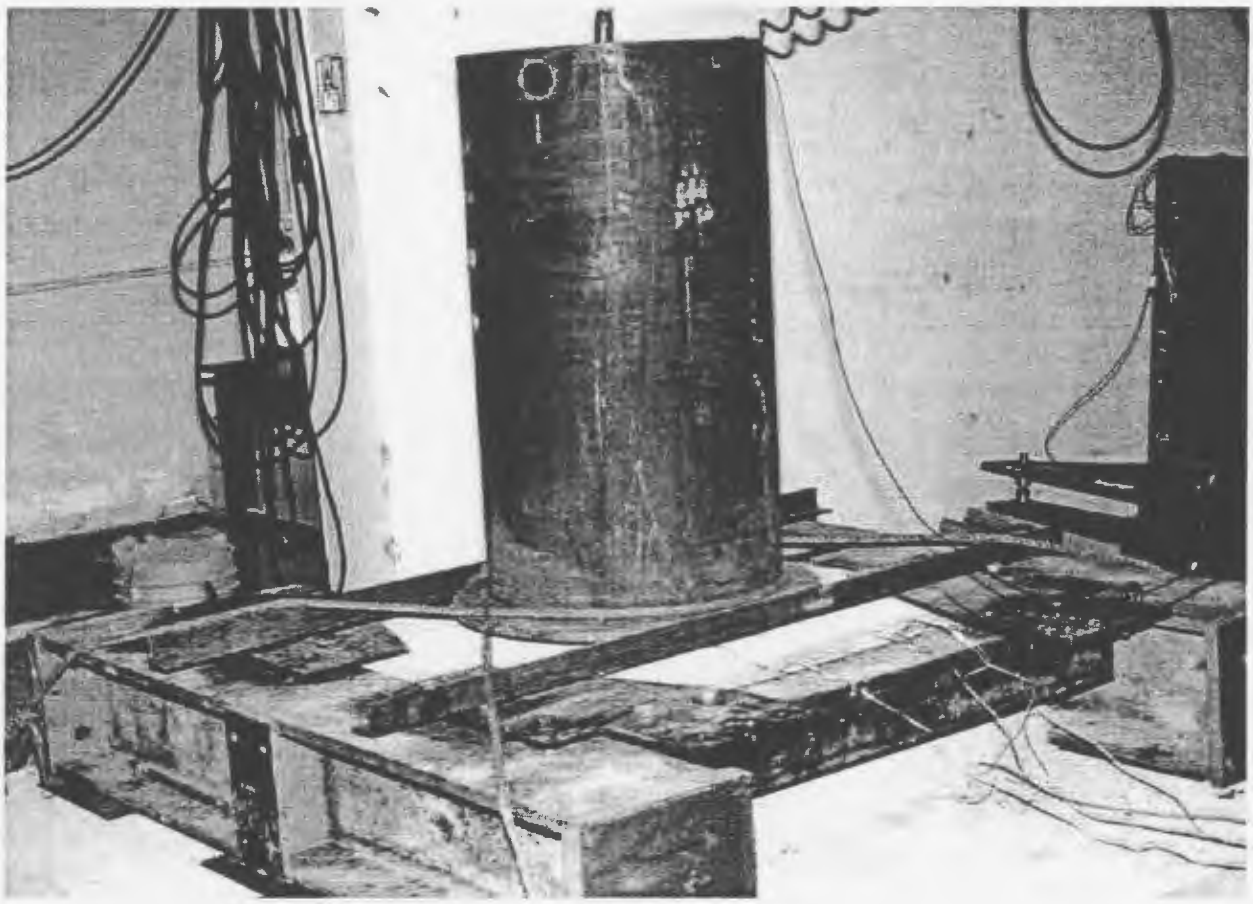

Figure 3.11. Complete test frame with guide steel cylinder

Figure 3.12. Test set-up for a fixed specimen

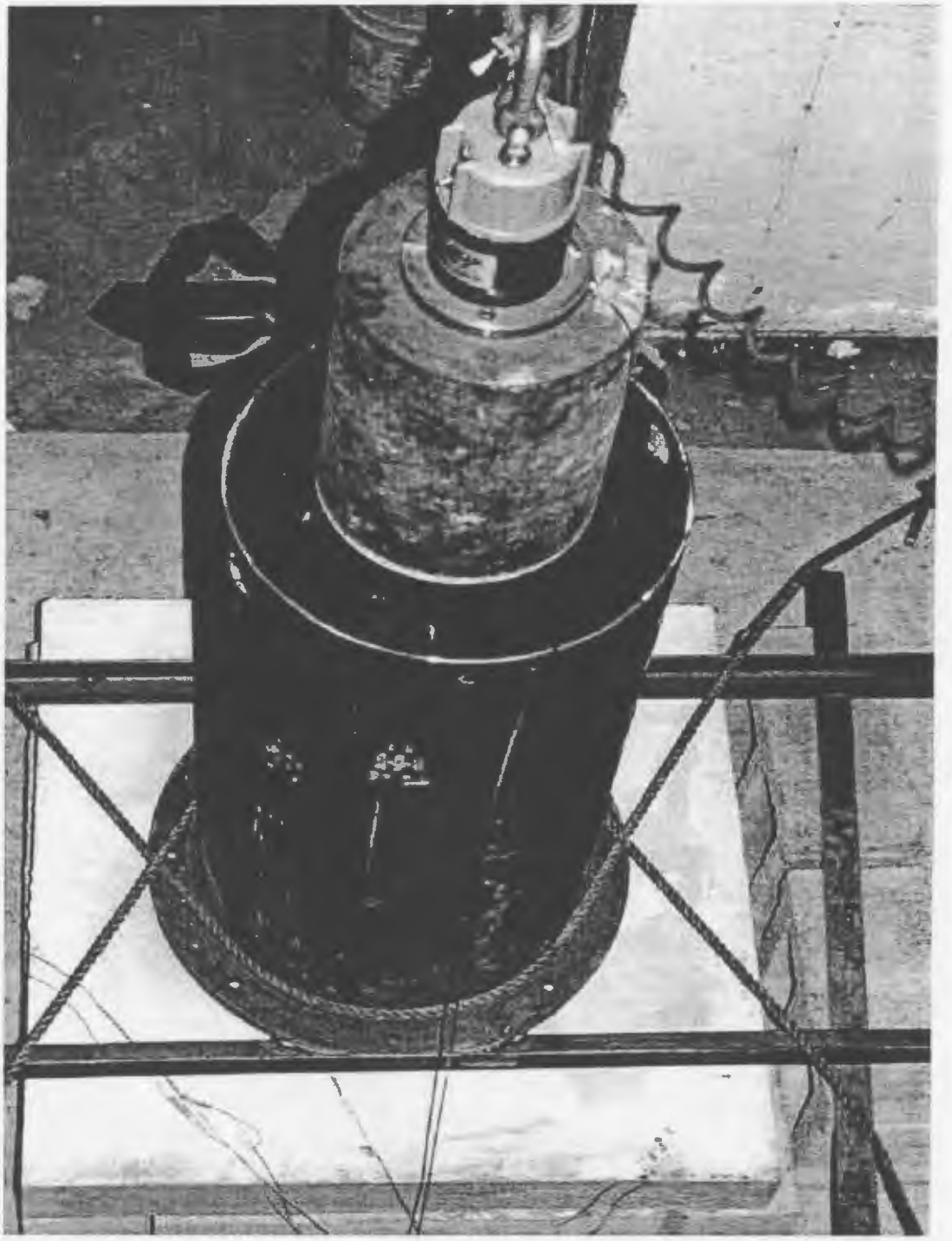

Figure 3.13. Test set-up for simply-supported specimen

Figure 3.14. A specimen during impact testing

Figure 3.15. LPDT fixed at the center of specimen

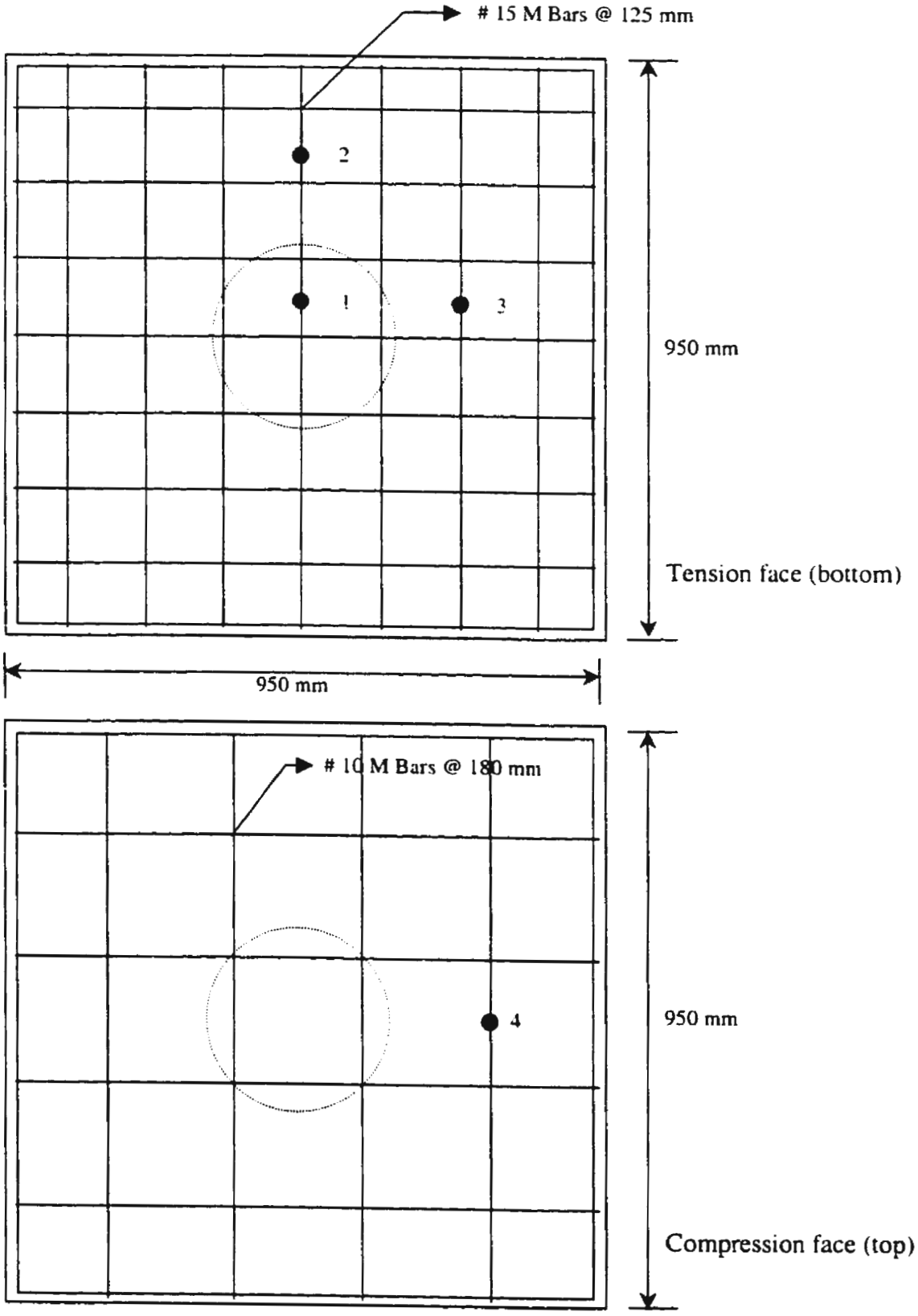

Figure 3.16. Locations of steel strain gages on tension and compression faces

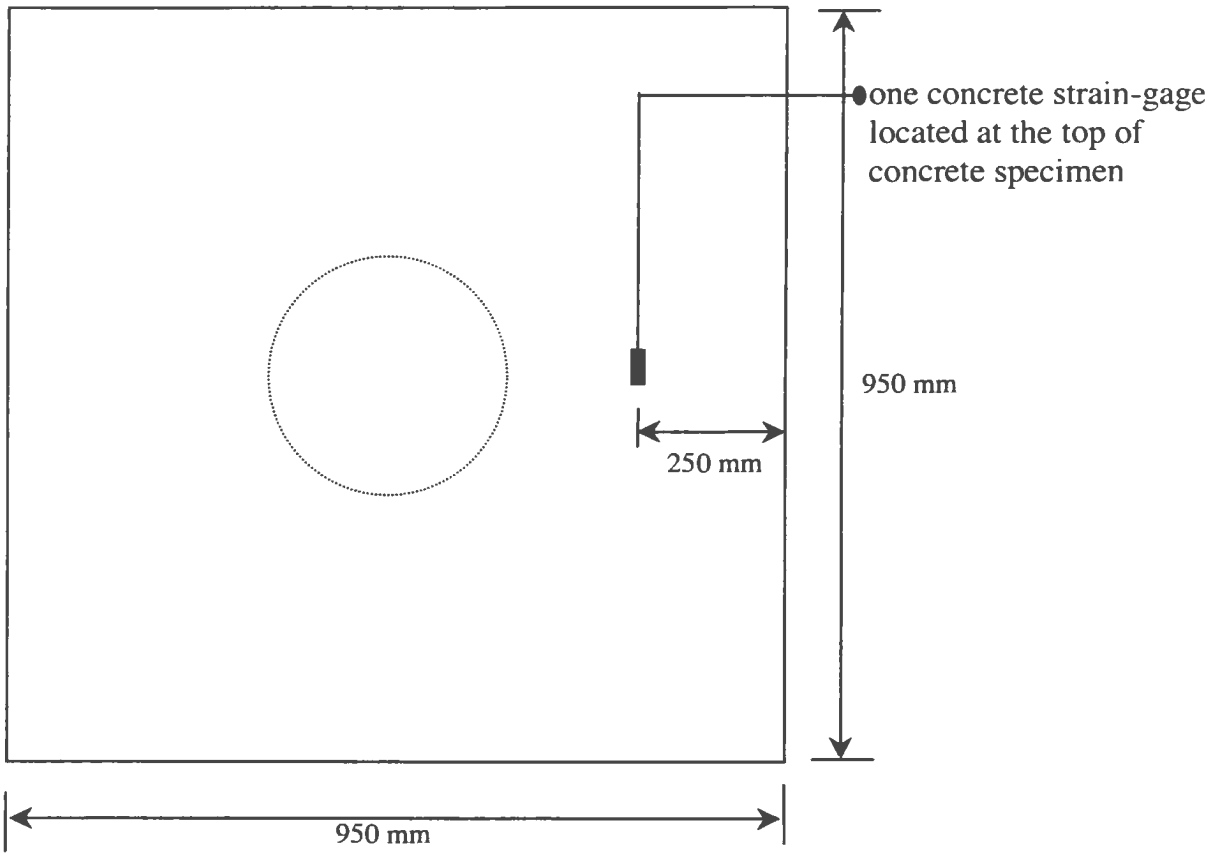

Figure 3.17. Concrete strain-gage location

Figure 3.18. Data acquisition system

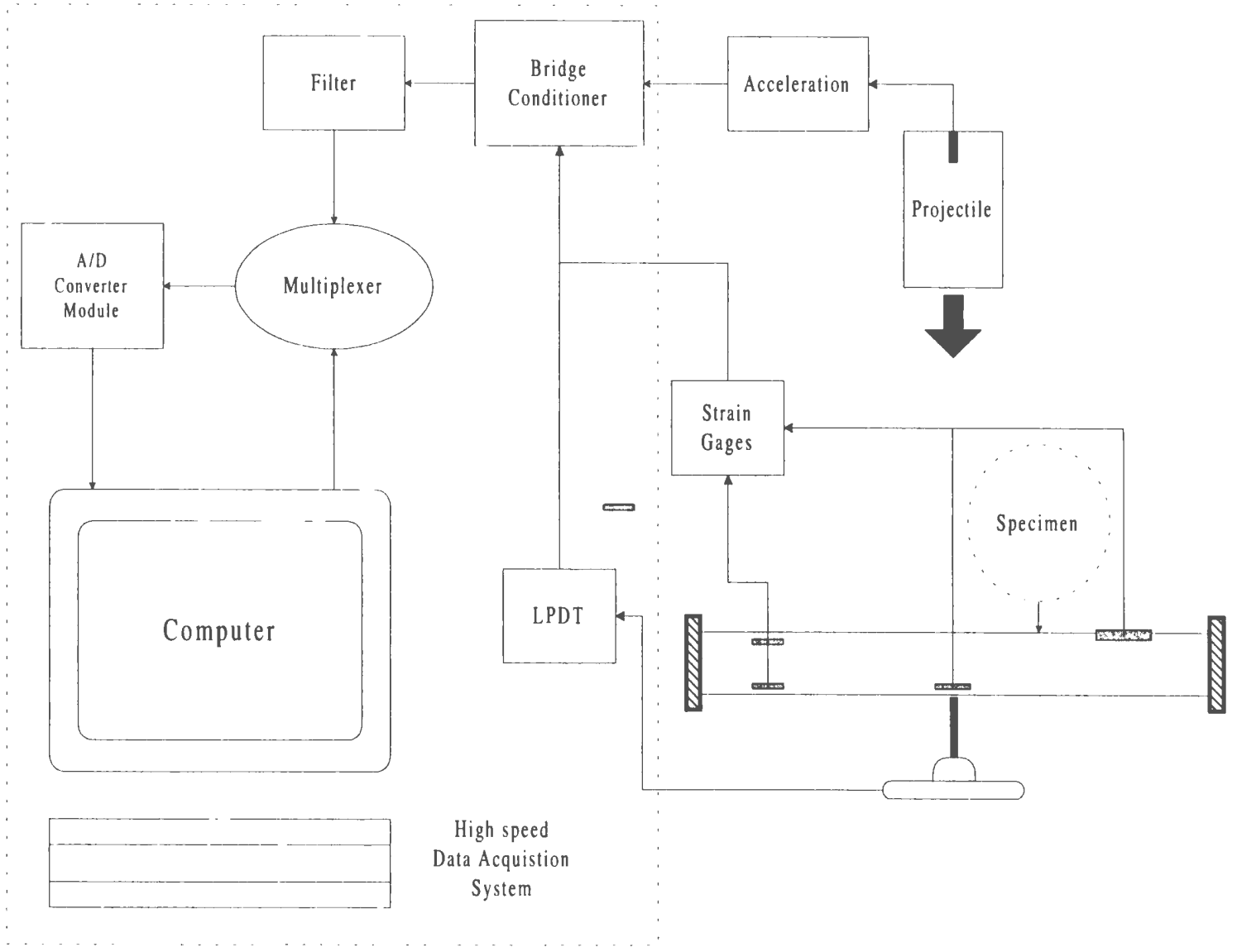

Figure 3.19. Instrumentation block-diagram

Chapter 4

TEST RESULTS AND DISCUSSION

This chapter discusses the test results of the present research investigation including the crack patterns, ultimate loads, deflections, ductility and energy absorption, modes of failure, strains both in concrete and steel reinforcement. A comparison was made between high-strength and normal-strength concrete slabs tested under static loading in the same laboratory by previous research workers, Marzouk and Hussein (1990).

Measurements obtained from laboratory investigation are presented in the following section. Due to the large amount of recorded data, only a few representative of the test results are selected in this presentation. In addition, the crack patterns at failure are represented graphically by means of photograph.

4.1. Cracking Characteristics

The crack patterns, after failures, are depicted in Figures 4.1 through 4.4 for tension face damages. While the stripping of the concrete cover from the compression face shown in Figure 4.5. Both the tension face and the compression face of all specimens showed very similar cracking damage.

It was not possible to determine a reliable value for the shear-cracking load, i.e. the load at which the shear cracks started up. The estimation of such load from the crack pattern was uncertain because there was no fundamental difference between shear crack and flexural crack expanding in tangential direction. However, employing the decrease of the steel strain in the reinforcement can be used as a guide for determining the shear cracking loads. As proposed by Kinnunen and Nylander (1960), the observed punching loads of two-way concrete slabs without shear reinforcement were around 70-80 percent of the ultimate load.

For dynamic loading, a slight trend of more tension face damage and more concrete stripping occurred at a larger reinforcement steel ratio ρ than the smaller ratio. The same observation was more evident for the case of high-strength concrete than normal-strength concrete. Radial cracks expanding to the edges of the specimens were evident on all the test specimens. The crack indicates that bending and shear failure mechanisms were detected in all the specimen. Therefore, it can be concluded that all the specimens were failed under a ductile shear failure.

4.2. Load-Deflection Characteristics

The impact loads versus the deflection at the center of the plates for the different test series are presented in Figure 4.6 through 4.13. The load-time curves for the different test series have also shown in Figure 4.14 through 4.17, while the deflection -time curves given in Figure 4.18 through 4.21.

The deflections for all tested specimens were obtained using LPDT measurements at the center of specimen. Using dynamic equilibrium in the vertical direction, the impact

load was obtained from the accelerations that was provided from the accelerometer. The dynamic equilibrium in the vertical direction is described in the following equation:

$$F(t) = (m_p + 0.5\, m_s)\, a_p$$

where, $F(t)$ = impact loading

m_p = mass of projectile

m_s = mass of specimen

a_p = acceleration of projectile.

The load versus deflection curve can be used for estimating the energy absorption capacity by calculating the area under the load-deflection curve. In addition, load-displacement curve can be approximated by several straight lines with different slopes. The ascending curve has a slope that represents to the stiffness of the specimen before cracked. Within a given curve, the pre-cracking stage represented by the slope of the ascending curves is normally steeper than the descending curve of the post-cracking stage. As expected, the stiffness of concrete plates were decreased after cracking.

Load-deflection curves of the test specimens shown in Figures 4.6 through 4.9 were made with different steel reinforcement ratio, and had the same concrete strengths as well as the same support conditions. Figures 4.6 to 4.9 show that for pre-cracking stages, the slope of ascending curve of the bigger reinforcement ratio were slightly higher than those from plates with smaller reinforcement ratio. This indicates that the plate stiffness increased with the increase of reinforcement ratio.

Repeating the same mentioned procedure for different specimens with different concrete strength and support conditions are shown in Figures 4.10 through 4.13. All the figures indicated that the plate stiffness increased with the increase of concrete-strength.

The stiffnesses of concrete plates were slightly increased with the change of end-conditions from simply supported to fixed.

4.3. Dynamic Fracture Energy

The energy absorption capacity is defined as the area under the load-displacement curve. The test results are given in Table 1. The results include the energy absorption capacity of all tested specimens at failure.

Table 4.1. Test results

Series No:	Slab No:	Support Condition	f_c' (MPa)	Reinforcement ρ (%)	Reinforcement ρ' (%)	Speed (m/s)	Accel (g)	Displ. at center (mm)	Energy Absorption (kN.mm)
1	HSS1	Simply supported	81.7	0.95	0.68	7.00	110	12.0	276
2	HSS2	Simply supported	81.7	1.26	0.68	7.67	110	14.0	421
3	HSS3	Simply supported	81.7	1.90	0.74	8.29	115	23.0	876
4	HSS4	Simply supported	81.7	2.32	0.82	8.86	118	29.0	1227
5	HSF1	Fixed	79.1	0.95	0.68	7.00	-	15.8	N/A
6	HSF2	Fixed	79.1	1.26	0.68	7.67	102	17.0	364
7	HSF3	Fixed	79.1	1.90	0.74	8.29	115	25.0	812
8	HSF4	Fixed	79.1	2.32	0.82	8.86	121	34.9	1245
9	NSS1	Simply supported	33.1	0.95	0.68	5.42	70	5.5	77
10	NSS2	Simply supported	33.1	1.26	0.68	6.26	76	7.9	162
11	NSS3	Simply supported	33.1	1.90	0.74	7.00	95	10.8	181
12	NSS4	Simply supported	33.1	2.32	0.82	7.67	106	11.2	255
13	NSF1	Fixed	36.6	0.95	0.68	4.43	72	4.7	61
14	NSF2	Fixed	36.6	1.26	0.68	4.95	78	6.0	110
15	NSF3	Fixed	36.6	1.90	0.74	5.42	85	8.4	186
16	NSF4	Fixed	36.6	2.32	0.82	5.86	98	10.0	260

It is evident from the given table that the energy absorption capacity increased as the concrete strength increased. Test results of the specimens made with different

concrete strength, and had the same reinforcement-ratio and support condition revealed that energy absorption increased with the increase of concrete strength. The use of high-strength concrete plate can be employed to improve the energy absorption capability of the concrete plate by about 4 times higher than normal-strength concrete plate.

The effect of support-condition on the energy absorption capacity was not a significant factor. As the end-condition changed from fixed to simply-supported, a slight change in the energy absorption capacity of the test plate was recorded. On the other hand, the effect of reinforcement ratio on the energy absorption capacity was significant. For example, increasing the reinforcement ratio from 1% to 2%, the energy absorption capacity of the specimen increased by about three times, both for the case of high-strength and normal-strength concrete.

4.4. Steel and Concrete Strains

Figures 4.22 through 4.37 show the distribution of the measured steel strains and concrete strains of all specimens. The strains were measured at points of special interest in order to obtain information on the state of stress, as mentioned in sections 3.6.3.1 and section 3.6.3.2. Unfortunately, not all the measured data are reported since some strain gages were lost due to electrical problems and damages to the gages during casting.

All the tested specimens experienced yielding of steel reinforcement before punching failure occurred. The tension reinforcement reached the yield point at strain of about 0.0025. Comparing the tension steel strain at approximately same location from the compression face, it has been found that the steel strains in the case of impact loading were about twice higher than those recorded for static loading as reported previously.

There was a concentration of stresses at the area under impact load. While a large area of steel had yielded, the strain at the concrete compression face just reached to a maximum of 1700 micro strain at failure. This is approximately half the value that obtained experimentally at the same location under static loading as reported previously. Since, in the case of impact loading, the concrete surface suddenly perforated, the concrete surface have been separated, hence the concrete strains on the separate face were not recorded.

4.5. Modes of Failure

Modes of failure of conventional two-way plates under static load can be classified into three categories:

(1) Pure flexural failure

(2) Pure shear failure

(3) Ductile shear failure.

Pure flexural failure takes place in plates where most of the reinforcement yields before punching occurs. Consequently, the plates exhibit large deflections prior the failure. Usually this type of failure happens in the case of lightly reinforced plates. As the reinforcement ratio decreases, more steel yielding approaches to the total area of the tension steel reinforcement.

The second category of failure is pure shear failure. Pure shear failure occurs when the yielding of the tension steel is very localized at the center of loading. Usually, specimens with heavy reinforcement ratio failed under punching shear. The third type of

failure is ductile shear failure or shear failure with ductility. This type of failure is a case of transition between pure punching and pure flexure failures.

As mentioned in the Section 4.1, all specimens failed under ductile shear failure. This failure can be categorized under the third type of failure. The impact punching load increased as the concrete-strength increased and the steel reinforcement ratio increased.

The failure surface of some of the tested specimens were carefully removed and examined. The observed angles of failure surface had some variation. For normal-strength concrete plates, the observed angle of failure surface was about 60 degree, while for high-strength concrete plates, the angle was found to about 65 degree. In addition, the punching shear radius on the tension face happened at a distance of (1.6-2.0) times the plate depth (d) from the edge of loaded area for most of the tested specimens compared to a distance $d/2$ for static loading.

4.6. Effect of Concrete Strength

The designed compressive strength targets for this investigation were 35 MPa for normal-strength and 80 MPa for high-strength concrete as described in section 3.1. Increasing the concrete compressive strength from normal-strength to high-strength concrete increased the energy absorption capacity, critical velocity of perforation, and deflection at the center of specimens.

The energy absorption capacity increased by range of about 3-5 times, while the critical velocity of perforation increased by a range of about 20-30 percent. The displacements at the center of specimen also increased around twice. This observation indicated that high-strength concrete can provide higher ductility for concrete plates.

4.7. Effect of Steel Reinforcement Ratio

The tension reinforcement ratios were 1%, 1.5%, 2%, and 2.5%. As tension steel ratio was increased from about 1% to 1.5%, the critical velocity of perforation increased by about ten percent. The energy absorption capacity has also increased by about fifty percent for high-strength concrete and hundred percent for normal-strength concrete.

Increasing tension steel ratio from 1% to 2%, the critical velocity of perforation increased by about twenty percent. While, the energy absorption capacity of the specimen increased by about three times, both in high-strength and in normal-strength concrete. In addition, when the tension steel ratio increased from 1% to 2.5%, the critical velocity of perforation increased by about thirty percent. In this case, the energy absorption capacity has also increased by about four times for high-strength concrete as well as normal-strength concrete.

4.8. Effect of Support Pattern

As mentioned in section 3.3, this study was conducted on 16 specimens under two types of support patterns, fixed and simply supported. The effect of support pattern can be described briefly in the following section.

Energy absorption capacity of the two types had nearly the same behavior both in the case of fixed and simply supported. Therefore, there was no significant effect of support pattern for specimens regarding the energy absorption capacity.

However, increasing the concrete strength from 35 MPa to 80 MPa resulted into a significant effect on the critical velocity of perforation. The critical velocity of

perforation increased by about 20-30 percent for specimens under simply supported end condition, and 50-60 percent for specimens under fixed end condition.

4.9. Effect of Dynamic Loading on Peak Strain

Comparing the static loading to the dynamic (impact) loading can be summarized in the following section. In case of static loading, the peak strain and the maximum deflection happen on the same time with the peak load. However, under dynamic loading, the peak strain occurs slightly delayed with respect to the peak load but ahead to the maximum deflection. An illustration of the difference behavior between normal-strength and high-strength concrete is shown in Figure 4.38.

Under impact loading, the tension steel strain is estimated by about twice that under static loading. On the other hand, the concrete strain on the outer side area of contact loading decreased by about half. As described in the previous section, the concrete surface suddenly perforated under dynamic loading, hence the concrete strains on the separated area could not be recorded.

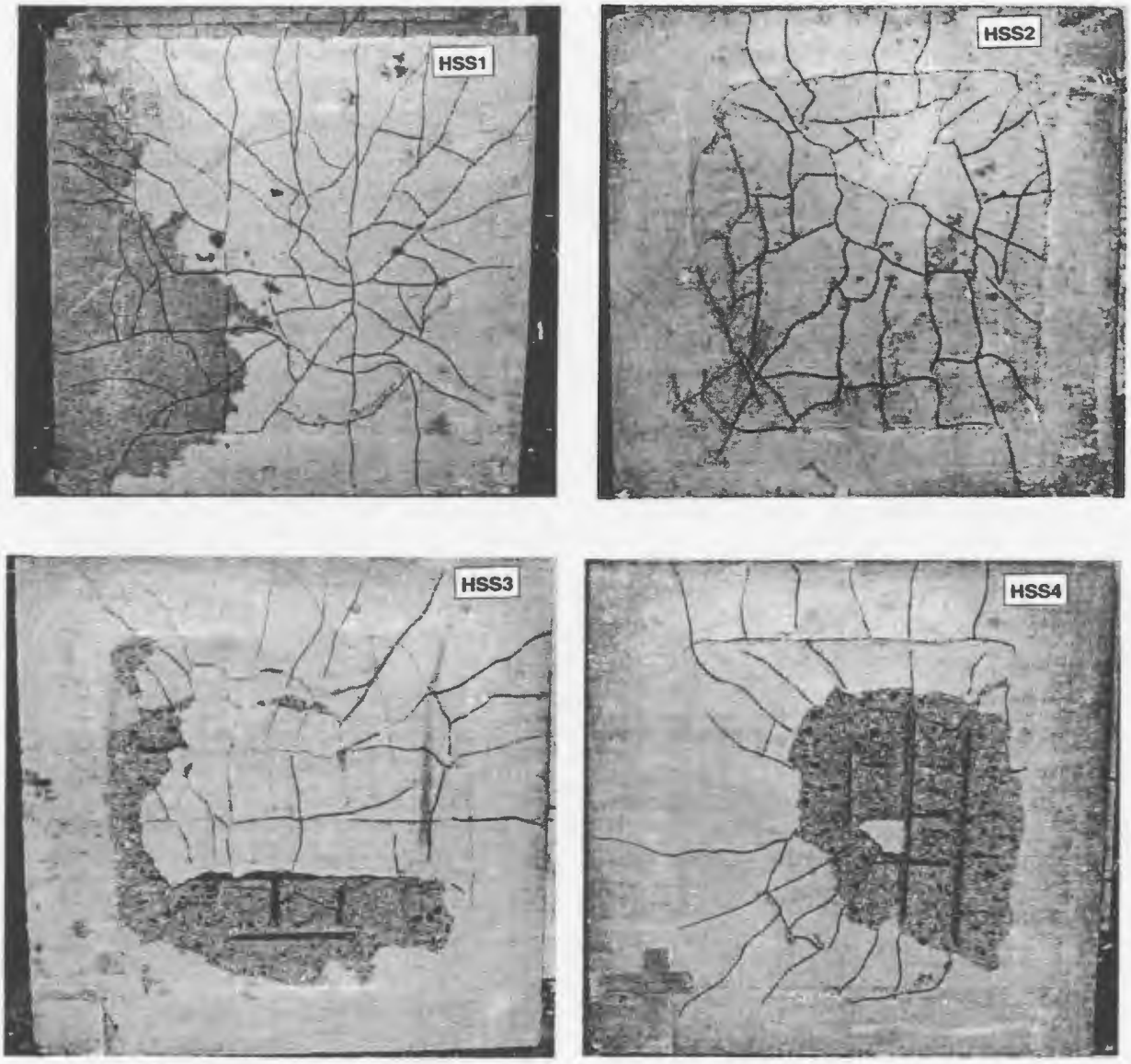

Figure 4.1. Failure patterns of test specimens HSS1, HSS2, HSS3, and HSS4

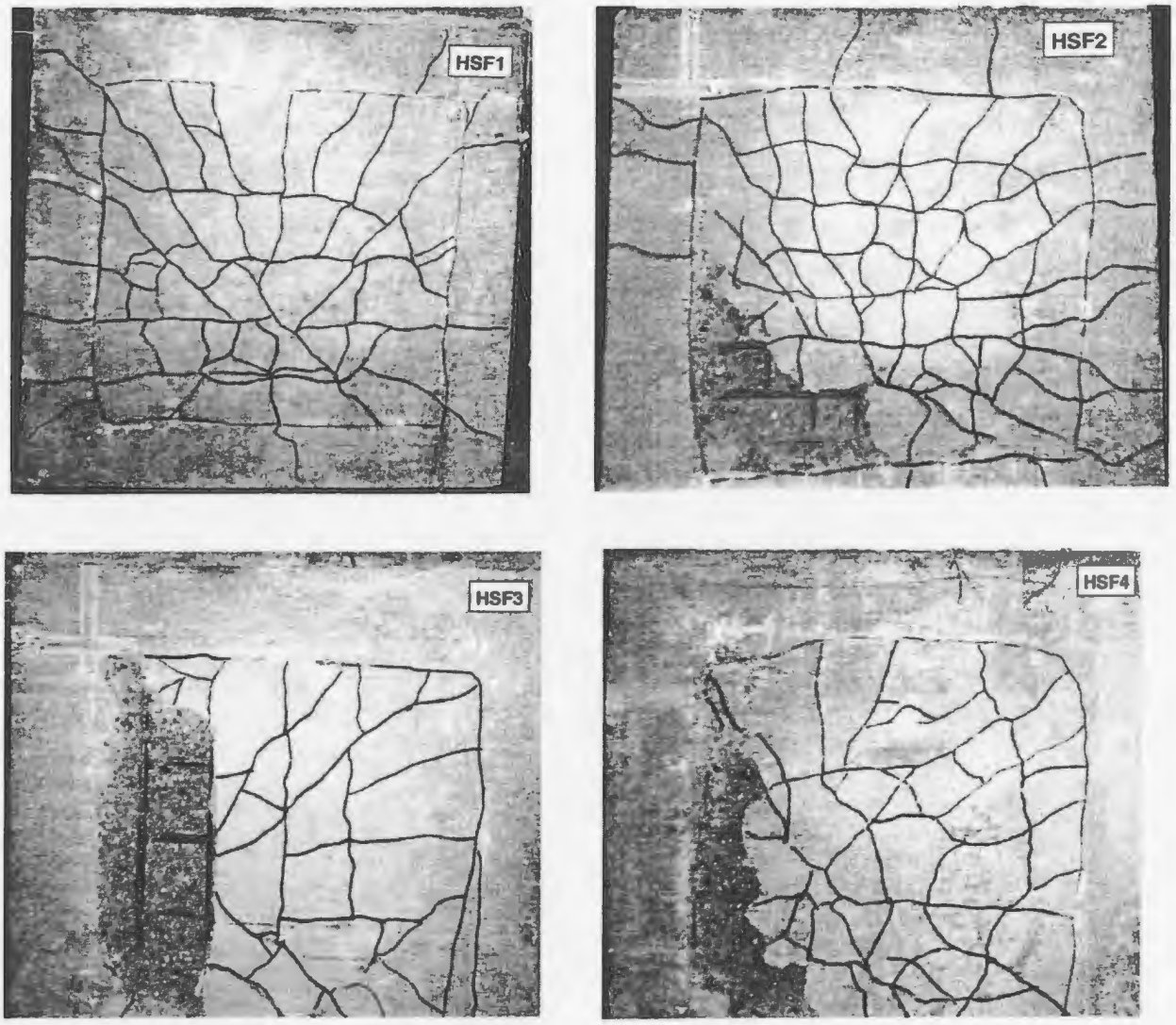

Figure 4.2. Failure patterns of test specimens HSF1, HSF2, HSF3, and HSF4

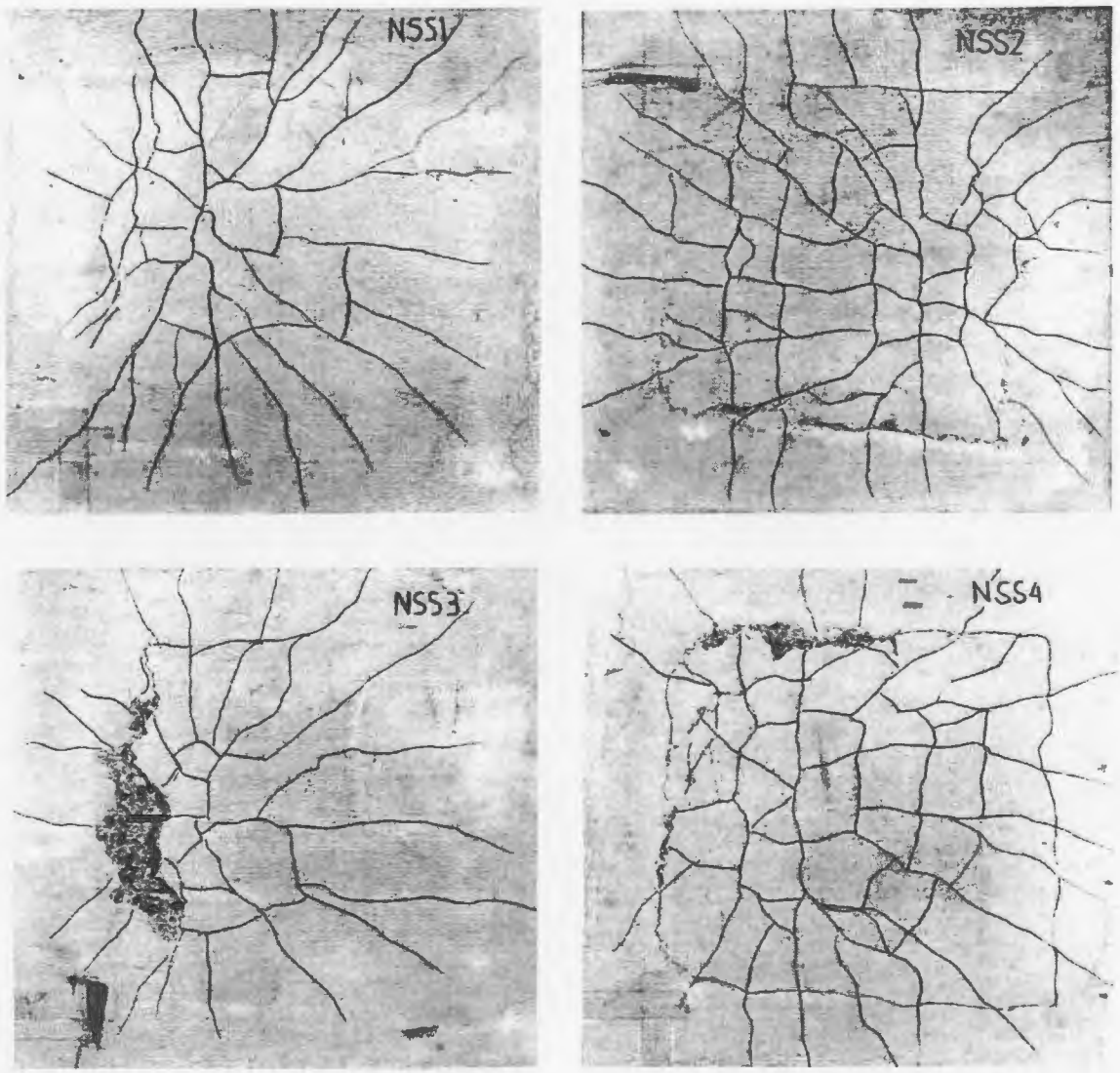

Figure 4.3. Failure patterns of test specimens NSS1, NSS2, NSS3, and NSS4

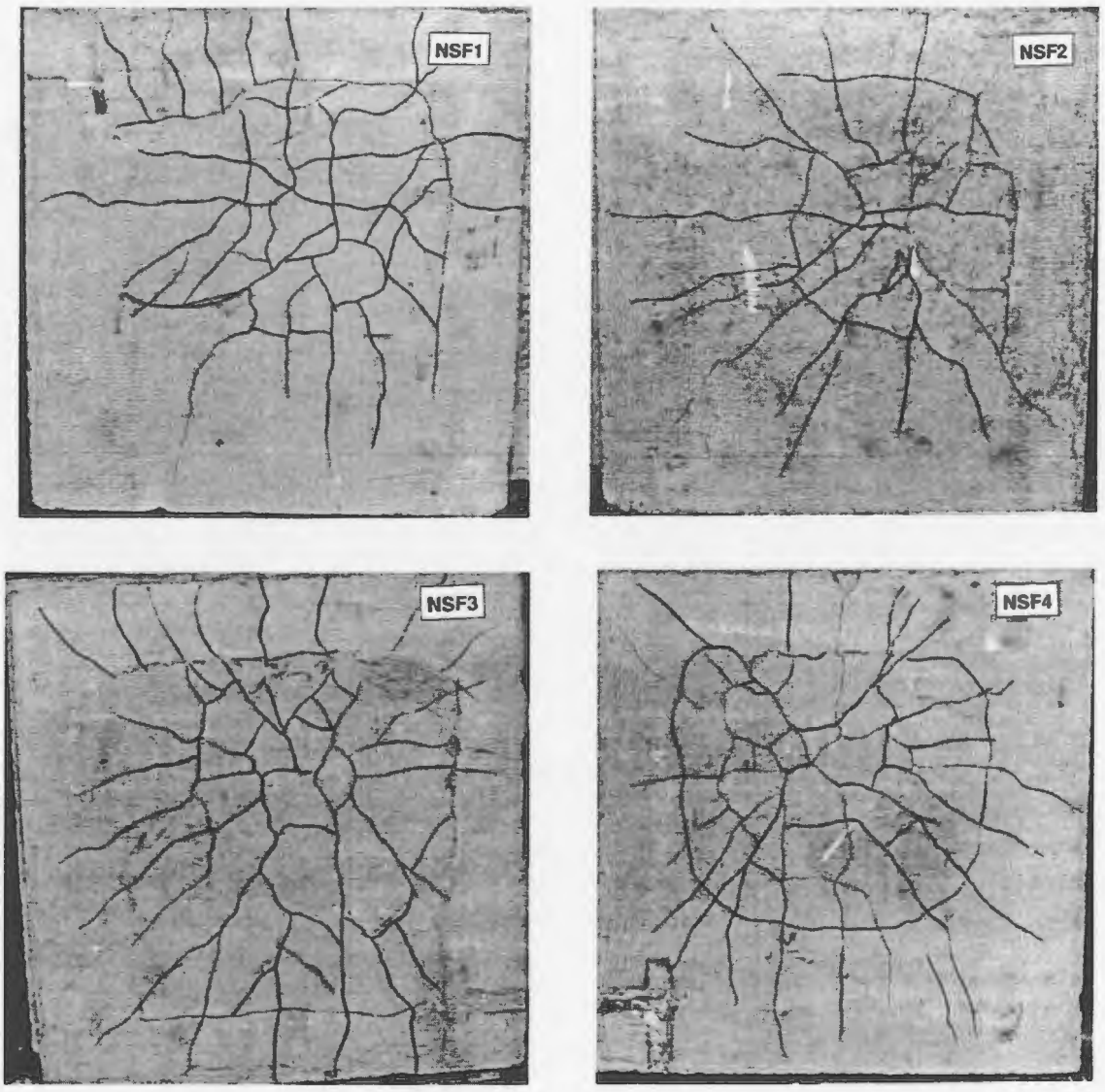

Figure 4.4. Failure patterns of test specimens NSF1, NSF2, NSF3, and NSF4

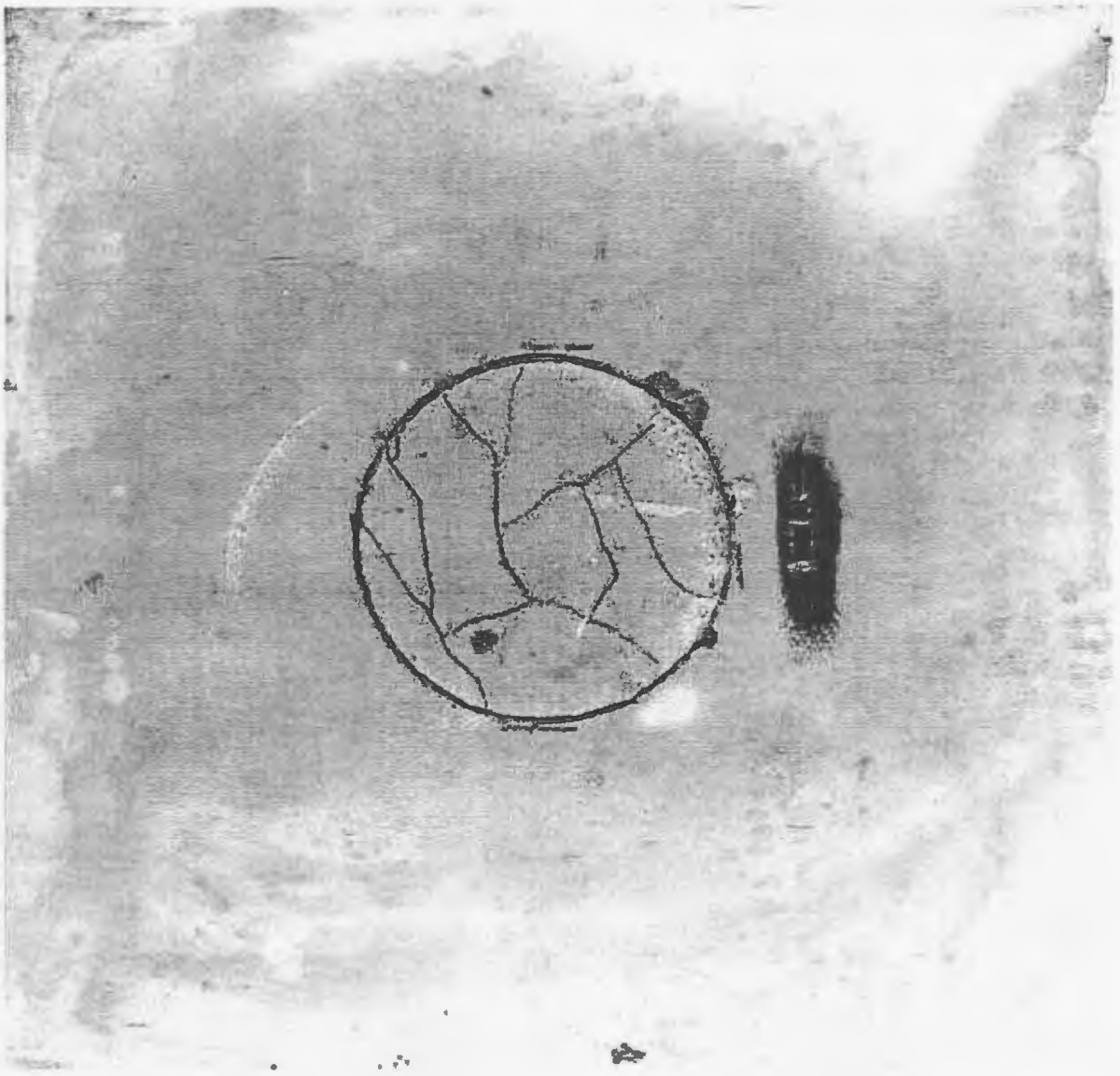

Figure 4.5. Failure pattern of a typical test specimen at the compression face

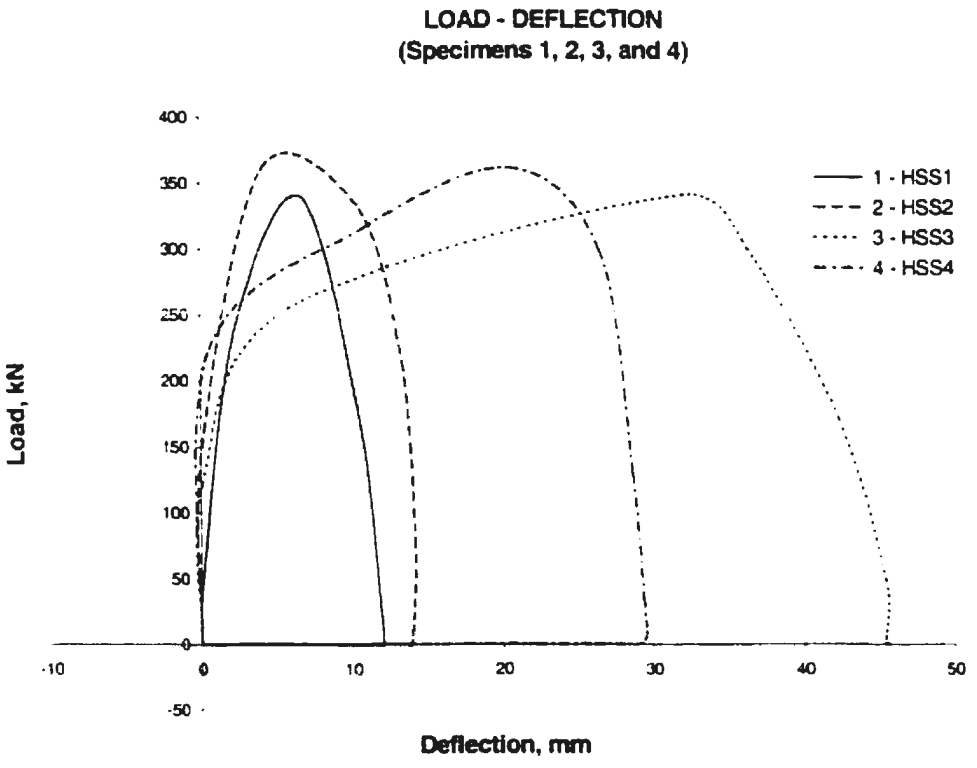

Figure 4.6. Load-deflection curves for specimen no. 1, 2, 3 and 4

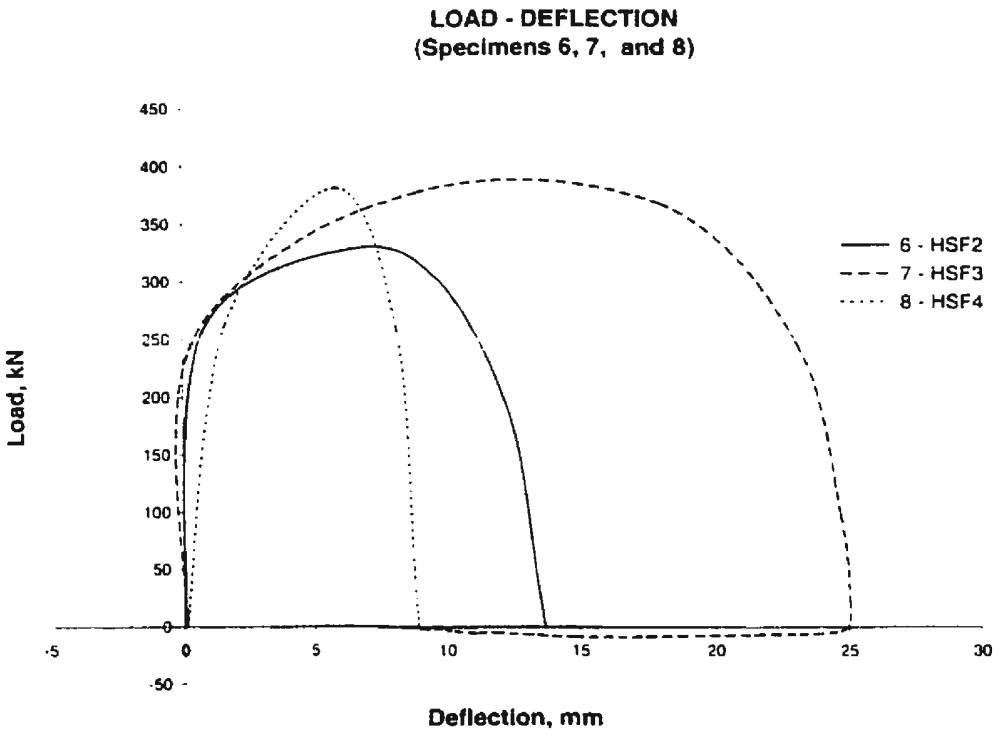

Figure 4.7. Load-deflection curves for specimen no. 6, 7, and 8

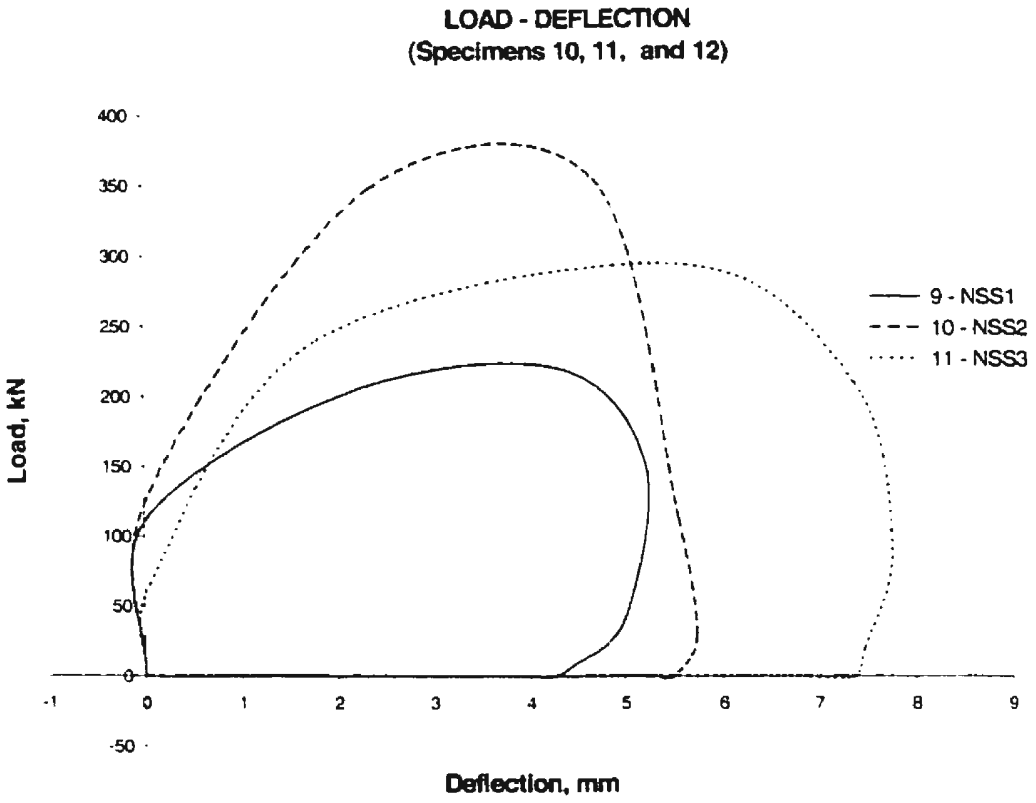

Figure 4.8. Load-deflection curves for specimen no. 9, 10, and 11

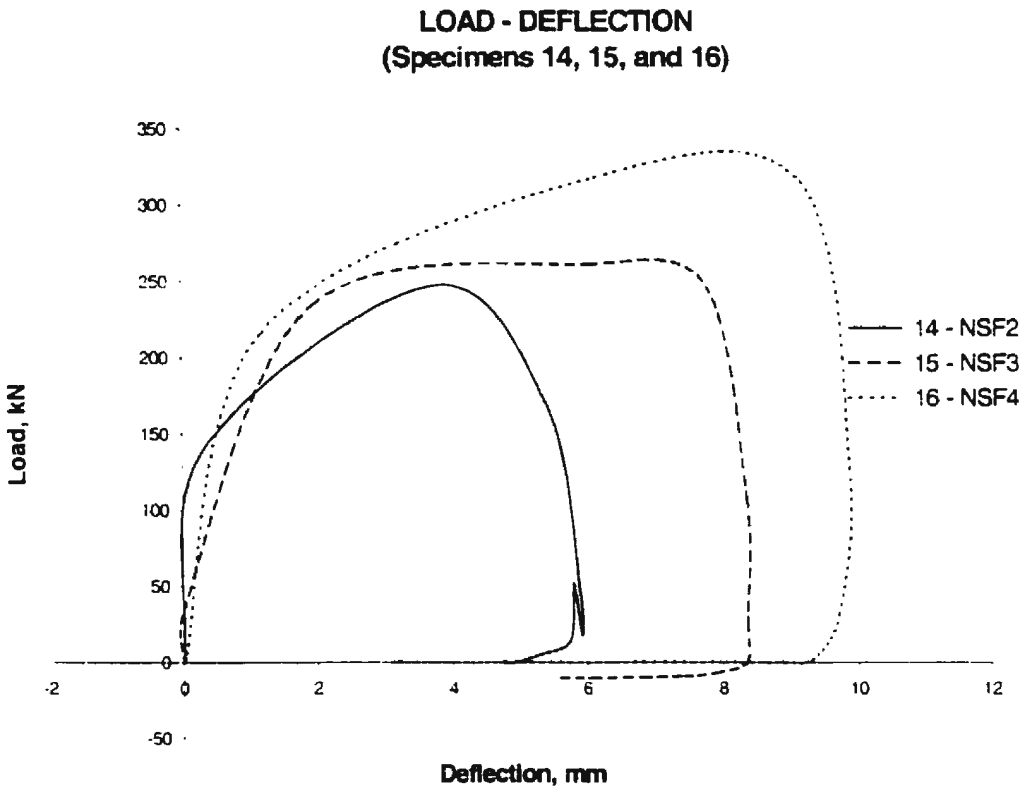

Figure 4.9. Load-deflection curves for specimen no. 14, 15, and 16

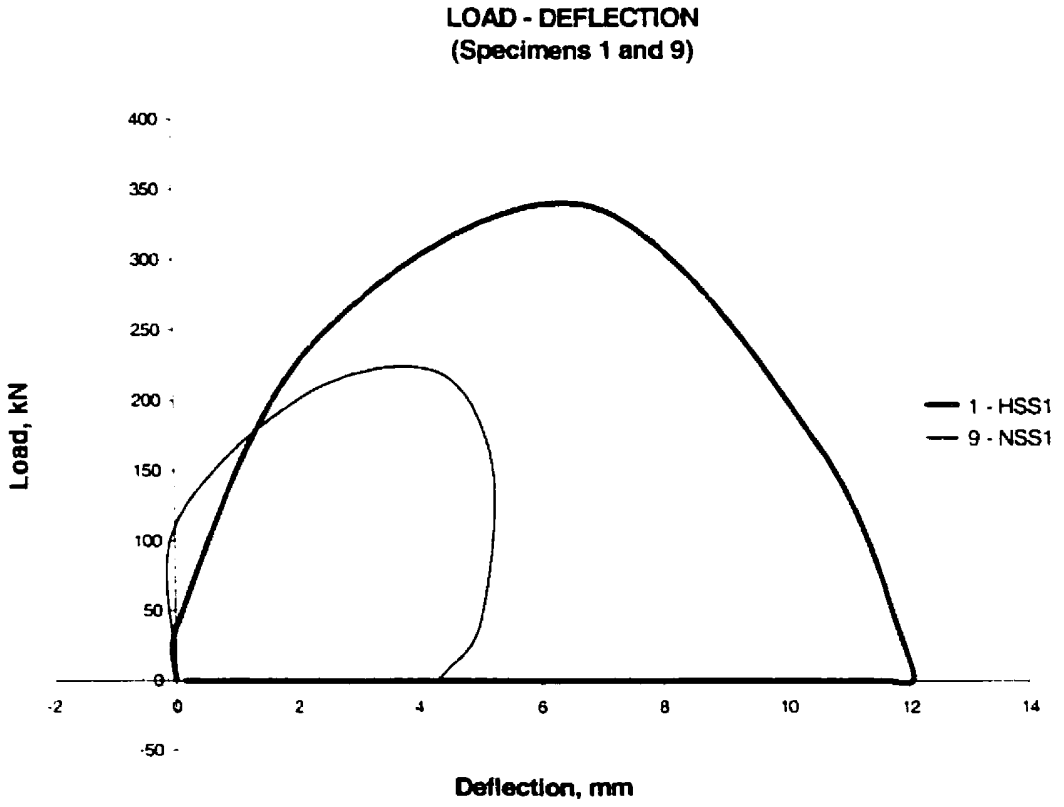

Figure 4.10. Load-deflection curves for specimen no. 1 and 9

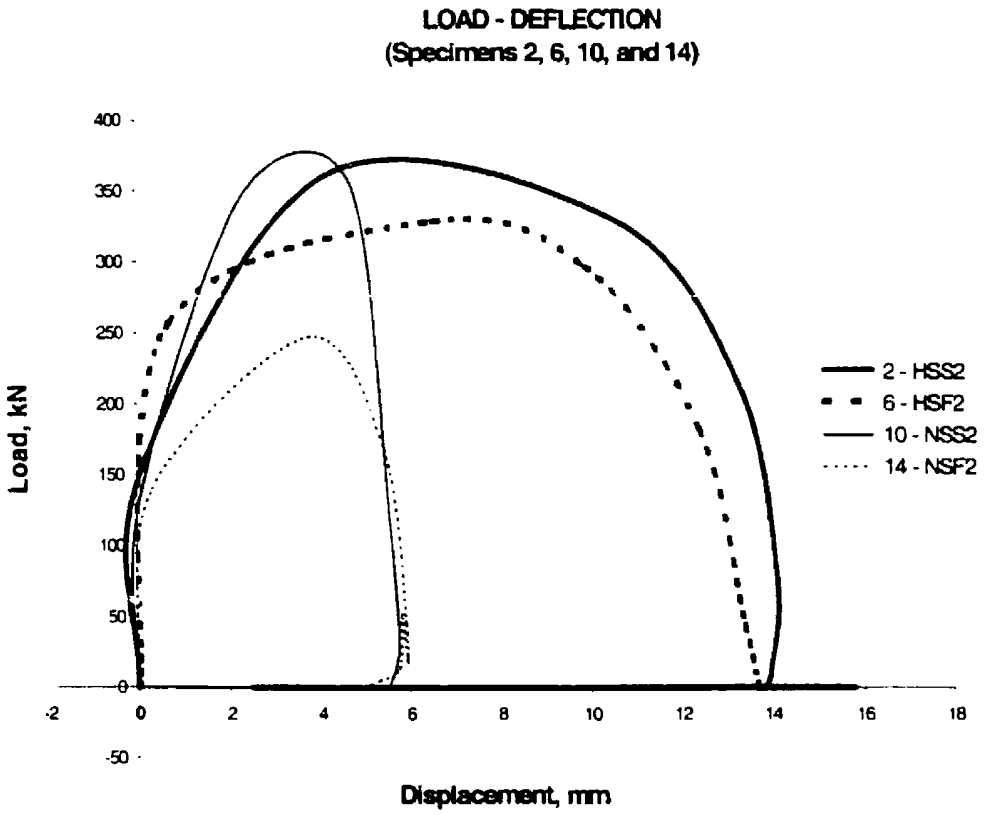

Figure 4.11. Load-deflection curves for specimen no. 2, 6, 10, and 14

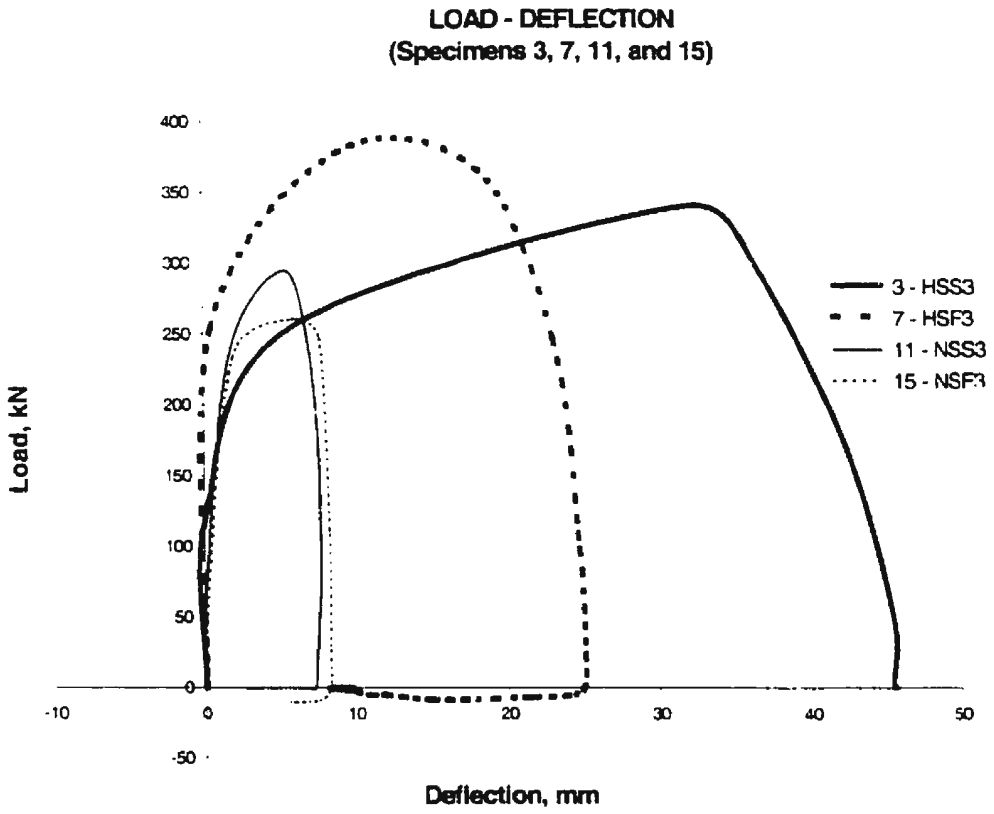

Figure 4.12. Load-deflection curves for specimen no. 3, 7, 11, and 15

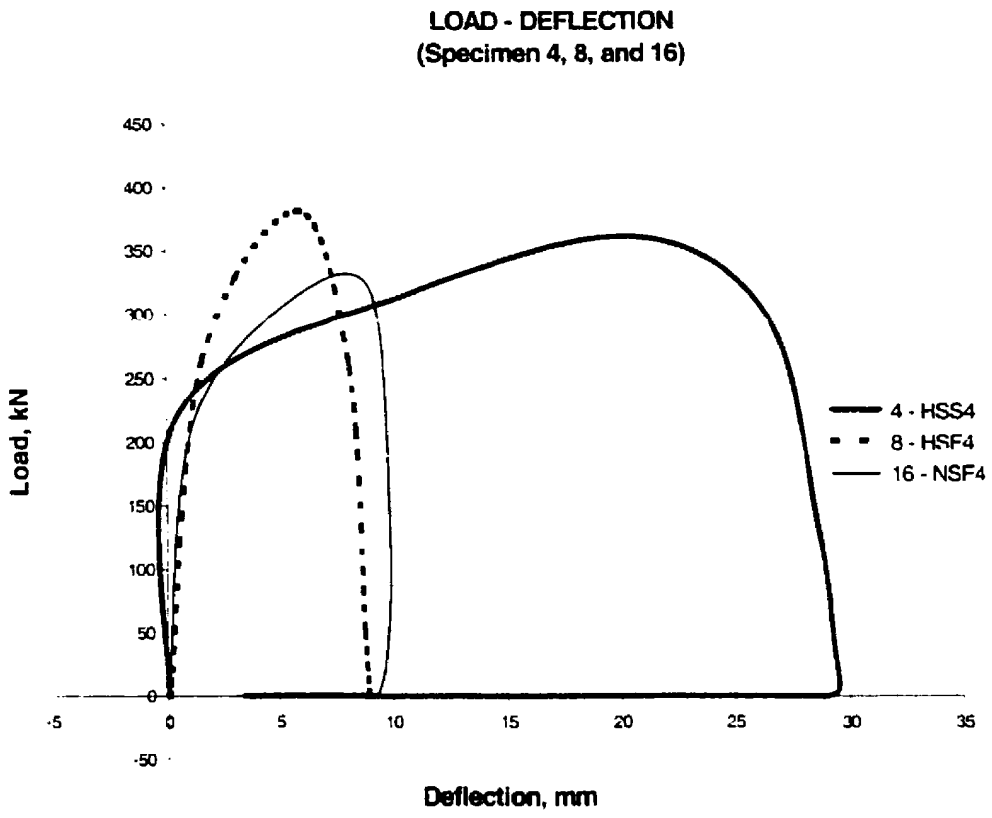

Figure 4.13. Load-deflection curves for specimen no. 4, 8, and 16

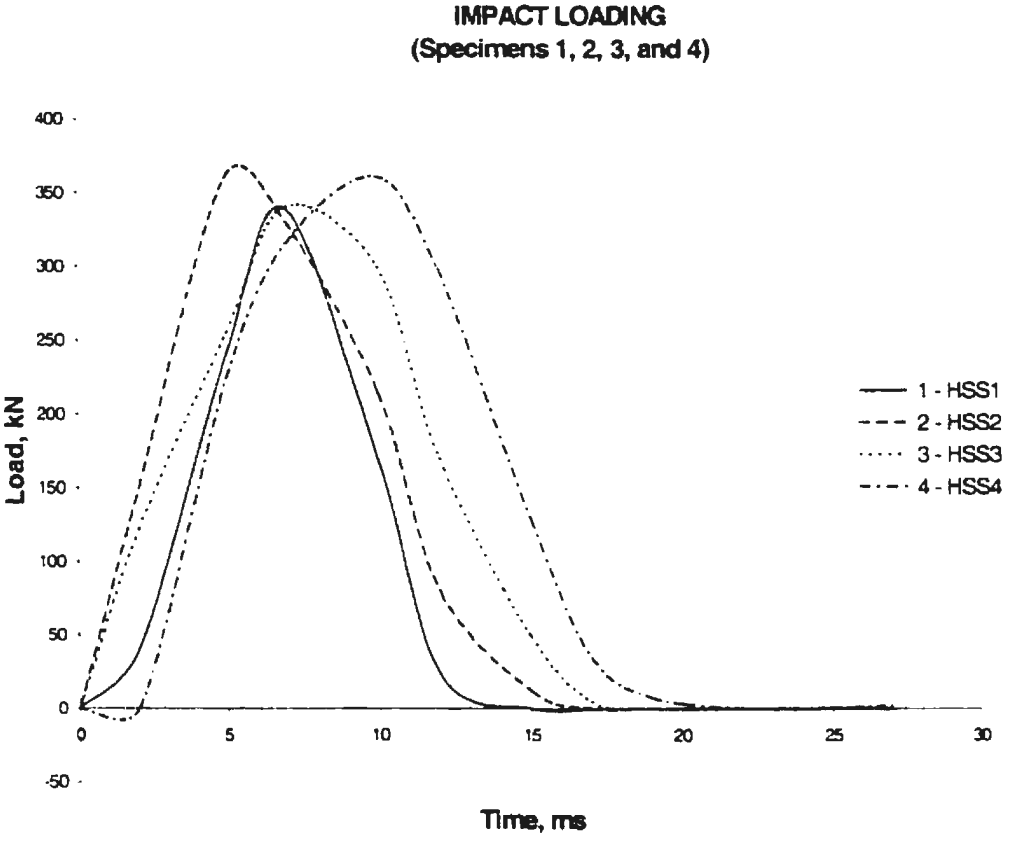

Figure 4.14. Load-time curves for specimens no. 1, 2, 3, and 4

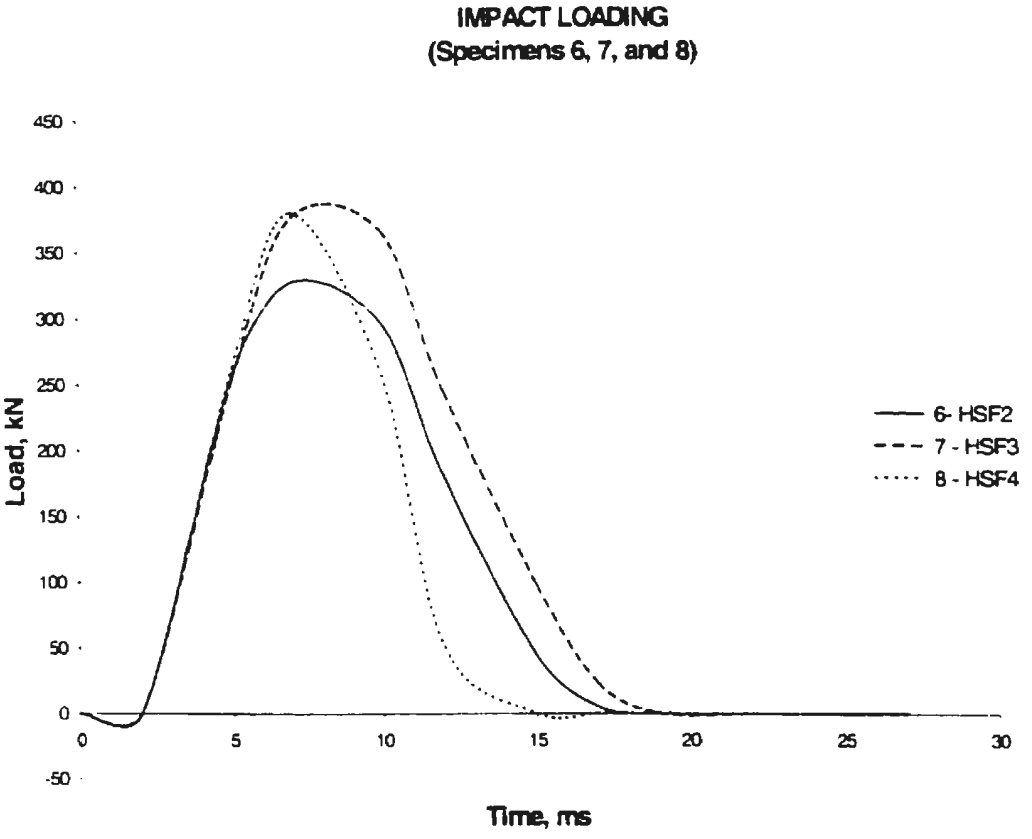

Figure 4.15. Load-time curves for specimens no. 6, 7, and 8

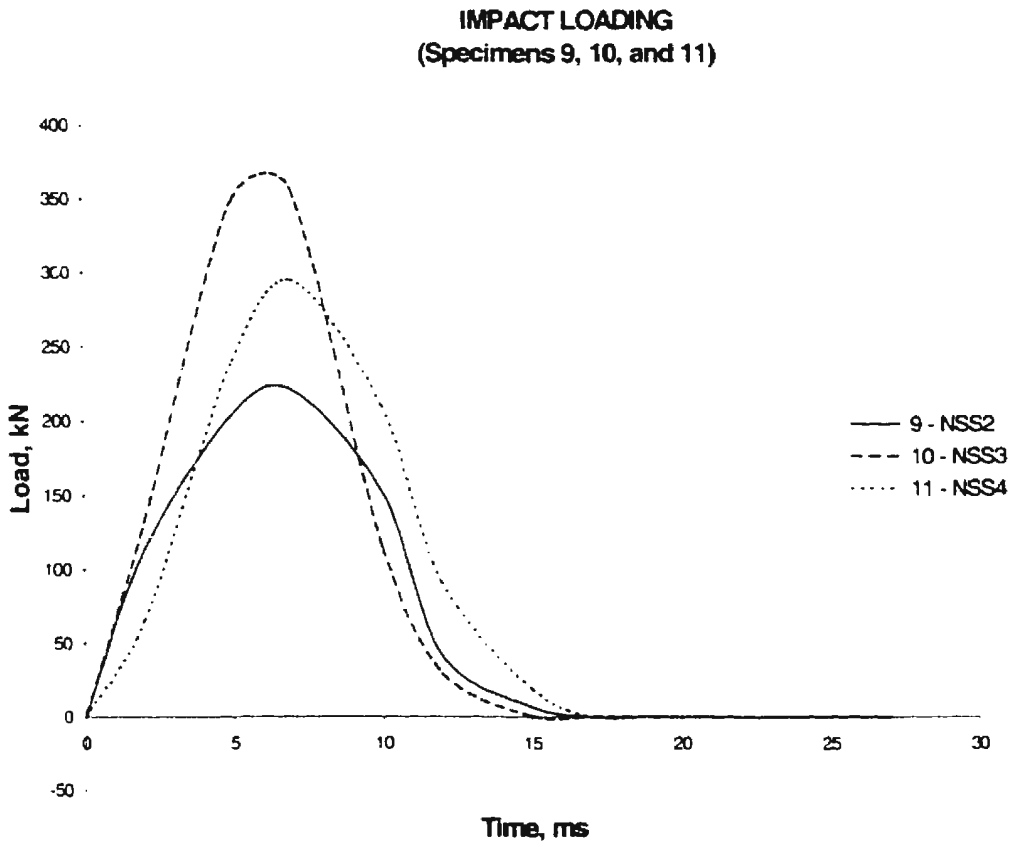

Figure 4.16. Load-time curves for specimens no. 9,10, and 11

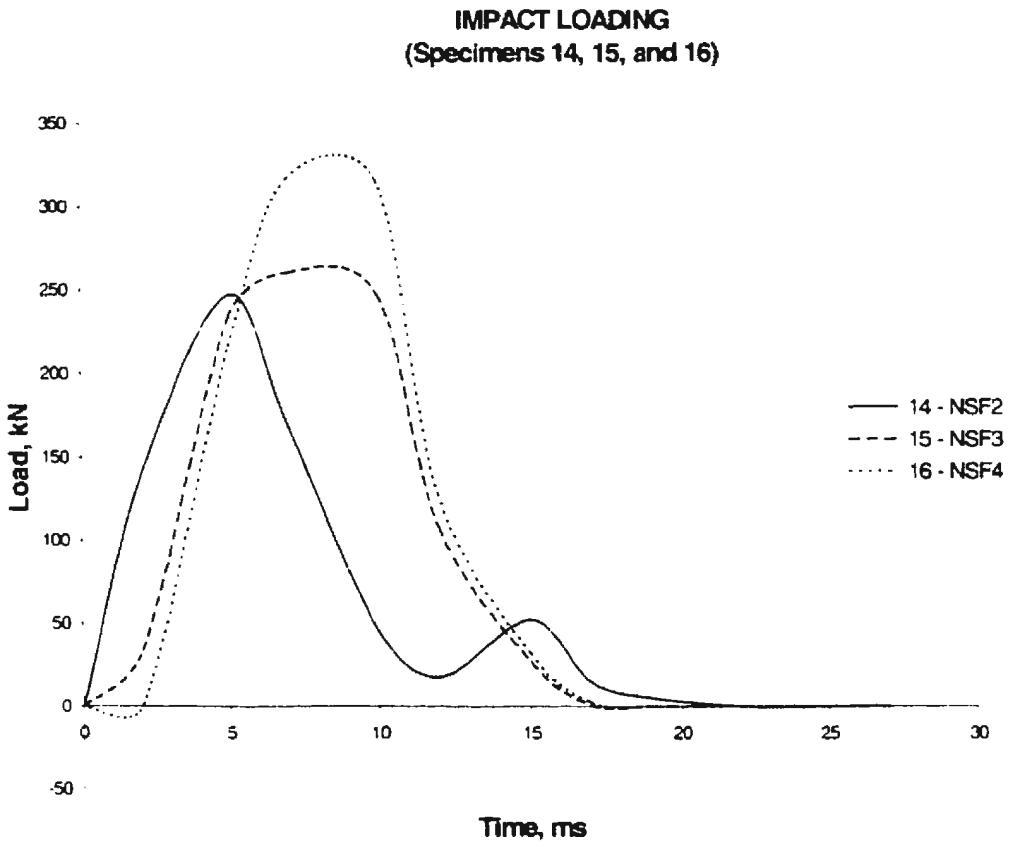

Figure 4.17. Load-time curves for specimens no. 14, 15, and 16

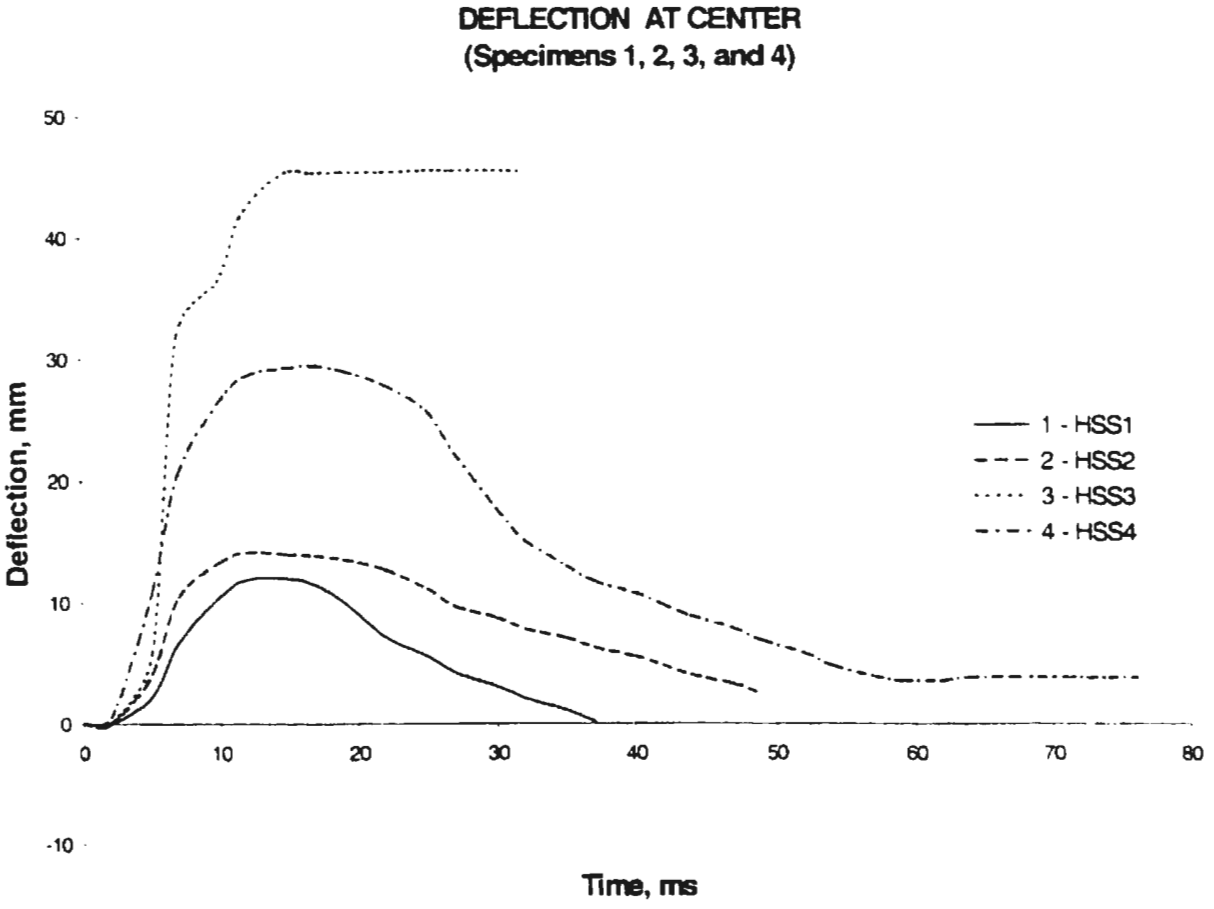

Figure 4.18. Deflection-time curves for specimens no. 1, 2, 3 and 4

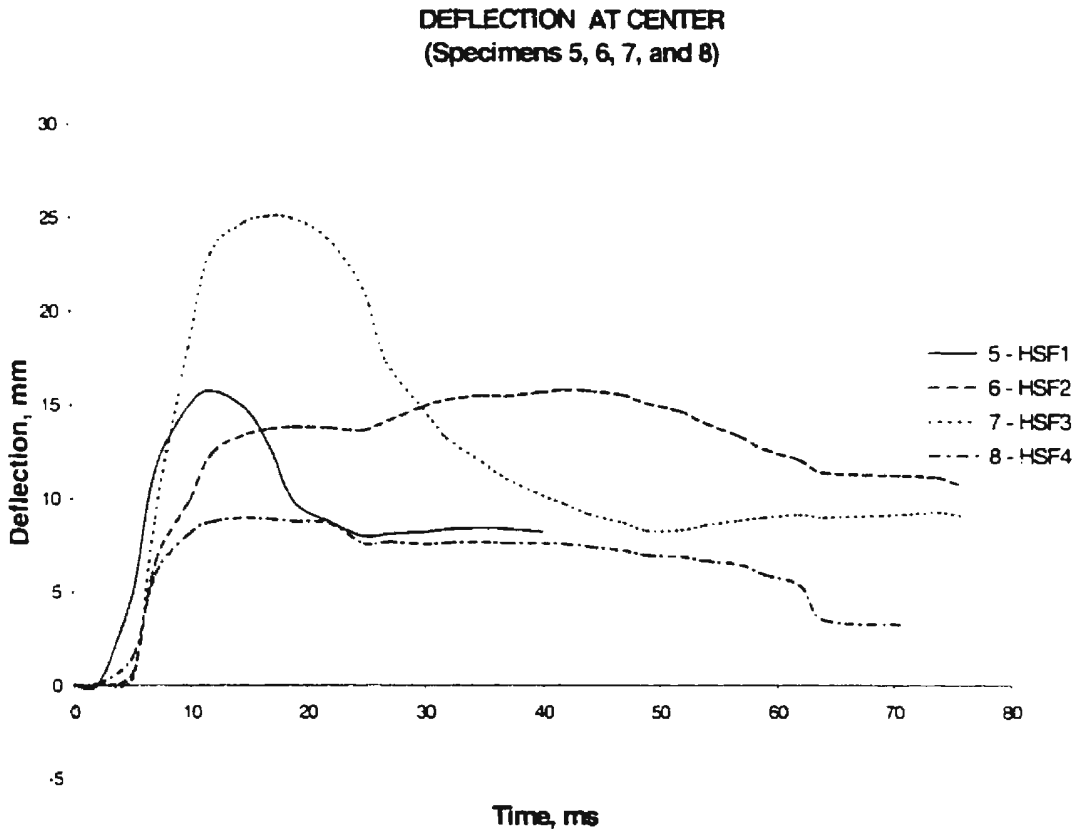

Figure 4.19. Deflection-time curves for specimens no. 5, 6, 7, and 8

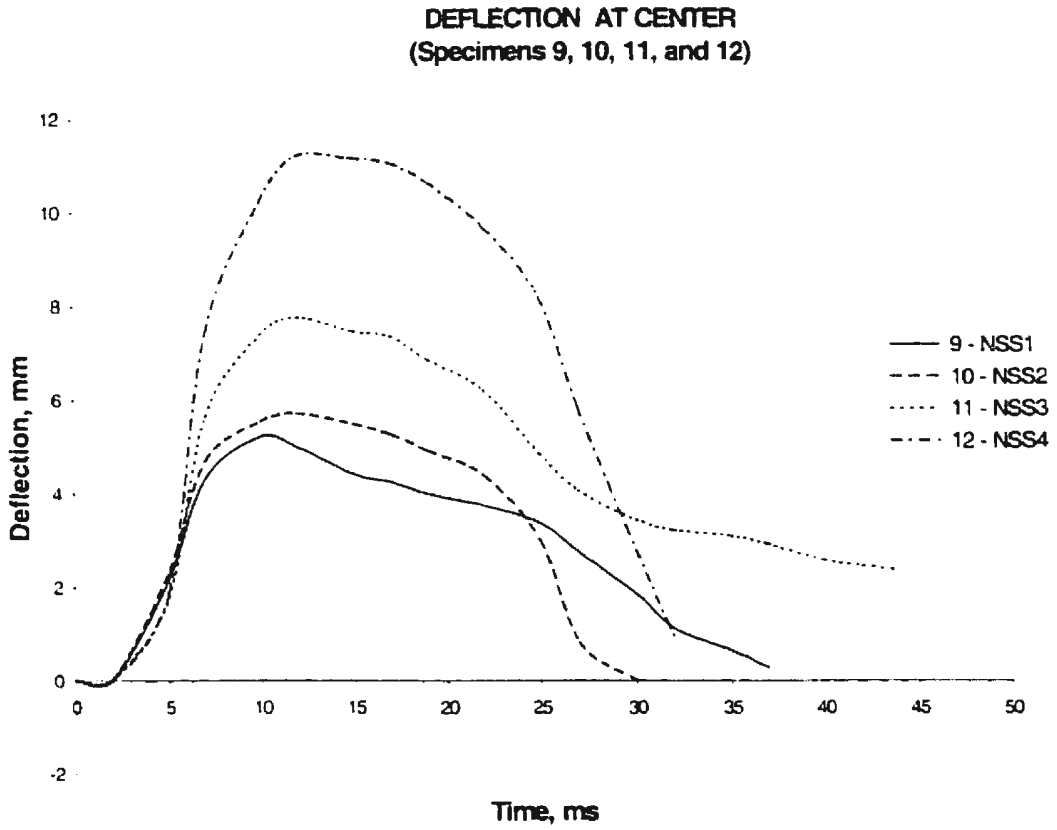

Figure 4.20. Deflection-time curves for specimens no. 9, 10, 11, and 12

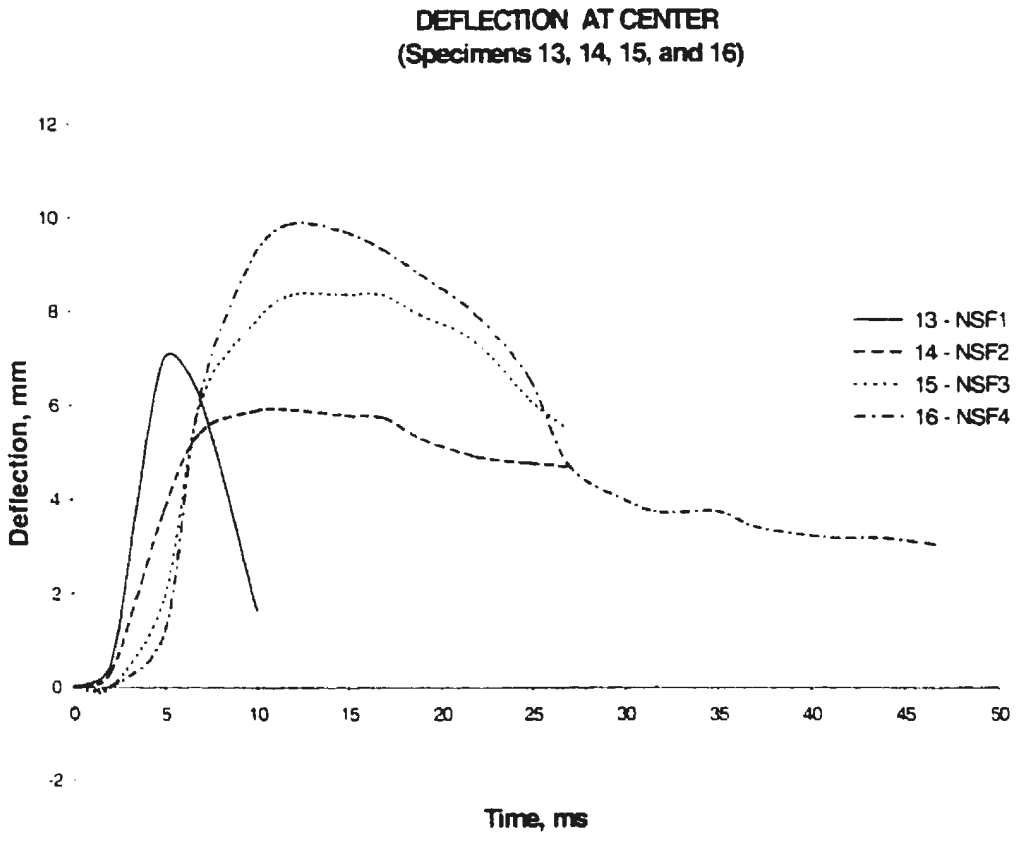

Figure 4.21. Deflection-time curves for specimens no. 13, 14, 15, and 16

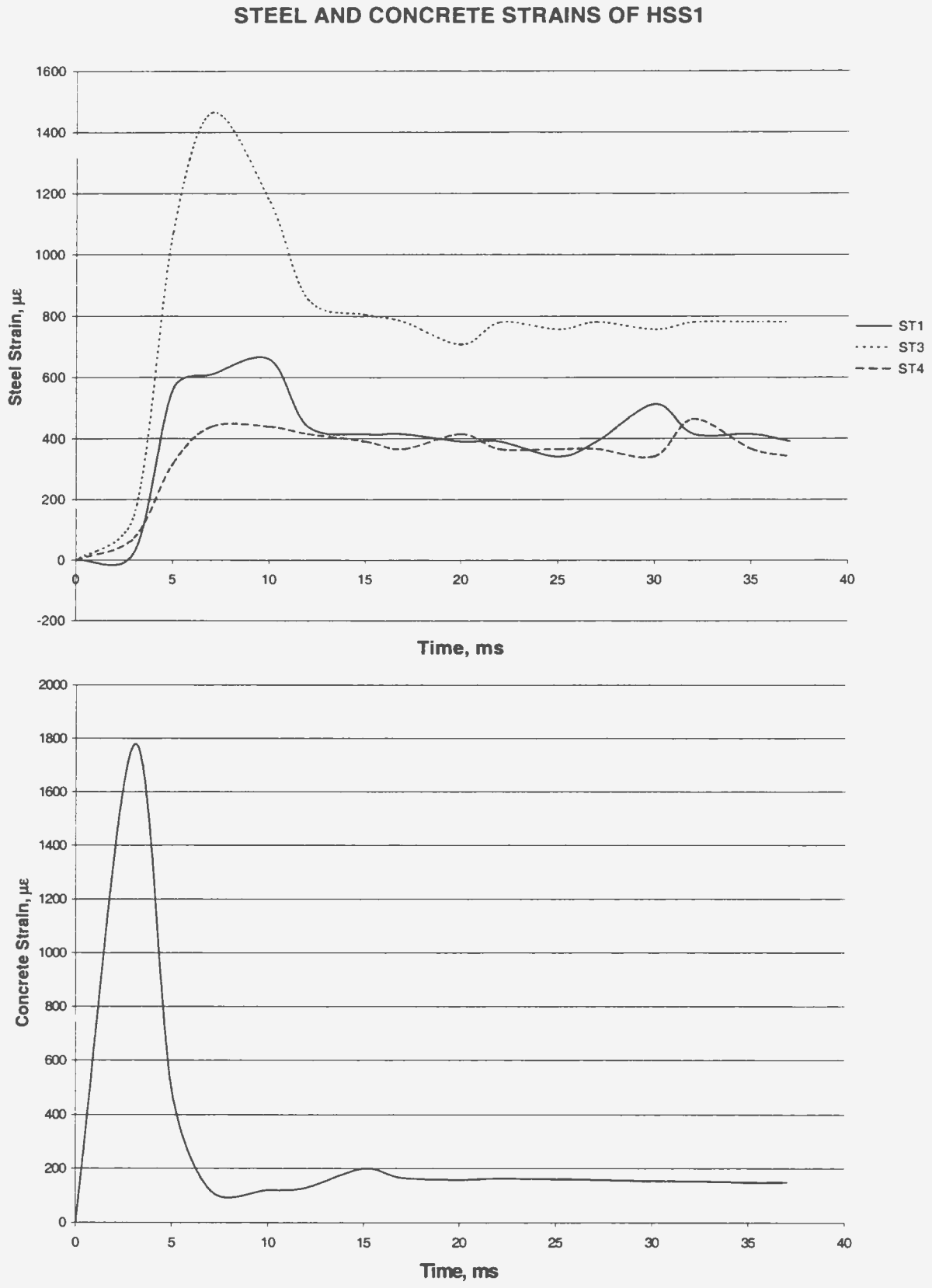

Figure 4.22. Steel and concrete strains of specimen HSS1

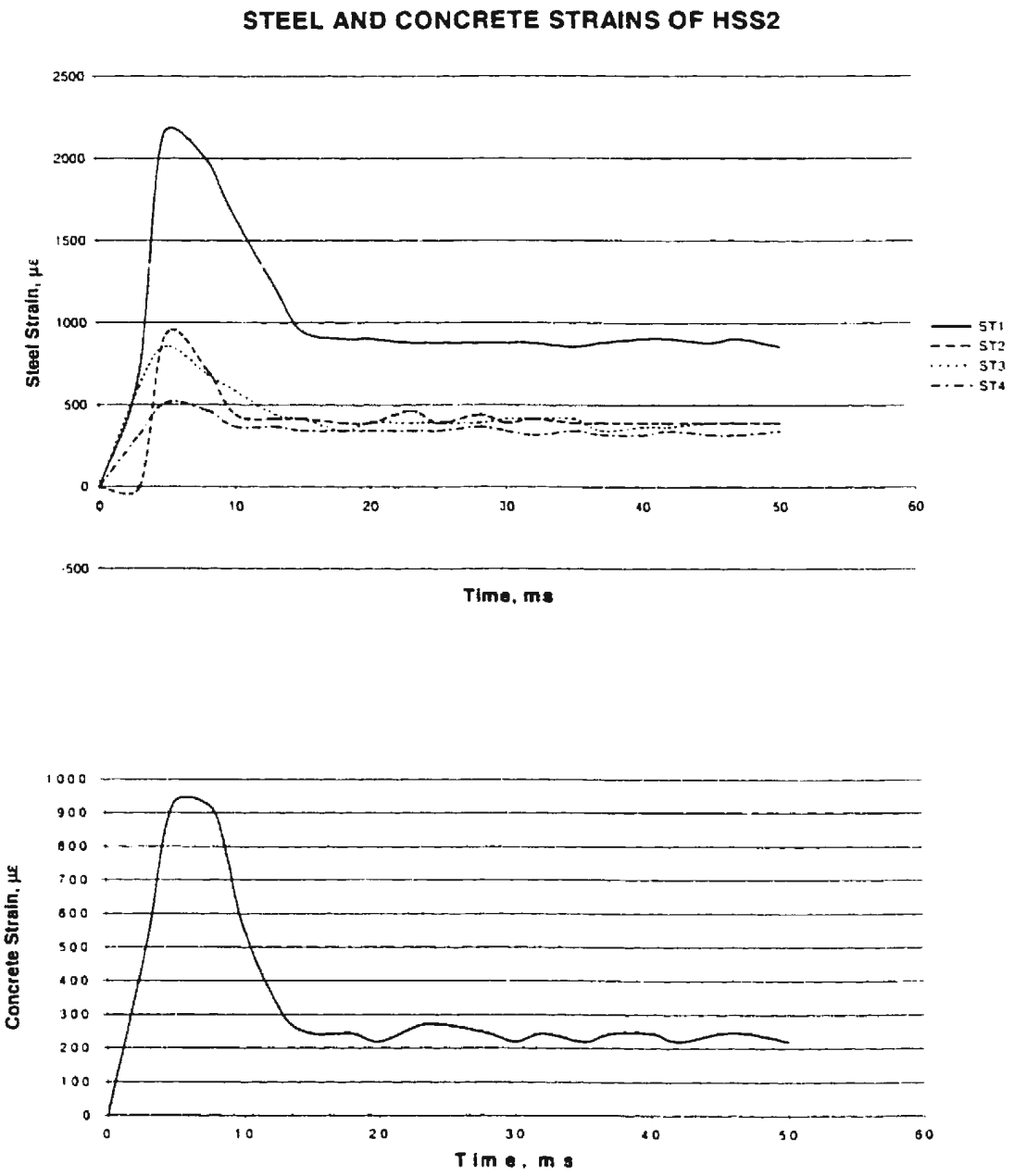

Figure 4.23. Steel and concrete strains of specimen HSS2

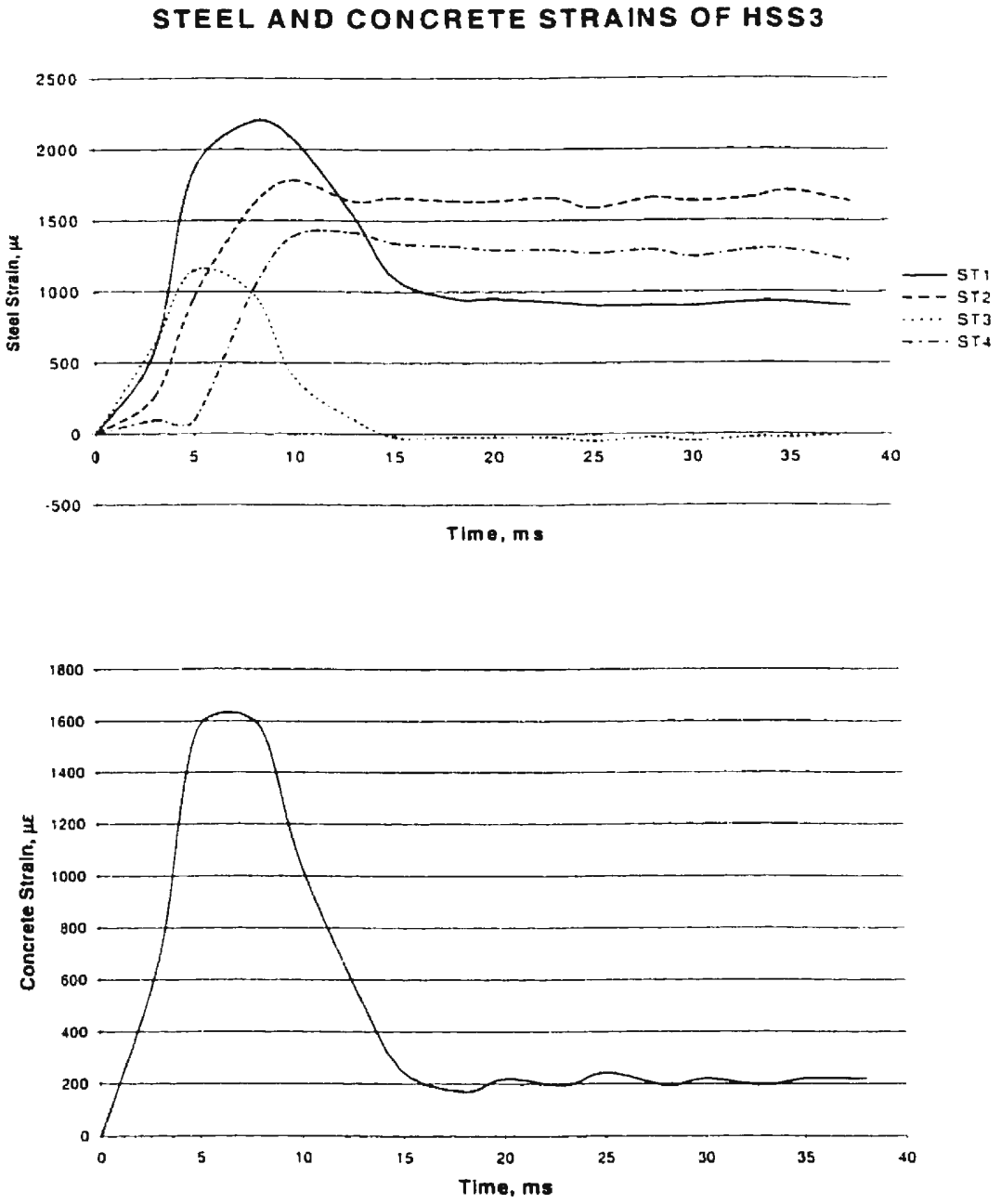

Figure 4.24. Steel and concrete strains of specimen HSS3

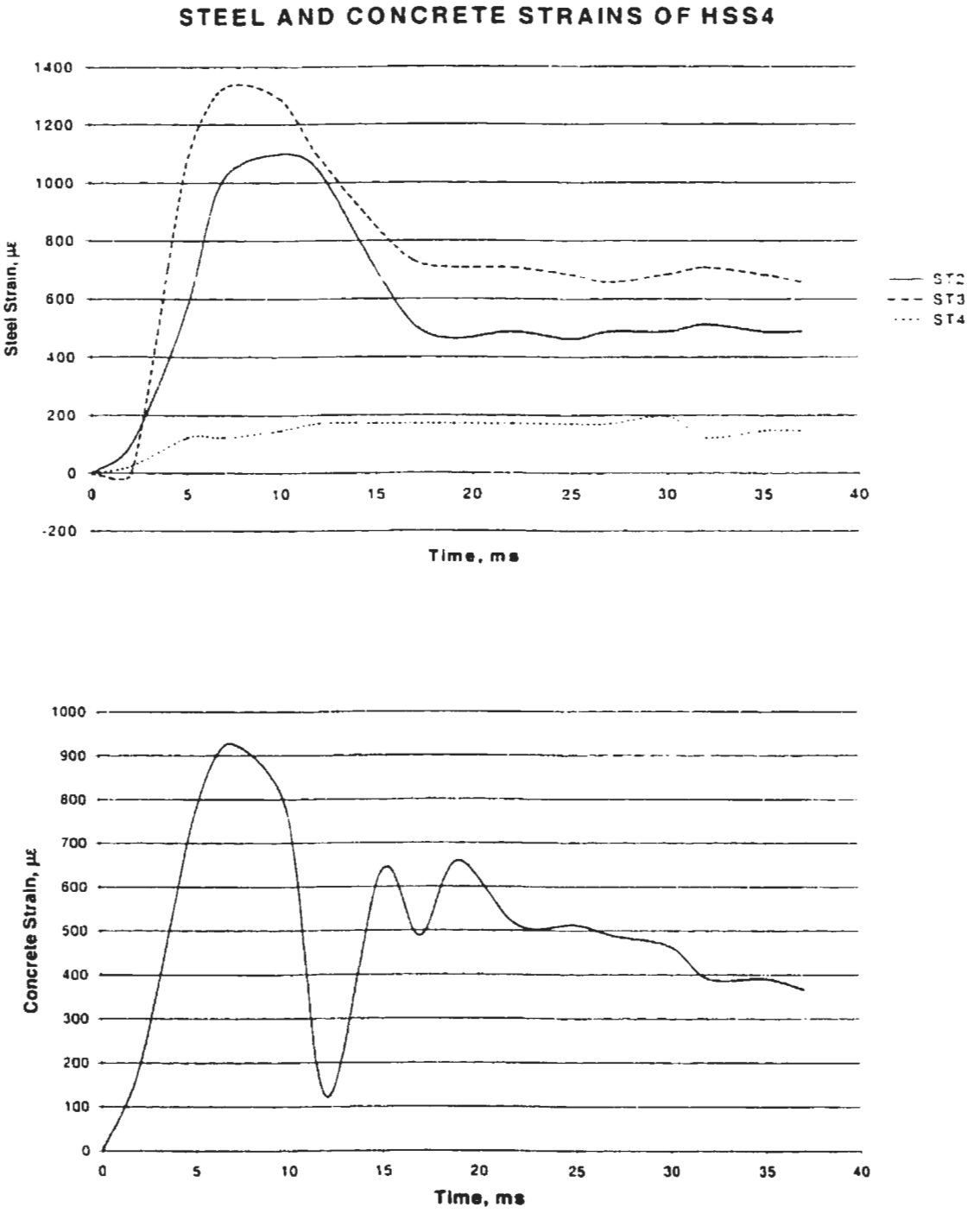

Figure 4.25. Steel and concrete strains of specimen HSS4

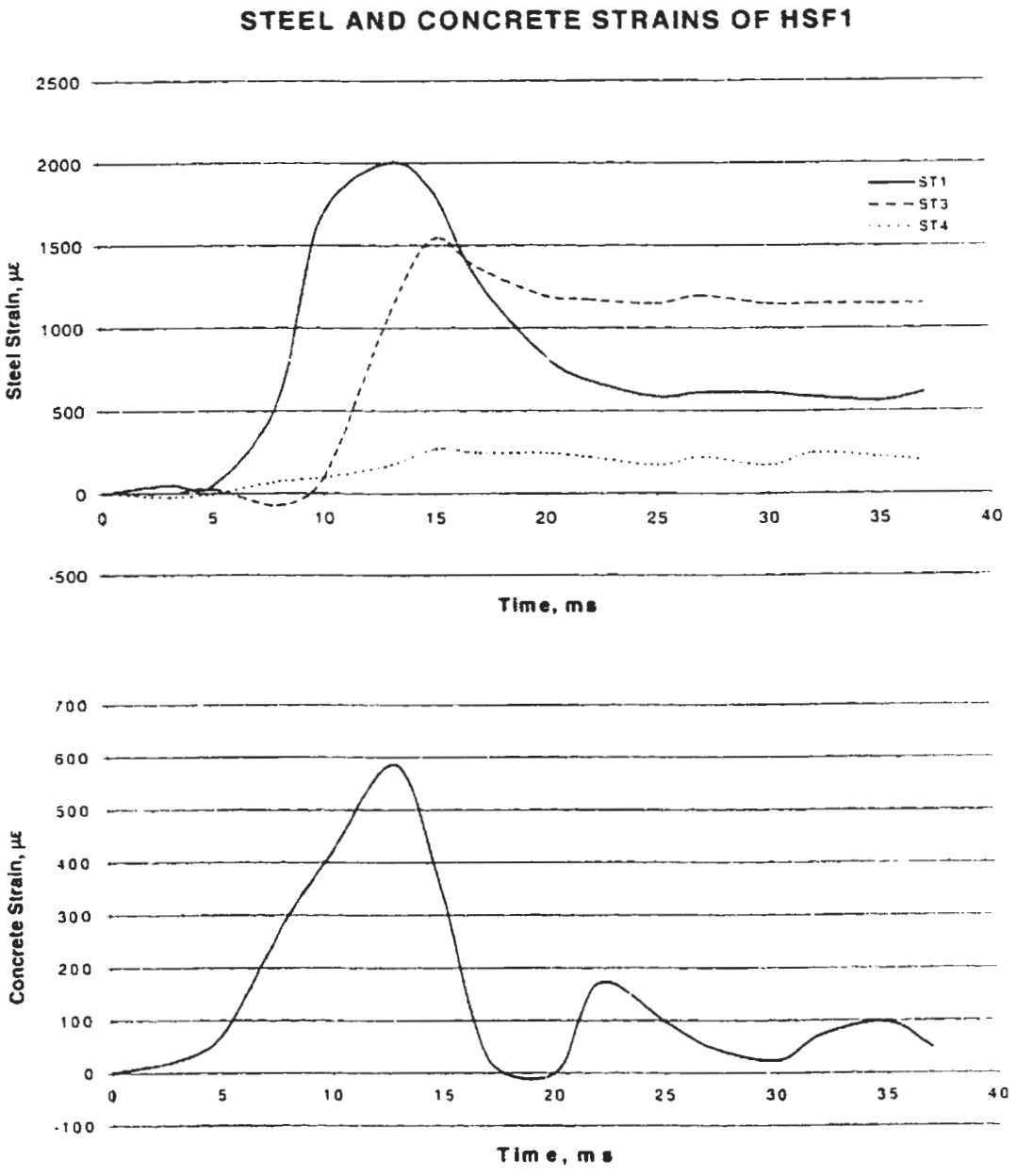

Figure 4.26. Steel and concrete strains of specimen HSF1

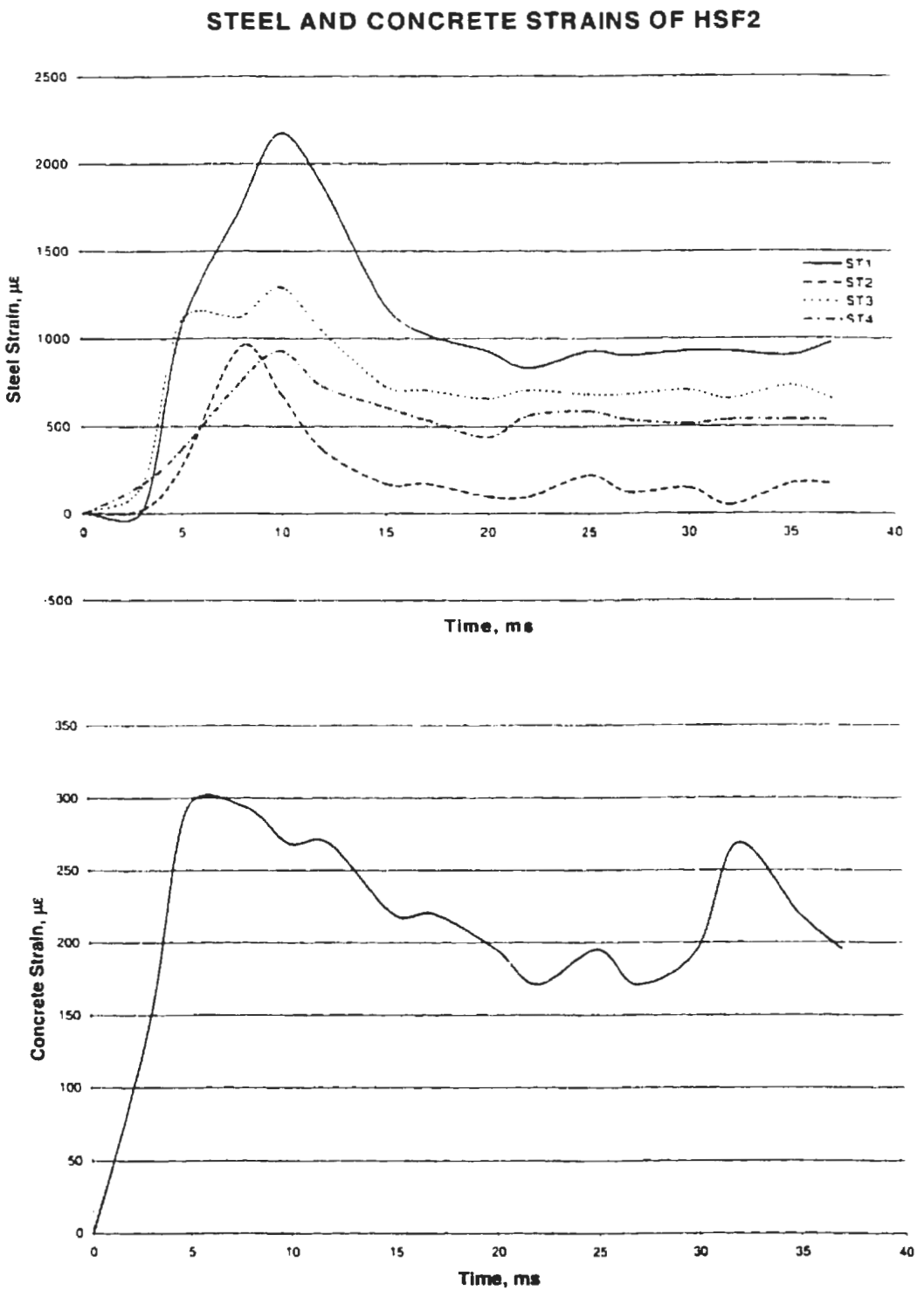

Figure 4.27. Steel and concrete strains of specimen HSF2

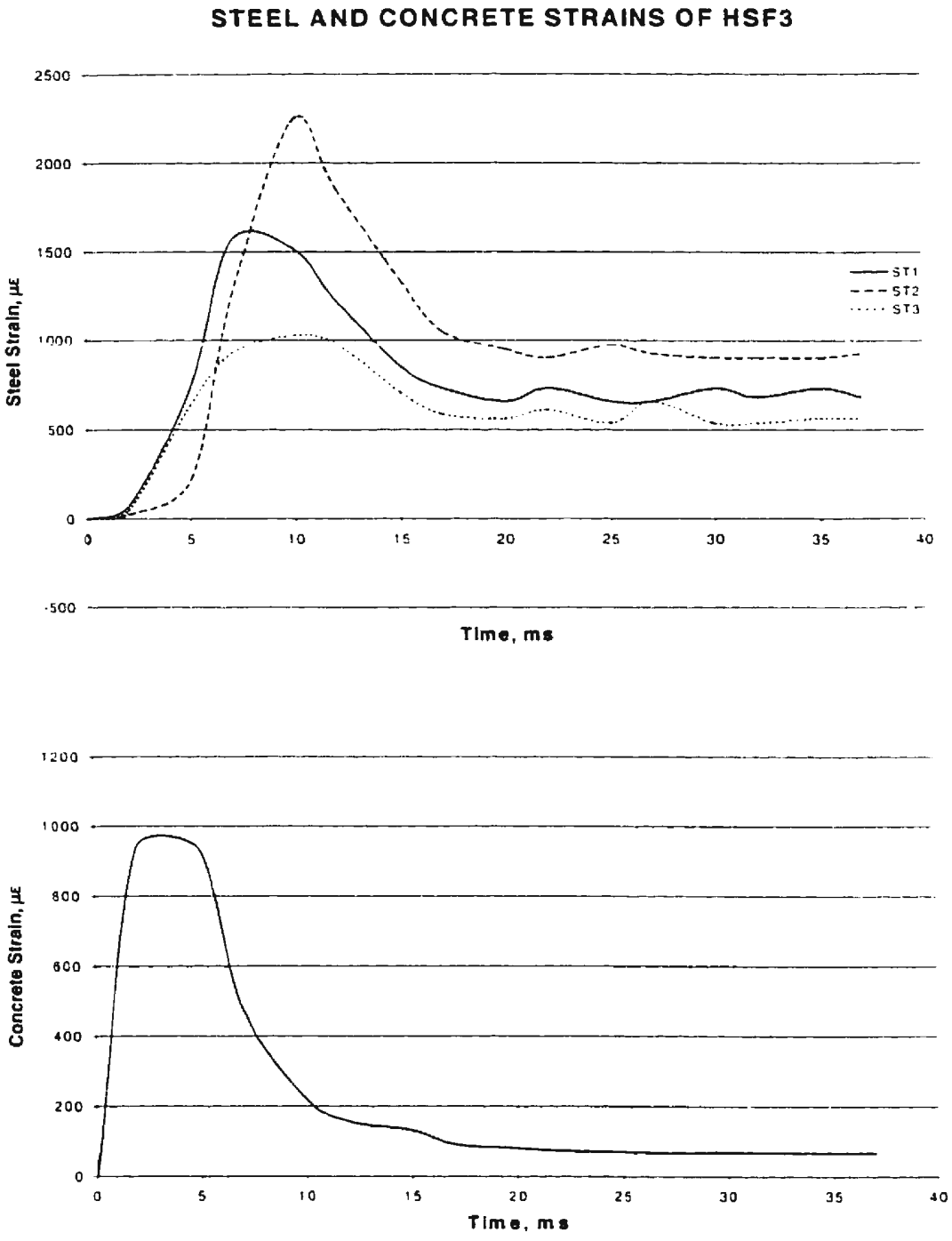

Figure 4.28. Steel and concrete strains of specimen HSF3

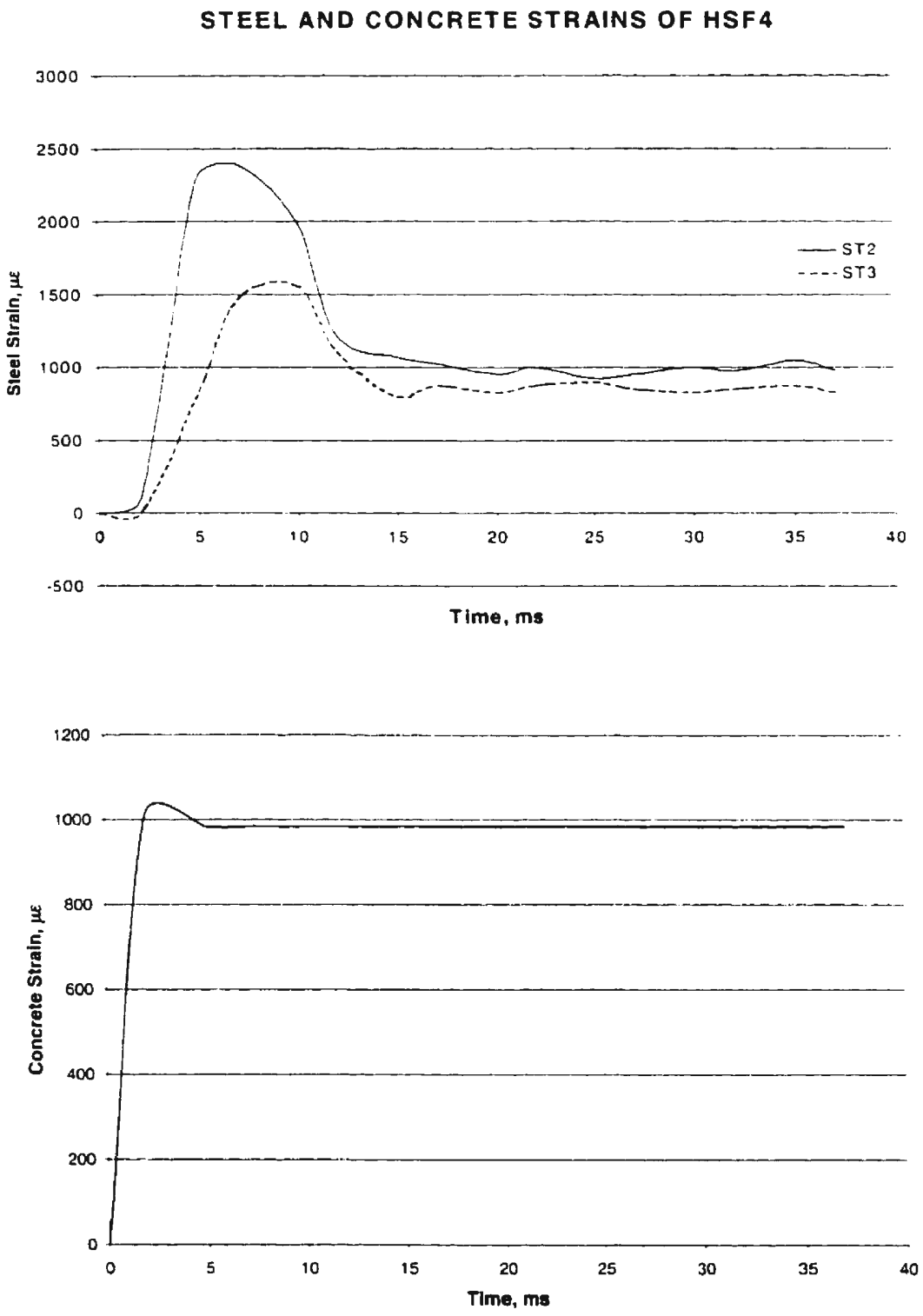

Figure 4.29. Steel and concrete strains of specimen HSF4

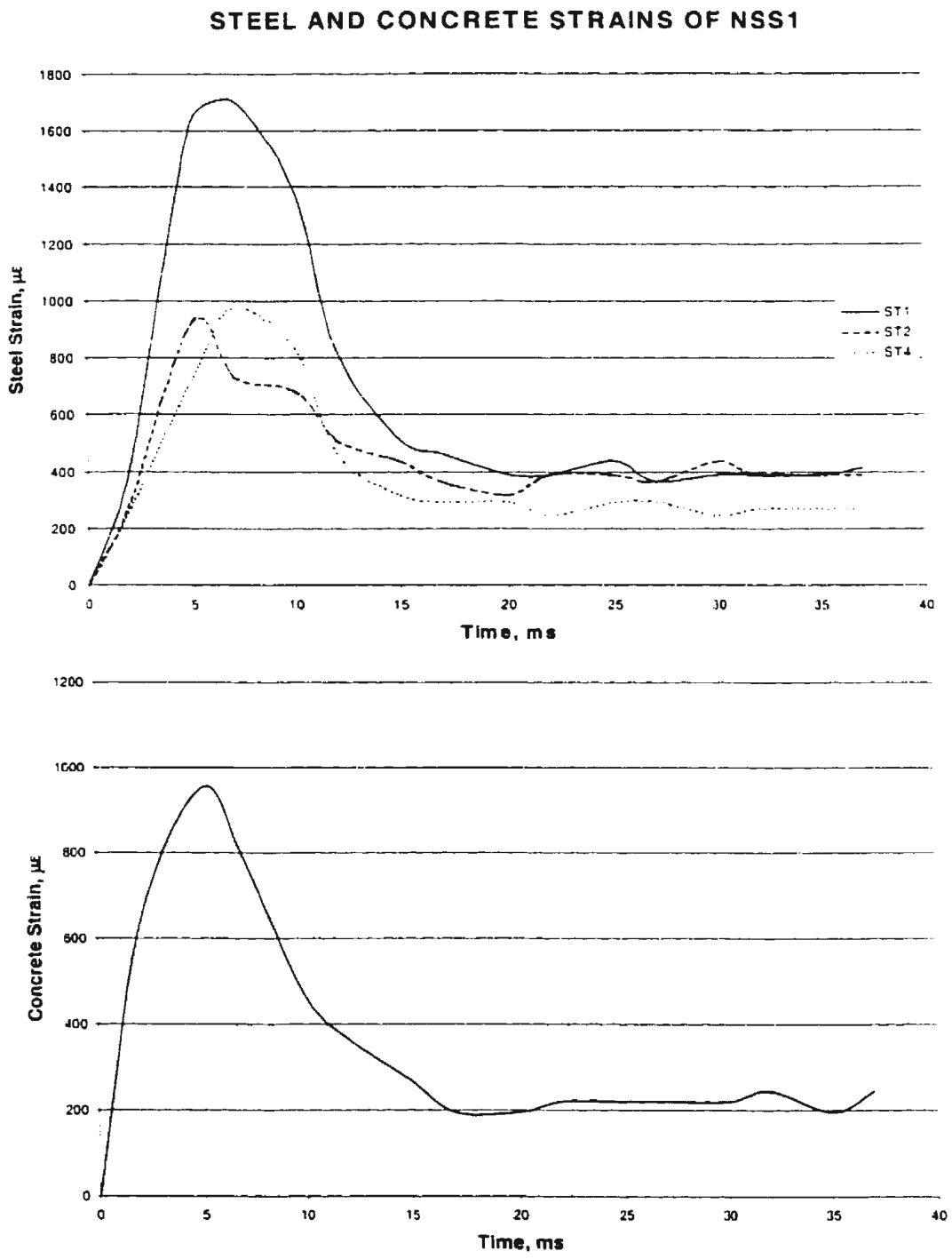

Figure 4.30. Steel and concrete strains of specimen NSS1

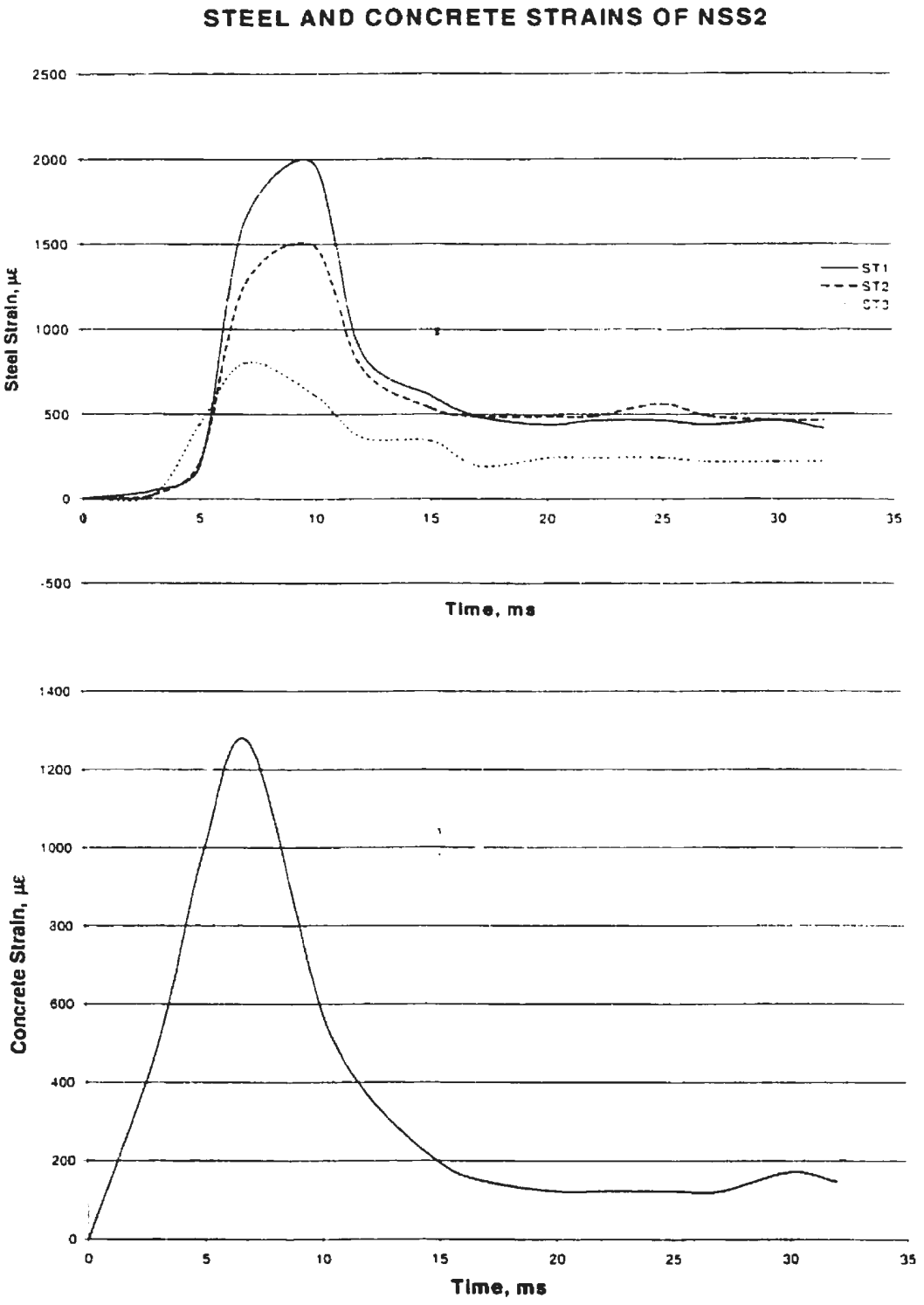

Figure 4.31. Steel and concrete strains of specimen NSS2

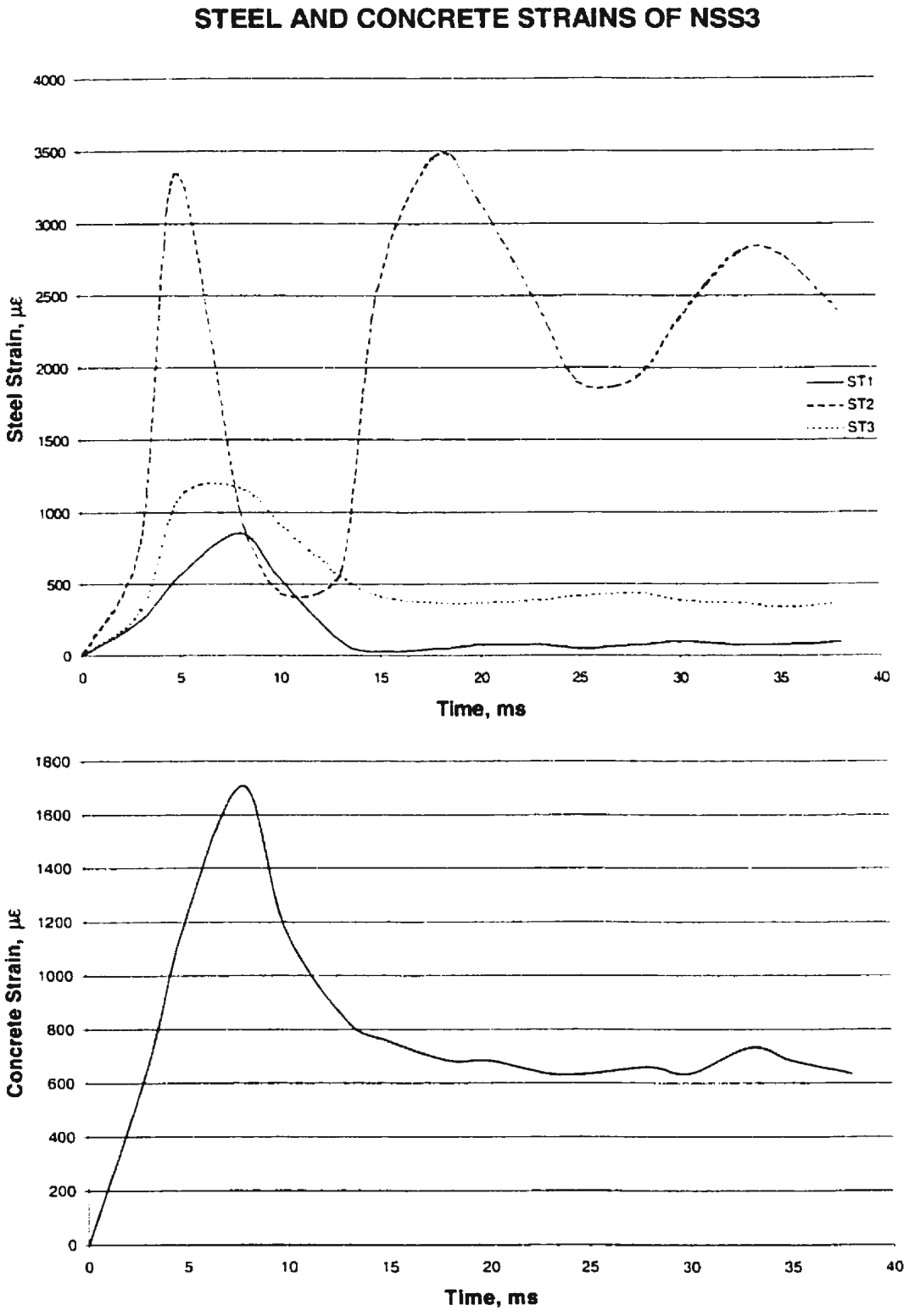

Figure 4.32. Steel and concrete strains of specimen NSS3

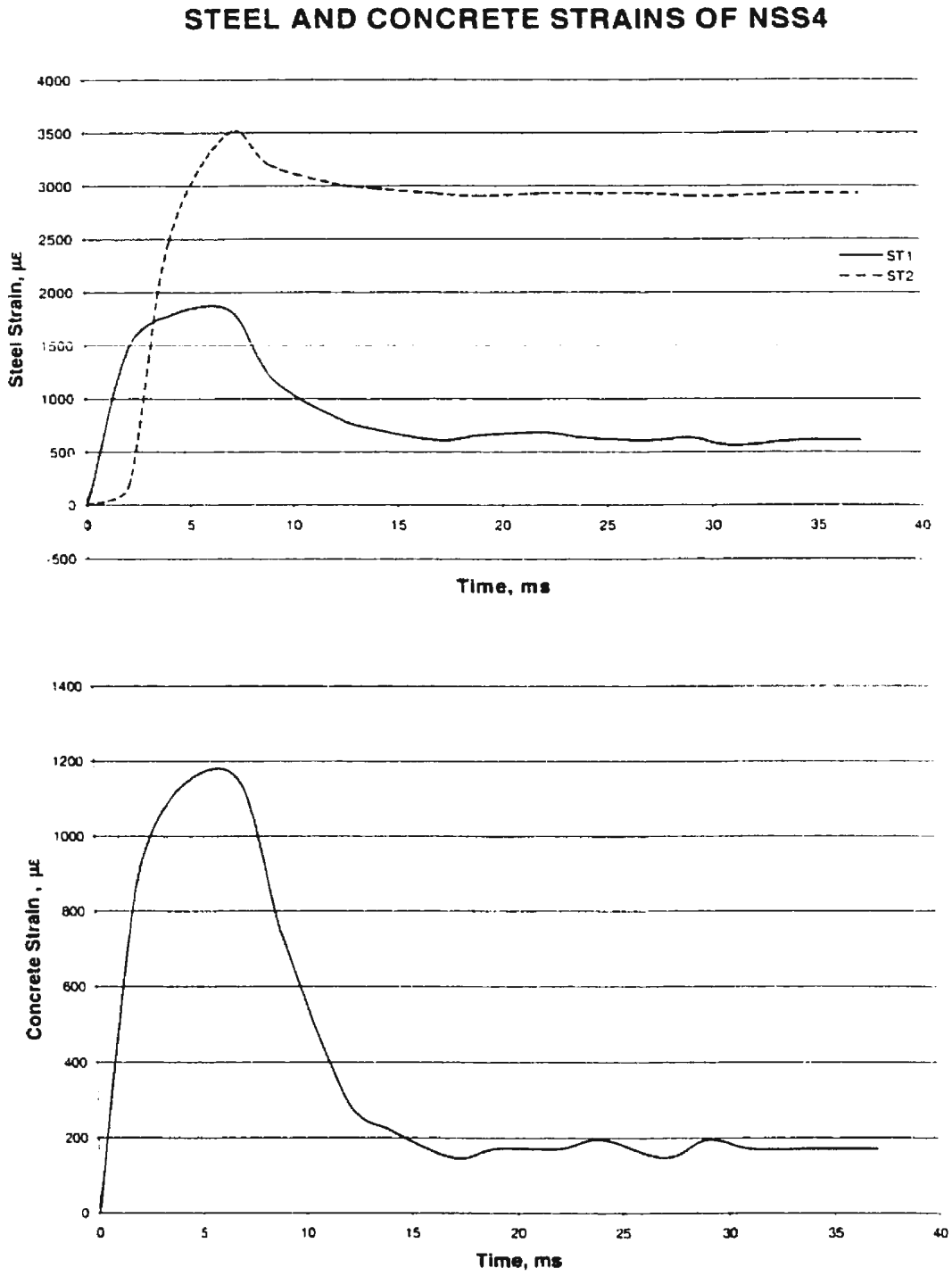

Figure 4.33. Steel and concrete strains of specimen NSS4

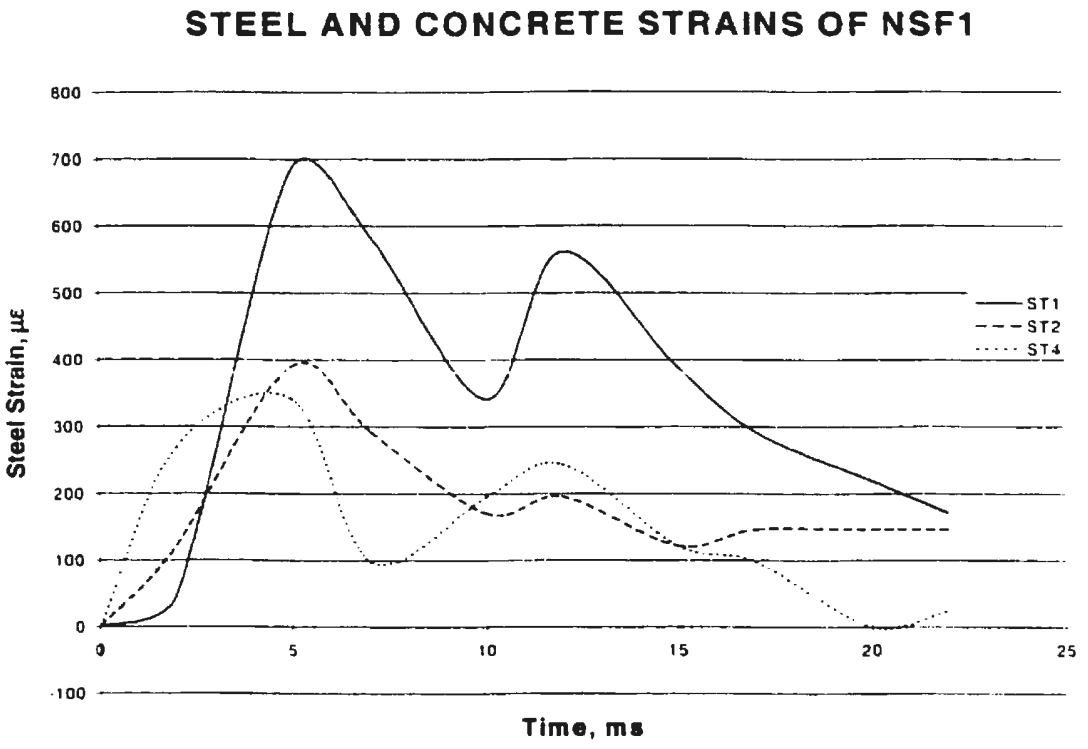

(Concrete strains are not available)

Figure 4.34. Steel and concrete strains of specimen NSF1

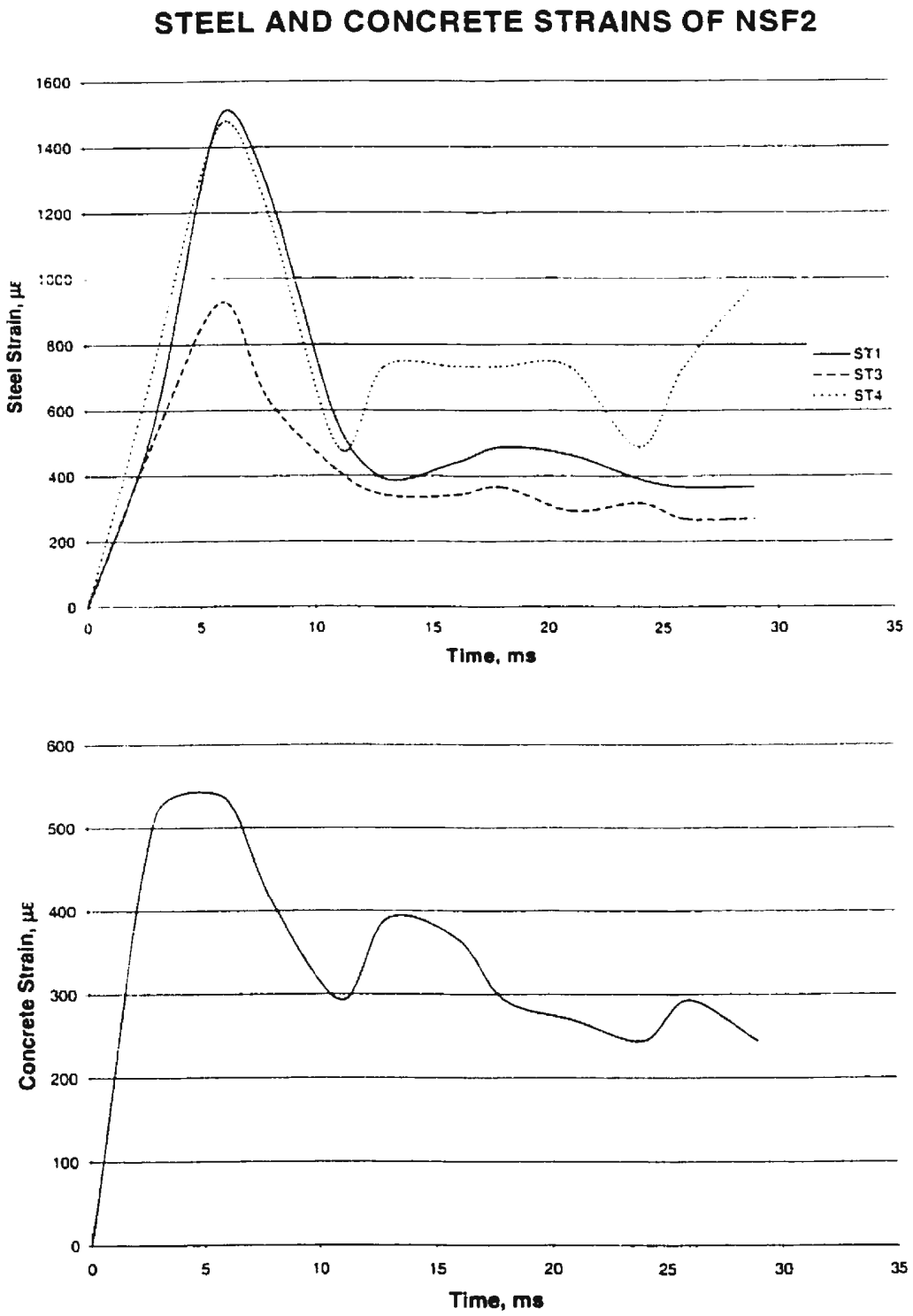

Figure 4.35. Steel and concrete strains of specimen NSF2

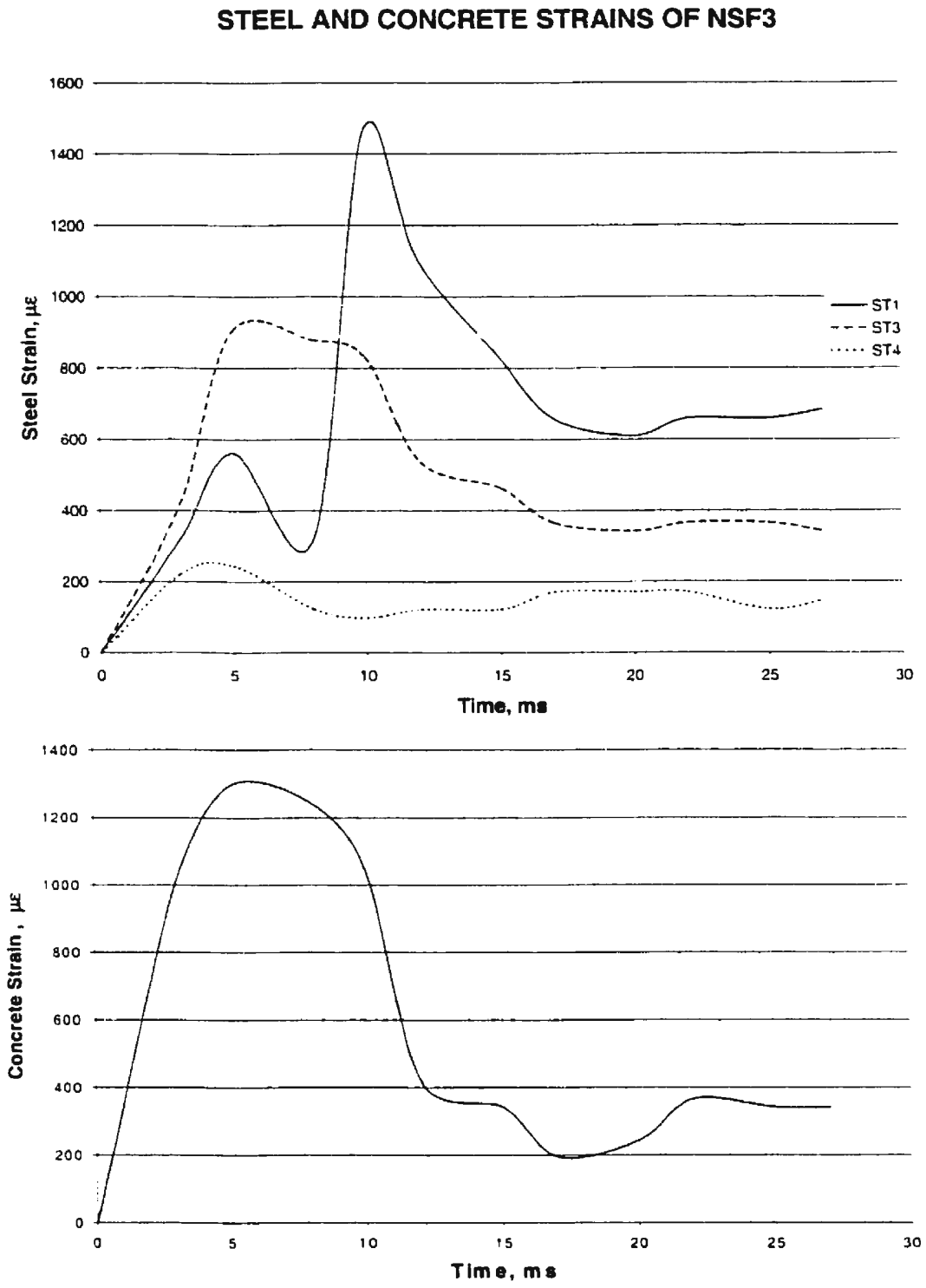

Figure 4.36. Steel and concrete strains of specimen NSF3

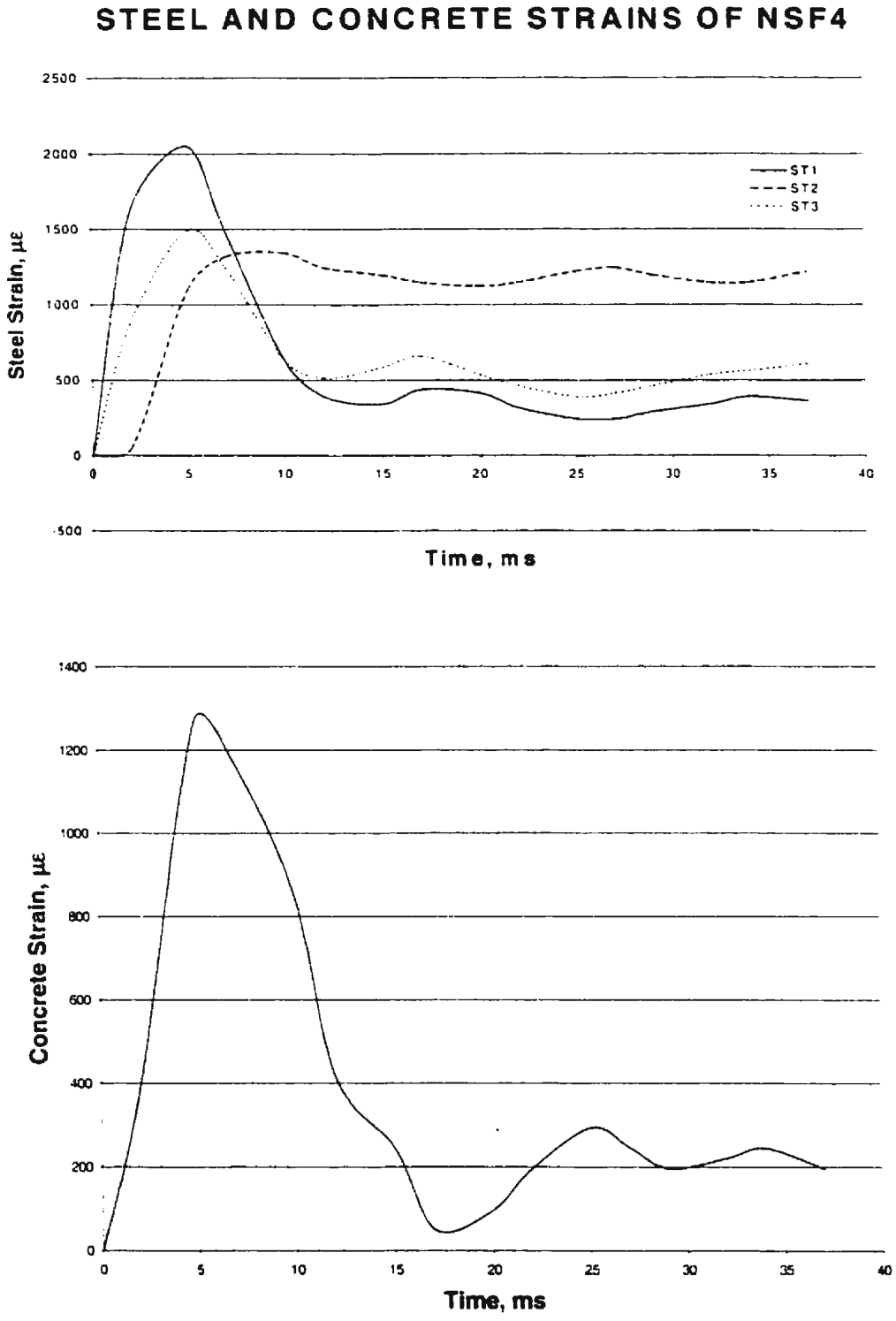

Figure 4.37. Steel and concrete strains of specimen NSF4

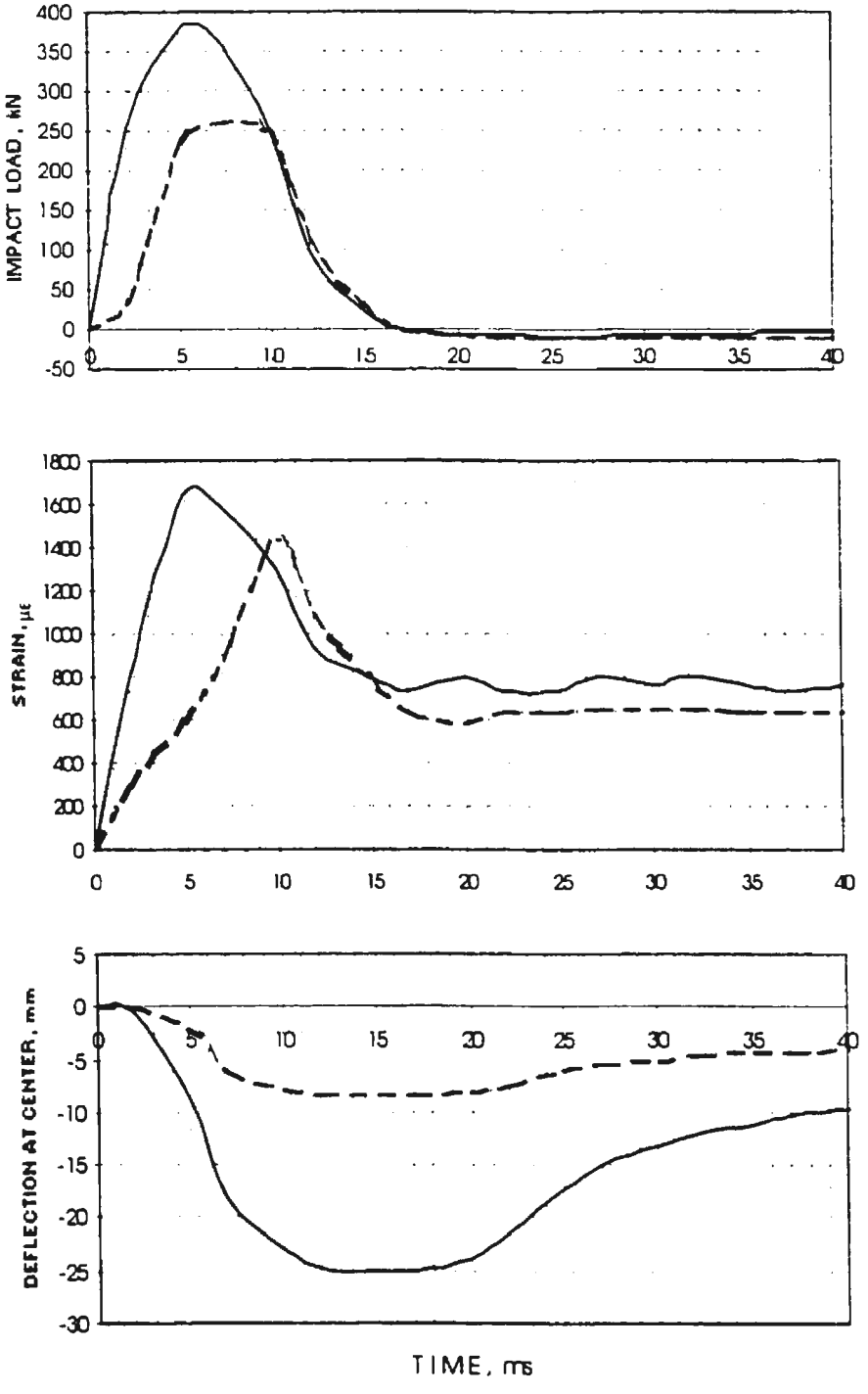

Figure 4.38. High-strength versus normal-strength concrete plate behavior under impact loading

Chapter 5

NUMERICAL EVALUATION

5.1. Introduction

High-strength concrete has a different behavior than normal-strength concrete. It fails by cracking through the aggregates resulting in a smooth fracture surface, while normal-strength concrete fails by the aggregate pulling out of the matrix resulting in a rough fracture surface. This phenomenon can significantly affect the structural performance of concrete material in many applications. For example, the shear transfer mechanism in reinforced concrete structures relies partially on aggregate interlocking across the shear cracks. This mechanism will be reduced greatly for high-strength concrete as a result of its failure mode.

This chapter presents a numerical evaluation of the test results. The performances of numerical evaluation are evaluated against North American codes and some European codes such as BS-8110 (1985), CEB-FIP (1990), and NS-3473 (1992). The analysis will include a comparison between the ratios of dynamic to static impact load. The static punching shear strength capacities according to the current code predictions will be

examined with respect to the experimental results. The values of the critical velocity of perforation calculated from the test results are compared to values calculated according to the dynamic code CEB (1988).

A fracture mechanics analysis was used to evaluate the impact loads on high-strength concrete plate. The fracture mechanics approach is considered a good promising approach for investigating the brittle failure of structural concrete elements accurately. The fracture mechanics approach is used to investigate the effect of the rate of loading on a brittle material based on linear elastic fracture mechanics (LEFM). One of the objectives of the present study is to provide the design engineers with a rate sensitivity number for high-strength concrete plates.

5.2. Impact Load

In order to calculate the impact load of the test results, the vertical equation of dynamic equilibrium, ignoring damping, can be written as:

$$F(t) = m_t . a_t \tag{5.1}$$

where $F(t)$ is the total force, a_t is the total accelerations, and the total mass m_t is the sum of the projectile mass and half of the specimen mass. If a_t is equal to the projectile acceleration a_p, while m_p and m_s are the masses of the projectile and the specimen, respectively, Equation (5.1) can then be written as:

$$F(t) = \left(m_p + 0.5\, m_s\right) a_p \tag{5.2}$$

Equation (5.2) can then be used for calculating the impact test load $P_{test} = F(t)$

5.3. Punching Shear (Static Capacity)

The design shear strength equation incorporated in building codes are a direct result of empirical procedures developed from laboratory tests. As mentioned previously, the North American codes are based principally on Moe's (1961) work, while the British codes are based mainly on Regan's (1981) work. It becomes necessary to examine the existing formula strength of high-strength concrete plates of 80 MPa compressive strength.

Maximum shear stress resistance provided by a concrete plate without shear reinforcement, v_c, calculated according to ACI-318 (1995) under S.I. unit, shall be the smallest of:

$$v_c = \left(1 + \frac{2}{\beta_c}\right)\frac{1}{6}\sqrt{f_c'} \tag{5.3a}$$

$$v_c = \left(\frac{\alpha_s\, d}{b_o} + 2\right)\frac{1}{12}\sqrt{f_c'} \tag{5.3b}$$

$$v_c = \frac{1}{3}\sqrt{f_c'} \tag{5.3c}$$

where, β_c = ratio of long side to short side of the concentrated load

f_c' = specified compressive strength of concrete

α_s = factor which adjusts v_c for support dimensions

d = distance from extreme compression fiber to centroid of tension reinforcement

b_o = perimeter of critical section for shear in plates.

The Committee recommended that the following design equation for calculating ultimate shear load,

$$V_u = v_u \, b_o \, d \tag{5.4}$$

The critical section shall be a section perpendicular to the plane of the plate and located so that its perimeter, b_o, is a minimum. But, the section need not approach closer than $d/2$ to the perimeter of the concentrated load. Therefore, $b_o = \pi \, (c + d/2)$, where c is the diameter of loaded area.

The British Codes, BS-8110 (1985), and code of practice for structural use of concrete, CP-110 (1972), recommended the following equation for calculating punching shear capacity as:

$$V_u = K_a \, K_{sc} \sqrt[3]{\frac{100 \, A_s}{bd} f_{cu}} \, (2.69 \, d)\left(\sum C + 7.85 \, d\right) \tag{5.5}$$

where, V_u = ultimate shear force (N)

K_a = 0.13 for normal concrete 0.105 for lightweight concrete

K_{sc} = 1.15 [4 π (column area) / (column perimeter)^2]$^{1/2}$

$\frac{100 \, A_s}{b \, d}$ = steel ratio

f_{cu} = cube strength of concrete (MPa)

d = effective depth of the slab (mm)

$\sum C$ = perimeter of the column (mm)

The shear perimeter for a rectangle column is located at distance 1.25 d out from the column, for a circular column is located 1.25 d out from the column. According to the

code predictions, the above limit of 40 MPa of the cube strength of Equation (5.5) was neglected when calculating the shear strength.

Nominal shear stress, v_c, according to CEB-FIP (1990) is:

$$v_c = 0.18 \left(1 + \sqrt{\frac{200}{d}}\right) \sqrt[3]{100\ \rho\ f_c'} \qquad (5.6)$$

The highest concrete strength considered in CEB-FIP (1990) is 80 MPa. The control perimeter is the minimum length taken from $2d$ from the concentrated load periphery. Equation (5.4) can also be used for calculation the punching shear capacity, where, the perimeter b_o for circular loaded area is $= \pi\ (c + 2d)$.

The Norwegian code NS-3473 (1992) specifies the punching shear capacity as:

$$V_{cd} = 0.33\ (f_{td} + k_A\ \rho / \gamma_c)\ u\ d\ k_v \leq 0.66\ f_t\ u\ d\ k_v \qquad (5.7)$$

where, f_{td} = design tensile strength of concrete

γ_c = material coefficient for reinforced concrete = 1.0

k_A = 100 N/mm^2

$1.0 < k_v\ (= 1.5\ d / d_1) < 1.4$, d_1 = 1.0 m

d = mean plate depth in the two reinforcement directions

u = the length of perimeter of the governing section at a distance 1.0 d from loaded area

ρ = tension reinforcement ratio.

Compressive strength is usually given as the reference value for a concrete grade. According to the CEB-FIP (1990) recommendation for mean values, the tensile strength of concrete can be estimated from compressive strength by:

$$f_{td} = 0.20 f_c^{2/3} \quad (5.8)$$

The measured test impact loads P_{test} and the calculation of the shear strength by different codes are tabulated in Table 5.1.

5.4. Code Recommendations

In order to evaluate the validity of the current design specifications, the calculations of the formulas for static punching shear capacities listed in Table 5.1 are to be discussed briefly in present section. The static punching shear tests of all specimens can be used as a reference for all of the dynamic impact tests.

The static punching shear capacities calculated according to ACI-318 (1995) and the dynamic test results are used for the dynamic shear capacities. The ratio of dynamic to static punching shear is in the range of 1.39-2.31; it the same ratio ranged between 1.50-1.82, 1.36-1.65, and 1.87-2.33 according to the BS-8110 (1985), CEB-FIP (1990), and NS-3473 (1992), respectively.

The impact test results indicate that the punching failures were at a much higher load level than the static punching shear capacity. The ratio of impact versus static load according to the North American codes is normally varied between a wider range compared to the European codes. The ratio of dynamic to static punching shear according to NS-3473 (1992) is almost consistent and higher than other codes predictions. In conclusion, the results can be used as a design guide for engineers to predict the dynamic capacity of high-strength concrete plates.

Table 5.1. Comparison of test results (impact) with code predictions (static)

No.	Specimen	fc' (MPa)	ρ (%)	P_{impact} (kN)	P_{static}(Code) ACI (kN)	BS 8110 (kN)	CEB-FIP (kN)	NS 3473 (kN)	P_{impact}/P_{static} ACI	BS 8110	CEB-FIP	NS 3473
1	HSS1	81.7	0.95	338.17	240.45	196.45	214.52	164.73	1.41	1.72	1.58	2.05
2	HSS2	81.7	1.26	354.27	240.45	215.84	235.69	175.56	1.47	1.64	1.50	2.02
3	HSS3	81.7	1.90	370.37	232.12	236.81	261.70	189.70	1.60	1.56	1.42	1.95
4	HSS4	81.7	2.32	380.03	232.12	253.12	279.72	203.76	1.64	1.50	1.36	1.87
5	HSF1	79.1	0.95	N/A	236.60	194.34	212.22	161.90	N/A	N/A	N/A	N/A
6	HSF2	79.1	1.26	328.50	236.60	213.52	233.17	172.73	1.39	1.54	1.41	1.90
7	HSF3	79.1	1.90	376.81	228.39	234.28	258.90	186.99	1.65	1.61	1.46	2.02
8	HSF4	79.1	2.32	389.70	228.39	250.40	276.72	201.05	1.71	1.56	1.41	1.94
9	NSS1	33.1	0.95	225.44	153.05	145.36	158.73	105.21	1.47	1.55	1.42	2.14
10	NSS2	33.1	1.26	244.77	153.05	159.71	174.40	116.04	1.60	1.53	1.40	2.11
11	NSS3	33.1	1.90	305.96	147.74	175.23	193.65	132.65	2.07	1.75	1.58	2.31
12	NSS4	33.1	2.32	341.39	147.74	187.29	206.98	146.71	2.31	1.82	1.65	2.33
13	NSF1	36.6	0.95	231.88	160.94	150.31	164.14	110.20	1.44	1.54	1.41	2.10
14	NSF2	36.6	1.26	251.21	160.94	165.15	180.34	121.03	1.56	1.52	1.39	2.08
15	NSF3	36.6	1.90	273.75	155.36	181.20	200.25	137.44	1.76	1.51	1.37	1.99
16	NSF4	36.6	2.32	315.62	155.36	193.67	214.03	151.50	2.03	1.63	1.47	2.08

5.5. Critical Velocity of Perforation

The values of the critical velocity of perforation can be calculated according the formula:

$$V_c = 1.3\, W^{1/6}\, f_c^{'1/2} \left(\frac{p h^2}{\pi M} \right)^{2/3} (\rho + 0.3)^{1/2} \qquad (5.9)$$

where, W = concrete density

$f_c^{'}$ = cylinder compressive strength

p = missile perimeter

h = concrete slab thickness

M = missile mass

ρ = reinforcement quantity.

The calculations of critical velocity then are given in Table 5.2 as follows:

Table 5.2. Critical velocity of perforation

Specimen	f_c (MPa)	W (kg/m3)	p (mm)	h mm)	M (kg)	ρ (%)	Vc (m/s)
HSS1	81.7	2400	304.8	100	220	0.95	7.05
HSS2	81.7	2400	304.8	100	220	1.26	7.61
HSS3	81.7	2400	304.8	100	220	1.90	8.51
HSS4	81.7	2400	304.8	100	220	2.32	8.98
HSF1	79.1	2400	304.8	100	220	0.95	6.94
HSF2	79.1	2400	304.8	100	220	1.26	7.49
HSF3	79.1	2400	304.8	100	220	1.90	8.37
HSF4	79.1	2400	304.8	100	220	2.32	8.83
NSS1	33.1	2400	304.8	100	220	0.95	4.49
NSS2	33.1	2400	304.8	100	220	1.26	4.85
NSS3	33.1	2400	304.8	100	220	1.90	5.41
NSS4	33.1	2400	304.8	100	220	2.32	5.71
NSF1	36.6	2400	304.8	100	220	0.95	4.72
NSF2	36.6	2400	304.8	100	220	1.26	5.10
NSF3	36.6	2400	304.8	100	220	1.90	5.69
NSF4	36.6	2400	304.8	100	220	2.32	6.01

In order to evaluate the prediction of Equation (5.9), the calculated critical velocity is then compared to the actual test velocity. The comparison between the calculated critical velocity and the actual test velocity are given in Table 5.3. below:

Table 5.3. Calculated critical velocity compared with test velocity

Series No:	Notation	Maximum Acceleration (g)	Maximum Displacement at Center (mm)	Critical Velocity from code (m/s)	Test Velocity (m/s)	Ratio $\frac{V\ test}{V\ code}$
1	HSS1	110	12	7.05	7.00	0.99
2	HSS2	110	14	7.61	7.67	1.01
3	HSS3	115	23	8.51	8.29	0.97
4	HSS4	118	29	8.98	8.86	0.98
5	HSF1	-	16	6.94	7.00	1.01
6	HSF2	102	17	7.49	7.67	1.02
7	HSF3	115	25	8.37	8.29	0.99
8	HSF4	121	35	8.83	8.86	1.00
9	NSS1	70	6	4.49	5.42	1.21
10	NSS2	76	8	4.85	6.26	1.29
11	NSS3	95	11	5.41	7.00	1.29
12	NSS4	106	11	5.71	7.67	1.34
13	NSF1	72	5	4.72	4.43	0.94
14	NSF2	78	6	5.10	4.95	0.97
15	NSF3	85	8	5.69	5.42	0.95
16	NSF4	98	10	6.01	5.86	0.98

It can be seen from Table 5.3 that under impact loading, both of the measured and calculated accelerations for high-strength concrete were higher than normal-strength concrete. The acceleration for heavy reinforcement plates were higher than that for lighter reinforcement. This indicates that the acceleration magnitude increased when the concrete strength and steel reinforcement ratio were increased. Increasing concrete strength from normal-strength to high-strength, from about 35 MPa to 80 MPa, increased

the acceleration by about 40% in the case of simply-supported and increased about 30% in the case of fixed support. In addition, as the steel reinforcement ratio increased by about 0.5%, the acceleration increased by about 10%.

The critical velocity of perforation according to CEB (1988) were very close to the test results for high-strength concrete plates, both in the case of fixed and simply-supported. However, for normal-strength concrete, the critical velocities were different. Under fixed condition, the test results of normal-strength concrete plates were much higher by about 30% than the code prediction. On the other hand, for simply-supported plates, the test results were slightly lower by about 4% than the CEB (1988) prediction. In conclusion, the prediction of critical velocity based on the CEB (1988) Equation (5.9) is adequate and can be used to estimate the critical velocity of high-strength concrete plates subjected to impact loading accurately.

5.6. Fracture Mechanics Analysis of Impact Load

The strength of materials depends on how rapidly the stress is applied. Thus, the rate of loading effect is extremely important, since it sets a limit on the allowable stresses in structures based on the expected time under load. One of the main objective is to use fracture mechanics to provide a more detailed estimate of the rate of loading effects on the behavior of the concrete plate under impact.

The fracture mechanics approach to the rate of loading effect in brittle materials is based on the classical Griffith (1925) theory. The fracture is governed by equation:

$$\sigma_c = \left(\frac{2E\gamma}{\pi a} \right)^{1/2} \tag{5.10}$$

where, σ_c = fracture strength

E = modulus of elasticity

γ = fracture surface energy

a = crack length

If $G_c = 2\gamma$ is the critical strain energy release rate, then the Equation (5.10) can also be written in the form:

$$\sigma_c = \left(\frac{E G_c}{\pi a} \right)^{1/2} \tag{5.11}$$

An intrinsic material property called fracture toughness, K_c, can then be defined as:

$$K_c = \sqrt{E G_c} \tag{5.12}$$

In order to states that fracture will occur when the crack length, a, reaches some critical value, substituting Equation (5.12) into Equation (5.11) give:

$$\sigma_c = \frac{K_c}{(\pi a)^{1/2}} \tag{5.13}$$

Subcritical crack growth is defined as the growth of cracks that are too small to cause failure under the prevailing stress. During subcritical crack growth, an empirical relationship is also utilized that describes the crack velocity as:

$$V = \frac{da}{dt} = A K_I^N \tag{5.14}$$

where, $V = \frac{da}{dt}$ = rate of crack extension, while A and N are constants. K_I is the stress intensity factor and equal to K_c at the critical stress condition.

Assuming, $Y = \sqrt{\pi}$, Equation (5.13) become:

$$\sigma_c = \frac{K_c}{Y a^{1/2}} \tag{5.15}$$

Using a more general form, Equation (5.15) can be expressed as:

$$K = Y \sigma a^{1/2} \tag{5.16}$$

Combining Equation (5.16) with Equation (5.14) gives:

$$\frac{da}{dt} = A Y^N \sigma^N a^{N/2} \tag{5.17}$$

The rate of stress can be define as

$$\frac{d\sigma}{dt} = \dot{\sigma} \tag{5.18}$$

Alternatively, in other way, Equation (5.18) can be written as:

$$dt = \frac{d\sigma}{\dot{\sigma}} \tag{5.19}$$

Substituting Equation (5.19) into Equation (5.17) and leads to the integration gives:

$$\int_{a_i}^{a_f} a^{-N/2}\, da = \frac{A Y^N}{\dot{\sigma}} \int \sigma^N \, d\sigma \tag{5.20}$$

$$\frac{2}{(N-2)}\left[a_i^{-(N-2/2)} - a_f^{-(N-2/2)}\right] = \frac{A Y^N}{(N+1)\dot{\sigma}} \sigma_f^{N+1} \tag{5.21}$$

where the subscript i and f refer to the initial condition before testing and the final condition on fracture, respectively. Inserting Equation (5.15) into Equation (5.21), gives:

$$\sigma_f^{N+1} = \frac{2\dot{\sigma} Kc^{2-N} (N+1)}{A Y^2 (N-2)} \left[\sigma_i^{N-2} - \sigma_f^{N-2}\right] \tag{5.22}$$

Letting:

$$B = \frac{2 Kc^{2-N} (N+1)}{A Y^2 (N-2)} \tag{5.23}$$

Leads to:

$$\sigma_f^{N+1} = B\dot{\sigma}\left[\sigma_i^{N-2} - \sigma_f^{N-2}\right] \tag{5.24}$$

And,

$$\sigma_f^{N+1} + B\dot{\sigma}\sigma_f^{N-2} = B\dot{\sigma}\sigma_i^{N-2} \tag{5.25}$$

From Equation (5.25), if the final strength of a specimen is measured in a fracture test, the initial strength can be computed by knowing the stressing rate $\dot{\sigma}$. Conversely, if the initial strength of a specimen is known, the fracture strength in any constant loading rate test can be defined from Equation (5.25) by numerical methods.

As reported by Nadeau, Bennet, and Fuller (1982), using the principles of linear elastic fracture mechanics, the dependence of strength on the rate of loading can be expressed by the logarithmic form of Equation (5.24). The expression can be written as follows:

$$\ln\sigma_c = \frac{1}{N+1}\ln B\dot{\sigma} + \frac{1}{N+1}\ln\left(\sigma_i^{N-2} - \sigma_f^{N-2}\right) \tag{5.26}$$

Analysis of Equation (5.26) implies that a plot of $\ln\sigma_c$ versus $\ln\dot{\sigma}$ would have a slope of $[1/(N+1)]$ at lower values of $\dot{\sigma}$. Finally, it would reach a constant value (zero slope) at high values of $\dot{\sigma}$. This is consistent with the subcritical crack growth model that at very high loading rates, the strength would be largely independent of loading rate. Since, there is not enough time for subcritical crack growth to occur, the initial and final strength are essentially equal.

In recent years, there are three independent methods for evaluating the constant B in Equation (5.23) by determining the constant N based on:

(1) direct observations of crack growth measurements where the constant N is the slope and the constant A is the intercept of the V-K plot, where V is crack velocity and K is intrinsic material property, plot on a logarithmic scale,

(2) the rate of loading effect in which the first two terms of Equation (5.26) are plotted giving both the slope N and from the intercept B,

(3) a logarithmic plot of the applied stress against the time to failure, the slope of this plot is $[-1/N]$.

Mindess (1984) reported that the values of N obtained from impact tests are essentially the same as those obtained from constant rate of loading tests (the second method). This would suggest that even at these very high stress rate, the fracture processes are much the same.

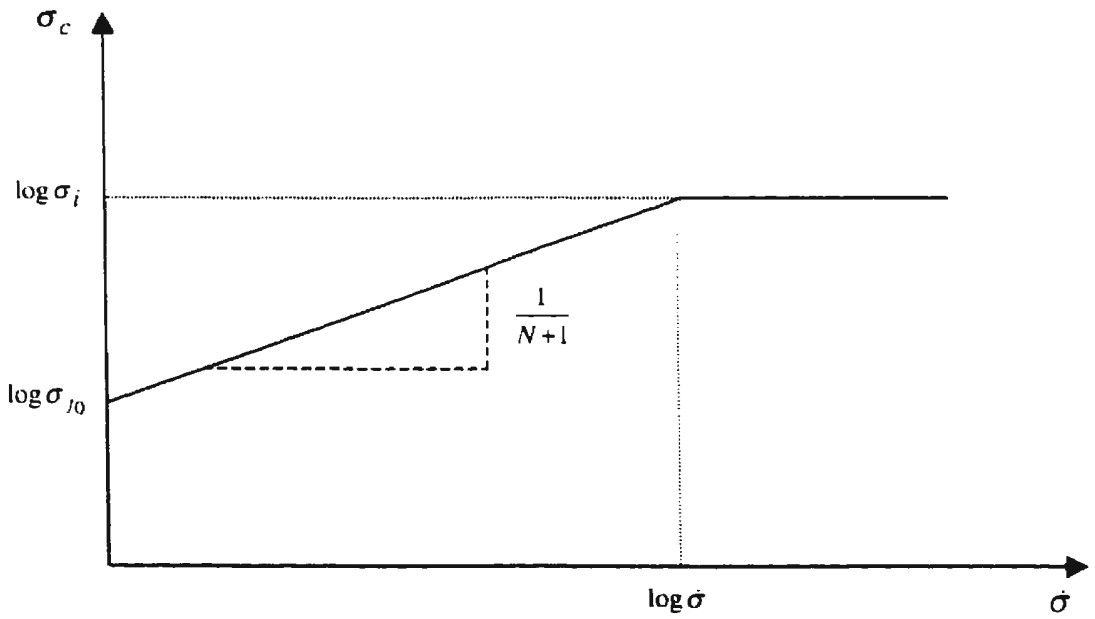

Figure 5.1. Method of calculating N from stressing rate data

The method of calculating N from stressing rate data is shown in Figure 5.1 when materials can be assumed to behave in a linear elastic manner. The strength, σ_c, can be expressed as a function of stress rate, $\dot{\sigma}$. Then, the slope of $\log\sigma_c$ versus $\log\dot{\sigma}$ is defined as $[1/(N+1)]$. When materials can be assumed to behave in a linear elastic, the stress rate in a test can be related to the strain rate, $\dot{\epsilon}$, through a simple relation: $\dot{\sigma} = E\dot{\epsilon}$. The first hump at strain versus failure time plot indicates inertial strain and the second hump is where the brittle matrix fractures. Since the matrix crack created during the second hump, the value of N in present research obtained from a logarithmic plot of applied strain versus the time to failure in rising part of the second hump. The slope of this plot is $[1/N]$.

The values of N in the present experiment are presented in Table 5.4. The table notices that the value of N varies between wide limits. In general, the values of N are higher than normally reported for other types of concrete. The test result indicates that concrete is known to be far more sensitive to stress rate under impact loading than in any other mode. This phenomenon probably caused by a lack of a linear response. Concrete is not ideally brittle and the $\sigma - \varepsilon$ response is far from linear. The values of N therefore may not be expected to capture the true nature of stress rate sensitivity in these materials. Therefore, as pointed by Mindess (1985), the assumption of a linear elastic fracture response assumed in Equation (5.14) is not entirely valid. However, the properties of high-strength concrete are close to more linear response than normal-strength concrete. Hence, the use of linear fracture mechanics for structures made with high-strength concrete are more valid than normal-strength concrete.

For specimens loaded slowly, more time is available for slow crack growth than specimens loaded rapidly. Therefore, the rate of loading effect on the tested specimens must be considered. Under very high rate of loading such as impact loading, the crack velocity (crack growth) depends on the values of N as defined by Equation (5.14). As the value of N increases, the crack velocity increases. It can be seen in Table 5.4 that the crack velocity increase as well as in the case of an increase of the concrete strength and in the case of a decrease in steel reinforcement ratio.

Table 5.4. Values of N from impact tests

No.	Specimen	fc' MPa	ρ %	N
1	HSS1	81.7	0.95	28
2	HSS2	81.7	1.26	28
3	HSS3	81.7	1.90	24
4	HSS4	81.7	2.32	23
5	HSF1	79.1	0.95	-
6	HSF2	79.1	1.26	33
7	HSF3	79.1	1.90	24
8	HSF4	79.1	2.32	22
9	NSS1	33.1	0.95	28
10	NSS2	33.1	1.26	24
11	NSS3	33.1	1.90	16
12	NSS4	33.1	2.32	14
13	NSF1	36.6	0.95	28
14	NSF2	36.6	1.26	24
15	NSF3	36.6	1.90	21
16	NSF4	36.6	2.32	17

However, some researchers like Reinhardt (1985) suggested an alternative explanation of the observed trends given on the basis of non-linear fracture mechanics. It has been recognized that immediately ahead of a moving crack is a zone of micro-

cracking, called process zone. The size of the zone of micro-cracking depending on the velocity of the crack. A faster crack has a larger zone of micro-cracking ahead of it. At a higher stress rate that crack propagates faster, and therefore the process zone will be bigger. This increased micro-cracking may explain the higher fracture energy requirements at higher stress rates.

The previous argument seems to contradict with the argument presented above. The sub-critical crack growth, predicts less micro-cracking in high-stress rate loading situations. However, these two phenomena occur on the opposite sides of the peak load. The concept of sub-critical crack growth is applicable prior to the peak load while the concept of larger process zone applies for the post-peak load region where the unstable crack propagation commences.

5.7. Dynamic Fracture Energy

When the projectile hits the specimen, a sudden transfer of energy from the projectile to the specimen occurs. The energy lost by the projectile is partly transferred to the specimen and partly stays within the projectile in the form of elastic strains and vibrations. The energy received by the specimen from the projectile is the energy given by the area under bending load versus deflection curve, as described in the following equation:

$$G_f(t) = \int_0^t P(t)\, du \tag{5.27}$$

where, $G_f(t)$ = bending energy received by the specimen

$P(t)$ = punching load

$u(t)$ = deflection at the load point

The deflection $u(t)$ can be obtained by double integration of the extrapolated acceleration at the load point, $\ddot{u}(t)$, by equation:

$$u(t) = \int_0^t \int_0^t \ddot{u}(t)\, dt\, dt \tag{5.28}$$

Figure 5.2 illustrates a typical load versus deflection plot. The area under load-deflection curve represents the fracture energy received by the specimen subjected to impact loading.

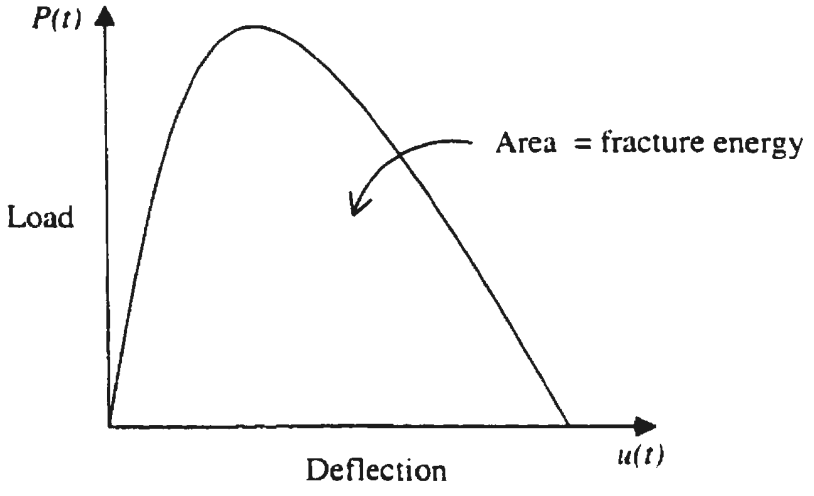

Figure 5.2. Typical load-deflection curve

The dynamic fracture energy values under impact loading for all tested specimens are then compared to static fracture energy under static loading. The values of static fracture energy were obtained from previous investigators, i.e. Hussein (1990), Marzouk, Emam, and Hilal (1995), and Osman, Marzouk, and Helmy (1998).

The comparison of fracture energy between dynamic to static tests are then tabulated in Table 5.5. The results indicate that concrete under impact loading, especially high strength concrete, is more energy absorbing than under static loading. In general, concrete is a sensitive material to the change in the stress-rate. The ratios of impact to static fracture energy was found to be higher for high-strength concrete than normal-strength concrete. Therefore, high-strength concrete plates are considered to have more impact resistance than normal-strength concrete.

Table 5.5. Comparison of dynamic fracture energy with static fracture energy

Series No:	Notation	Support Condition	fc (MPa)	ρ (%)	Dynamic Fracture Energy (kN.mm)*10^3	Static Fracture Energy (kN.mm)*10^3	Ratio Dynamic / Static
1	HSS1	Simply supported	81.7	0.95	2.76	2.61	1.1
2	HSS2	Simply supported	81.7	1.26	4.21	2.74	1.5
3	HSS3	Simply supported	81.7	1.90	8.76	3.01	2.9
4	HSS4	Simply supported	81.7	2.32	12.27	3.18	3.9
5	HSF1	Fixed	79.1	0.95	N/A	2.32	-
6	HSF2	Fixed	79.1	1.26	3.64	2.56	1.4
7	HSF3	Fixed	79.1	1.90	8.12	2.44	3.3
8	HSF4	Fixed	79.1	2.32	12.45	2.61	4.8
9	NSS1	Simply supported	33.1	0.95	0.77	2.43	0.3
10	NSS2	Simply supported	33.1	1.26	1.62	2.55	0.6
11	NSS3	Simply supported	33.1	1.90	1.81	2.80	0.7
12	NSS4	Simply supported	33.1	2.32	2.55	2.96	0.9
13	NSF1	Fixed	36.6	0.95	0.61	2.16	0.3
14	NSF2	Fixed	36.6	1.26	1.10	2.38	0.5
15	NSF3	Fixed	36.6	1.90	1.86	2.27	0.8
16	NSF4	Fixed	36.6	2.32	2.60	2.43	1.1

Chapter 6

SUMMARY AND CONCLUSIONS

The dynamic behavior of the two-way reinforced concrete plates under impact loading are summarized briefly. The present research investigation combines into an experimental investigation and a numerical investigation. A summary of the two phases of the investigation is described in the following section.

The experimental testing program was conducted on sixteen reinforced concrete plates under variety of concrete strength, steel reinforcement ratios, and two end-conditions. The plates were tested under dynamic impact load. The impact load speed ranged between 4.0 to 9.0 m/s as acceleration ranged between 70 to 120 g. Eight specimens were constructed with high-strength concrete, while the other eight specimens were constructed with normal strength concrete. The concrete strength ranged between 35 to 80 MPa and had a variety of reinforcement ratios in the range of about 1.0%-2.5%, and were tested under fixed and simply supported end-condition. The behavior of high-strength concrete plates was evaluated in terms of deflection, concrete and steel strains, energy absorption, and fracture energy.

The numerical investigation was carried out to verify the validity of the codes' predictions. The recorded impact load capacities were compared with static capacities of current codes' prediction. In addition, a fracture mechanics impact load analysis based on linear elastics fracture mechanics (LEFM) was performed. The purpose of the numerical investigation was to provide a more detailed analysis on the effect of the rate of loading on the dynamic behavior of high-strength concrete plates. The dynamics fracture energy of the tested plates were compared to static fracture energy calculated from previous investigators.

6.1. Experimental Investigation

Experimental studies were conducted on sixteen reinforced concrete two-way plates subjected to impact loading. The following conclusions were reached from the present investigation concerning the effect of concrete strength, steel reinforcement ratio, and end-condition.

1. All specimens failed under ductile shear failure. The observed angles of failure were about 60 degree for normal-strength concrete and 65 degree for high-strength concrete. In addition, the punching shear surface on the tension face was located at a distance of 1.6-2.0 times the plate depth (d) from the edge of loaded area for the most of the tested specimens.
2. As the concrete strength increased from normal-strength to high-strength (35 MPa to 80 MPa), energy absorption capacity and critical velocity of perforation increased. The energy absorption capacity increased by a range of about 3-5 times, and the critical velocity of perforation increased by a range of about 20%-30%.

3. The steel reinforcement has a major effect on the dynamic behavior of high-strength concrete plates. Increasing reinforcement ratio from 1% to 1.5%, the energy absorption increased by 50% for high-strength concrete and 100% for normal-strength concrete, while the critical velocity of perforation increased by about 10% for both high-strength and normal-strength concrete. Increasing reinforcement ratio from 1% to 2%, the energy absorption increased by about 300% and the critical velocity of perforation increased by about 20% for both high-strength and normal-strength concrete. Increasing reinforcement ratio from 1% to 2.5%, the energy absorption increased by about 400% and the critical velocity increased by about 30% for high-strength concrete as well as normal-strength concrete.
4. The effect of the end-condition was less significant on the behavior of high-strength concrete plates under impact load. As concrete strength increased from normal-strength to high-strength, the critical velocity of perforation increased by about 20%-30% for the simply supported specimens. While under fixed-end condition, the critical velocity of perforation increased by about 50%-60%.
5. In the case of static loading, the peak-load, peak-strain and maximum-deflection occurred at the same time. However, in the case of impact loading, the peak-strain occurs slightly later than to the peak-load but ahead of maximum-deflection. In addition, the tension steel strain is estimated by about twice that recorded under static loading. The test results illustrate the difference between impact failure mechanism compared to static failure mechanism. All of the impact test specimens failed under ductile shear failure.

6.2. Numerical Investigation

An analytical investigation was carried out on the impact loading on a concrete plates. The recorded impact load capacities were compared to static capacities calculated by the formula of current codes. A fracture mechanics analysis based on linear elastics fracture mechanics (LEFM) was performed to evaluate the effect of rate of loading on the dynamic behavior of high-strength concrete plates. The dynamics fracture energy was compared to static fracture energy for all of the tested specimens. The significance and contribution of the present numerical investigation can be concluded as follows:

1. The punching shear capacity due to impact loading were about twice that of the static punching shear capacity. The ratio of impact punching shear capacity to static as estimated by the ACI-318 (1995) was in the range of 1.39-2.31. The same ratio based on BS- 8110 (1985), CEB-FIP (1990), and NS-3473 (1992) were 1.50-1.82, 1.36-1.65, and 1.87-2.33, respectively.
2. The critical velocities of perforation can be estimated accurately for all high-strength concrete specimens according to CEB (1988) code expression. However, for normal-strength concrete under fixed-end condition, the critical velocity of the test result was 30% higher than the code prediction. On the contrary, under simply-supported condition, the test result was slightly lower by about 4% than the code values. In general, the prediction of the CEB (1988) code can be used accurately to estimate the critical impact velocity, especially for high-strength concrete plates.
3. A linear elastic fracture mechanics impact load expression can be used to evaluate the effect of rate of loading on the dynamic behavior of high-strength concrete plates. High-strength concrete is more brittle and close to more linear response prior to peak

load than normal-strength concrete. Therefore, linear fracture mechanics can be used to provide a good degree of confidence.

4. The concrete fracture strength, σ_c, can be expressed as a function of the stress rate, $\dot{\sigma}$. The slopes of $\log \sigma_c$ versus $\log \dot{\sigma}$ were determined experimentally. The suggested values for N and subsequently the two constants A and B can be used to represent the stress rate sensitivity numbers for high-strength and normal-strength concrete plates. Therefore, the recommended values can be used by designer to predict the dynamic behavior of any plate under impact loading.
5. The dynamic versus static fracture energy ratio of high-strength concrete plate under impact load was found to be much higher than that for normal-strength concrete. Therefore, high-strength concrete plates are considered to be more efficient material for construction under impact loading. High-strength concrete is a better material than normal concrete in dynamic situations because of its increased impact resistance.

REFERENCES

ACI-ASCE Committee 316. 1962. Shear and Diagonal Tension. Proceedings, American Concrete Institute, Volume 59, pp. 1-30.

ACI Committee 212. 1983. Admixtures for Concrete. ACI Manual of Concrete Practice, ACI212.1 R-81, Detroit, 29 p.

ACI Committee 318. 1995. Building Code Requirements for Structural Concrete (ACI 318M-95) and Commentary (ACI 318RM-95). American Concrete Institute, Farmington Hills, MI, 371 p.

ACI Committee 357. 1985. Guide for Design and Construction of Fixed Offshore Structures. American Concrete Institute, Detroit.

ACI Committee 363. 1992. State of the Art Report on High-Strength Concrete. ACI 363R-92, Detroit, 55 p.

ACI Committee 421. 1992. Abstract of Shear Reinforcement for Slabs. ACI Structural Journal, V.89, No.5, pp. 587-589.

ASTM. 1997. American Society for Testing and Materials Standard in Building Codes: Specifications, Test Methods, Practices, Classifications, Terminology. American Society for Testing and Material, West Conshohocken, Pennsylvania.

Aitcin. P., and Neville, A. 1993. High Performance Concrete Demystified. Concrete International, American Concrete Institute, Detroit, pp. 21-26.

Ammann, W., and Nussbaumer, H. 1995. Behaviour of Concrete and Steel Under dynamic Actions. *In* Vibration Problems in Structures: Practical Guidelines.

Edited by H. Bachman. Institut fur Baustatik und Konstuktion eth Honggerberg, Birkhauser, Basel, Germany, pp. 177-183.

BAM (Bundesanstalt fur Materialprufung). 1982. Concrete Structures under Impact and Impulsive Loading. Proceeding of the International Symposium, Vol. 3, Berlin, p. 656.

Banthia, N., Yan, C., and Sakai, K. 1998. Impact Resistance of Concrete Plates Reinforced with a Fiber Reinforced Plastic Grid. ACI Materials Journal, V.95, No.1, pp. 11-18.

Banthia, N., Mindess, S., and Bentur, A. 1987. Impact Behaviour of Concrete Beams. RILEM, Materials and Structures, **20**, pp. 293-302.

Banthia, N., Mindess, S., and Trottier, J.F. 1996. Impact Resistance of Steel Fiber Reinforced Concrete. ACI Materials Journal, V.93, No. 5, pp. 472-479.

Barr, P., Carter, P.G., Howe, W.D., and Neilson A.J. 1982. Replica Scaling Studies of Hard Missile Impacts on Reinforced Concrete. Symposium on Concrete Structures under Impact and Impulsive Loading, BAM Proceedings, Berlin, pp. 329-344.

Brown, I.C., and Perry, S.H. 1982. An Experimental Method to Investigate Impact on Concrete Slabs. Symposium on Concrete Structures under Impact and Impulsive Loading, BAM Proceedings, Berlin, pp. 202-211.

BS 8110. 1985. Structural Use of Concrete: Part 1, Code of Practice for Design and Construction. British Standard Institute, London, U.K., 126 p.

Carrasquillo, R.L. 1985. Production of High-Strength Concrete Pastes, Mortars, and Concretes. Proceedings, Material Research Society, Volume 42, pp. 151-168.

CEB (Comite Euro-International du Beton). 1988. Concrete Structures Under Impact and Impulsive Loading. Synthesis Report, Bulletin No.187, Lausanne.

Chen, Z. and Marzouk H.1993. Nonlinear Analysis of High-Strength Concrete Slabs. Engineering & Applied Science Technical Report Series No. 93004, Faculty of Engineering & Applied Science, Memorial University of Newfoundland, St. John's, Newfoundland.

CP110. 1972. Code of Practice for the Structural Use of Concrete, Part 1. British Standards Institution London, U.K.,155 p.

CSA Standard A23.3-94. 1995. Concrete Design Handbook. Canadian Portland Cement Association, Ontario, Canada.

Farag, H.M., and Leach, P. 1997. The Elasto-Plastic Design of Reinforced Concrete Beams and Slabs Subject to Dynamic Loading. Proceeding of The Institution of Civil Engineers Structures and Buildings, Vol. 122, London, pp. 117-123.

Farny, J.A., and Panarese, W.C. 1994. High-Strength Concrete. Engineering Bulletin, Portland Cement Association, Illinois, 48 p.

Forsel, C., and Holemberg, A. 1964. Consentrated Loads on Concrete Slabs. Betong, Volume 31, No. 2, Stockholm, Sweden, pp. 95-123.

Gardner, N.J., and Shao, X. 1996. Punching Shear Capacity of Reinforced Concrete Slabs. ACI Structural Journal, Vol. 93, No. 2, pp. 218-228.

Griffith, A.A. 1925. The Theory of Rupture. Proceeding of 1st International Congress Applied Mechanics, Biezeho and Burgers ed., Waltman, pp. 55-63.

Hillerborg, A. 1985. The Theoretical Basis of a Method to Determine the Fracture Energy G_f of Concrete, Material and Structure. RILEM, 18(106), pp. 291-296.

Hussein, A. 1990. Behavior of Two Way Slabs Made With High-Strength Concrete. M.Eng. Thesis. Memorial University of Newfoundland, Canada.

Jensen, J.J., Hoiseth, K.V., and Hansen, E.A. 1993. Ductility of High-Strength Concrete at High Rate Loading. HSC Proceedings, Lillehammer, pp. 241-250.

Kinnunen, S., and Nylander, H. 1960. Punching of Concrete Slabs Without Shear Reinforcement. Transaction No. 158, Royal Institute of Technology, Stockholm, Sweden.

Labtech. 1992. Data Acquisition and Process Control Software. Laboratory Technologies Corporation, Wilmington, USA.

Malvern, L.E., Jenkins, D.A., Tang, T., and Ross, C.A. 1985. Dynamic Compressive Testing of Concrete. Proceeding 2nd Symposium The Interaction of Non-nuclear Munitions with Structures, Panama City Beach, Florida, pp. 194-199.

Marzouk, H., and Chen, Z. 1993. Finite Element Analysis of High-Strength Concrete Slabs. ACI Structural Journal, V.90, No.5, pp. 505-513.

Marzouk, H., and Chen, Z. 1995. Fracture Energy and Tension Properties of High-Strength Concrete. ASCE Journal of Materials in Civil Engineering, Vol.7, No.2.

Marzouk, H., and Chen, Z. 1993. Nonlinear Analysis of Normal- and High-Strength Concrete Slabs. Canadian Journal of Civil Engineering, **20**, pp. 696-707.

Marzouk, H., Emam, M., and Hilal, M.S. 1996. Effects of High-Strength Concrete Columns on the Behavior of Slab-Column Connections. ACI Structural Journal, V.93, No.5, Title no. 93-S51.

Marzouk, H., and Hussein, A. 1991. Experimental Investigation on the Behavior of High-Strength Concrete Slabs. ACI Structural Journal, V.88, No.6.

Marzouk, H., and Hussein, A. 1991. Punching Shear Analysis of Reinforced High-Strength Concrete Slabs. Canadian Journal of Civil Engineering, **18**, pp. 954-963.

Marzouk, H., and Jiang, D. 1996. Finite Element Evaluation of Shear Enhancement of High-Strength Concrete Plates. ACI Structural Journal, V.93, No.6, Title no. 93-S63.

Massicotte, B., Elwi, A.E., and MacGregor, J.G. 1990. Tension Stiffening Model for Planar Reinforced Concrete Members. Journal of Structural Engineering, ASCE, Volume 116, No. 11, pp. 3039-3058.

Mindess, S., Banthia, N., and Yan, C. 1987. The Fracture Toughness of Concrete Under Impact Loading. Pergamon Journals Ltd., Cement and Concrete Research, Vol. 17, USA, pp. 231-241.

Mindess, S. 1984. Rate of Loading Effects on the Fracture of Cementitious Materials. *In* Application of Fracture Mechanics to Cementitious Composites. *Edited by* S.P. Shah. NATO Advanced Research Workshop. Martinus Nijhoff Publisher, Dordrecht, pp. 617-636.

Moe, J. 1961. Shearing Strength of Reinforced Concrete Slabs and Footings Under Consentrated Loads. Development Department Bulletin D47, Portland Cement Association, Skokie.

Nadeau, J.S., Benneth, R., and Fuller, E.R. 1982. Explanation of the Rate-of-Loading and Duration-of-Load Effects in Wood in Term of Fracture Mechanics. Journal of Material Science, V.17, pp. 2831-2840.

Norwegian Standard NS 3473. 1992. Concrete Structures. Design Rules. Norwegian Council for Building Standardization (NBR), 4th edition.

Osman, M., Marzouk, H., and Helmy, S. 1998. Behavior of High-Strength Lightweight Concrete Interior Flat-Slab Connection under Static and Cyclic Loading. Engineering & Applied Science Technical Report Series No. 98001, Faculty of Engineering & Applied Science, Memorial University of Newfoundland, St. John's, Newfoundland.

Regan, P.E. 1981. Behavior of Reinforced Concrete Slabs. CIRIA Report No. 89, Construction Industry Research and Information Association, London.

Reinhardt, H.W. 1985. Tensile Fracture of Concrete at High Rates of Loading. *In* Application of Fracture Mechanics to Cementitious Composites. *Edited by* S.P. Shah. Martinus Nijhoff, The Hague, pp. 559-590.

Saucier, K. L., Smith, E.F., and Tynes, W.O. 1964. High-Compressive Strength Concrete: Development of Concrete Mixtures. Technical Report No. RTD-TDR 63-3114, U.S. Air Weapons Laboratory.

Takeda, J., Tachikawa, H., and Fujimoto, K. 1982. Mechanical Properties of Concrete and Steel in Reinforced Concrete Structures Subjected to Impact or Impulsive Loading. Symposium on Concrete Structures under Impact and Impulsive Loading, BAM Proceedings, Berlin, pp. 83-91.

Tomaszewicz, A. 1993. Punching Shear Capacity of Reinforced Concrete Slabs. *In* Utilization of High-Strength Concrete. *Edited by* I. Holand and E. Sellevold. Proceedings, Vol. 1, Symposium in Lillehammer, Norway, pp.393-401.

Walker, S and Bloem, D.L. 1960. Effects of Aggregate Size on Properties of Concrete. Journal of the American Concrete Institute, Proceeding, Vol. 57, No. 3, Detroit, pp. 283-298.